Landscape and depositional controls on palaeosols of a distributive fluvial system (Upper Cretaceous, Brazil)

Marcus Vinícius Theodoro Soares [a,*], Giorgio Basilici [a,b], Paolo Lorenzoni [c], Luca Colombera [d], Nigel Philip Mountney [d], Agustín Guillermo Martinelli [e], Áquila Ferreira Mesquita [a], Thiago da Silva Marinho [f,g], Richard Guillermo Vásconez García [a], André Marconato [h]

[a] Department of Geology and Natural Resources, Institute of Geosciences, State University of Campinas, 13083-870 Campinas, SP, Brazil
[b] Centro Regional de Investigaciones Científicas y Transferencia Tecnológica/CONICET, Argentina
[c] Professional consultant, Largo Trasimeno 1, 02100 Rieti, Italy
[d] Fluvial & Eolian Research Group, School of Earth and Environment, University of Leeds, Leeds LS2 9JT, UK
[e] CONICET - Sección Paleontología de Vertebrados, Museo Argentino de Ciencias Naturales "Bernardino Rivadavia", Av. Ángel Gallardo 470, CP1405 Buenos Aires, Argentina
[f] Centro de Pesquisas Paleontológicas L. I. Price, Complexo Cultural e Científico Peirópolis, Pró-Reitoria de Extensão Universitária, Universidade Federal do Triangulo Mineiro, Uberaba, Minas Gerais, Brazil
[g] Instituto de Ciências Exatas, Naturais e Educação (ICENE), UFTM, Av. Randolfo Borges Jr. 1700, Univerdecidade, 38064-200 Uberaba, MG, Brazil
[h] Department of Geology, Federal University of Ouro Preto, Ouro Preto, MG 35.400-000, Brazil

ARTICLE INFO

ABSTRACT

The stratigraphic record of distributive fluvial systems is commonly characterised by frequent and complex inter-stratification of palaeosols among channel and overbank deposits. However, current models focus primarily on sedimentation and pay only limited attention to palaeopedogenesis, thereby failing to incorporate important palaeoenvironmental and stratigraphic information. This study proposes a pedosedimentary model for distributive fluvial systems that depicts and accounts for two palaeopedogenetic trends: one downdip, in relation to distality from the fan apex, and one along-strike, in relation to distance from active channel belts. Palaeosols are reported in detail from an Upper Cretaceous succession of the Bauru Basin, southeastern Brazil, through the application of macro-, micromorphological and geochemical studies, combined with facies and architectural-element analyses of sediments. In the downdip palaeopedogenetic trend, the proximal zone of the depositional system is characterised by a dominance of well-drained Inceptisols that develop on amalgamated channel fills; in the medial zone, Inceptisols occur interlayered with overbank deposits containing Entisols and poorly drained Vertisols. The distal zone preserves more mature and poorly drained Inceptisols developed on deposits of overbank and sporadic distal channel fills. These pedotypes show an increase in maturity and hydromorphism, moving away from the apex to the fan toe. This is likely linked to (i) the progressive approach of the topographic surface to the water table, and (ii) the average increase in distance to an active channel belt in distal locations. The along-strike palaeopedogenetic trend culminates in poorly developed palaeosols in floodplain regions that correspond to topographic depressions located between channel belts and which were subject to recurrent floods. Because palaeopedogenesis in the floodplain region is penecontemporaneous to sedimentation, pedotypes show an increase in maturity, bioinduced calcification and hydromorphism with distance from the active channels; they pass laterally from Entisols and Inceptisols near active channels, to Vertisols away from active channels. Conversely, following avulsion, abandoned channel belts remain as topographically elevated alluvial ridges located at some distance from the newly active channels and positioned above the water table and this leads to the development of better drained and better developed Inceptisols relative to pedotypes of the floodplain region. Overall, both palaeopedogenetic trends demonstrate the overriding controls of topography, sedimentation rate and parent material on pedogenesis, with only minor climatic influence. This work offers a novel pedosedimentary model for distributive fluvial systems and highlights the palaeoenvironmental significance of palaeosol trends, providing new constraints for the recognition of distributive fluvial systems in the rock record.

© 2020 Elsevier B.V. All rights reserved.

1. Introduction

Distributive fluvial systems (DFS) are a common fluvial form in modern continental basins and their deposits are widely recognised

from ancient successions preserved in the rock record. The term DFS is used to cover the landforms and stratigraphic record of alluvial fans, fluvial fans and megafans (Weissmann et al., 2010), a suite of systems that share characteristics related to subaerial deposition on a fan surface, but which differ with respect to fan area (150–250 km^2 in alluvial fan; <10^3 km^2 in fluvial fans and 10^3–10^5 km^2 in megafans), fan slope (c. 1°–5° in alluvial fans and less than 0.2° in fluvial fans and megafans) (DeCelles and Cavazza, 1999), dominant sediment-transport mechanism (debris flows in alluvial fans versus streamflows in fluvial fans and megafans), and sedimentary deposits (conglomerates in alluvial fans and sandstones/mudstones in fluvial fans and megafans) (Blair and McPherson, 1994). Since first being classified as a distinctive type of fluvial system (Friend, 1978), many larger DFS forms have been investigated in terms of the hydraulic character of their channels and the avulsion and sedimentation patterns of channel belts. The sedimentary architecture of distributive fluvial systems records the effects of nodal avulsions at fan apices, which are in part driven by high fluctuations in water discharge in the catchment area (Leier et al., 2005), themselves often correlated to highly seasonal climate (Hansford and Plink-Björklund, 2020). Several DFS depositional (facies) models have been proposed and these serve to predict and quantify a combination of proximal-to-distal decrease in the overall thickness, grain size, dimension and amalgamation of channel deposits, and the concomitant increase in floodplain facies (Weissmann et al., 2010; Owen et al., 2015).

Since the advent of the earliest DFS models, research efforts concerning these systems have been focused almost exclusively on assessment of channel hydraulics and in-channel sedimentation, with only modest consideration of overbank sedimentation, and little to no attention given to palaeosols (Mukerji, 1976; Friend, 1978; Tunbridge, 1984; Olsen, 1987; Parkash et al., 1983; Abdullatif, 1989; Kelly and Olsen, 1993; North and Warwick, 2007; Weissmann et al., 2010). However, the sedimentary record of preserved DFS systems typically exhibits notable vertical and lateral occurrence of palaeosols (Nichols and Fisher, 2007; Sáez et al., 2007; Hartley et al., 2013; Basilici et al., 2019; Dal' Bó et al., 2019; Soares et al., 2018, 2020). Because DFS facies models do not fully account for such features, they fail to consider key geological criteria for interpreting characteristics of the palaeoenvironment of deposition (e.g., temperature, precipitation, topography, level of the water table) and its sediment dynamics (e.g., periods of bypass and erosion cycles). Palaeosols are intimately related to environmental parameters that actively control hydraulic discharge, sediment supply, erosive power and avulsion dynamics of fluvial systems and that, consequently, determine their depositional architecture. A preliminary model of modern distributive fluvial systems exists (Hartley et al., 2013) that deals with regional variations in DFS soils based on their macromorphological characteristics. This model demonstrates that, from fan apex to toe, palaeosol types are controlled by a regional increase in soil moisture. Although this downdip palaeosol trend provides a fairly robust criterion for recognising potential DFS successions in the rock record (cf., Atkinson, 1986; Besley and Fielding, 1989; Platt and Keller, 1992; McCarthy et al., 1997; Oest, 2015; Owen et al., 2015; Rosario, 2017; Dal' Bó et al., 2019), a higher-resolution scheme for palaeosol distribution based on local catenary variation is still needed. When analysed in detail, the sedimentary architecture of DFS successions typically reveals a much more complex arrangement of palaeosol types, which are dominantly controlled by local factors, rather than by regional factors (cf. Soares et al., 2018, 2020).

This study examines palaeosols present in an Upper Cretaceous fluvial-fan succession of the Bauru Basin in southeastern Brazil (Fig. 1A), which developed under the influence of varying semi-arid to subhumid climatic regimes (Soares et al., 2018, 2020). The aim of the study is to develop a pedosedimentary model with which to account for the distribution of sediments and palaeosols in both downdip and along-strike directions of the system, and that would generally be applicable to many types of ancient distributive fluvial systems. Specific research objectives are: (i) to unravel the regional and local controlling mechanisms on the formation and preservation of palaeosol types; (ii) to reconstruct the palaeotopographic and water-table profiles in both downdip and along-strike directions; (iii) to develop a semi-quantitative depositional model that considers periods between sedimentation episodes, so as to resolve the interavulsion and interflooding frequencies of channel-belt and floodplain environments; (vi) to unravel the control of sedimentation rate on the formation and preservation of palaeosols; and (v) to better understand palaeoclimatic influence on the distribution of sediments and palaeosols in the rock record of distributive fluvial systems.

By addressing these questions, this work provides an in-depth dataset based on the field description, micromorphology and geochemistry of palaeosols present in the proximal, medial and distal zones of an ancient distributive fluvial system. The resultant proposed model demonstrates how palaeosol types are preserved in downdip and along-strike directions, and this will potentially guide the identification of DFS successions in the rock record.

2. Geological setting

2.1. The Bauru Basin

The Bauru Basin is an Upper Cretaceous intracratonic basin located in the southeast and midwest of Brazil (Fig. 1A). The origin of the basin is associated with the opening of the South Atlantic Ocean during the breakup of the Gondwana supercontinent. During this process, the South American Craton experienced one of the greatest basalt effusions recorded on Earth; approximately 1700 m of basaltic material was emplaced over central-southeast Brazil to form basalts of the Serra Geral Formation (Riccomini, 1997; Fernandes and Coimbra, 2000). Later, a siliciclastic succession that is c. 400 m thick accumulated on top of the basalts from the Coniacian to Maastrichtian, as revealed by biostratigraphic data (Dias-Brito et al., 2001) and from relationships with contemporaneous igneous intrusions towards the basin margin (Coutinho et al., 1982). During this period, the palaeoclimate of the Bauru Basin was warm and dry overall (Chumakov et al., 1995), but with marked shorter humid periods (Dal' Bó et al., 2010; Arai and Dias-Brito, 2018).

Two lithostratigraphic groups are present in the basin fill: one in the northeast (Bauru Group), where more humid conditions prevailed, and one in the southwest (Caiuá Group), where instead more arid conditions prevailed (Fernandes and Coimbra, 1994; Fernandes and Basilici, 2009). Aptian-Albian ages are suggested for the Caiuá Group (Dias-Brito et al., 2001) whereas the age of the Bauru Group is inferred as Campanian-Maastrichtian based on its vertebrate, invertebrate and microfossil assemblage (Santucci and Bertini, 2001).

The Caiuá Group is made of the Rio Paraná, Goiô Erê and Santo Anastácio formations, from bottom to top. The Rio Paraná Formation is formed of a c. 280 m thick sandstone unit organised in large-scale cross-strata separated by low-angle superimposition surfaces and formed of well-rounded and well-sorted sand with frosted surfaces. The Goiô Erê Formation constitutes a c. 50 m unit of sandstone of well-rounded and well-sorted sand showing interstratifications of cross-strata, planar parallel lamination, subcritical climbing translatent strata and irregular to convolute cross-strata. Finally, the Santo Anastácio Formation is a c. 100 m thick unit formed of high-frequency interbedding of massive sandstone beds of poorly sorted, subangular, fine-grained sand. Together, these units correspond to a desert depositional system (Caiuá desert) formed of a central draa (Rio Paraná Fm.), with a peripheral sand sea controlled by water table oscillations (Goiô Erê Fm.) and an outer sand sheet (Santo Anastácio Fm.) (Fernandes and Coimbra, 2000).

The stratigraphy of the Bauru Group has been iteratively refined to better reflect its geological history, and it was recently organised into five lithostratigraphic units, from the base to the top: Araçatuba, Uberaba, Adamantina, Marília and Serra da Galga formations (Fig. 1C).
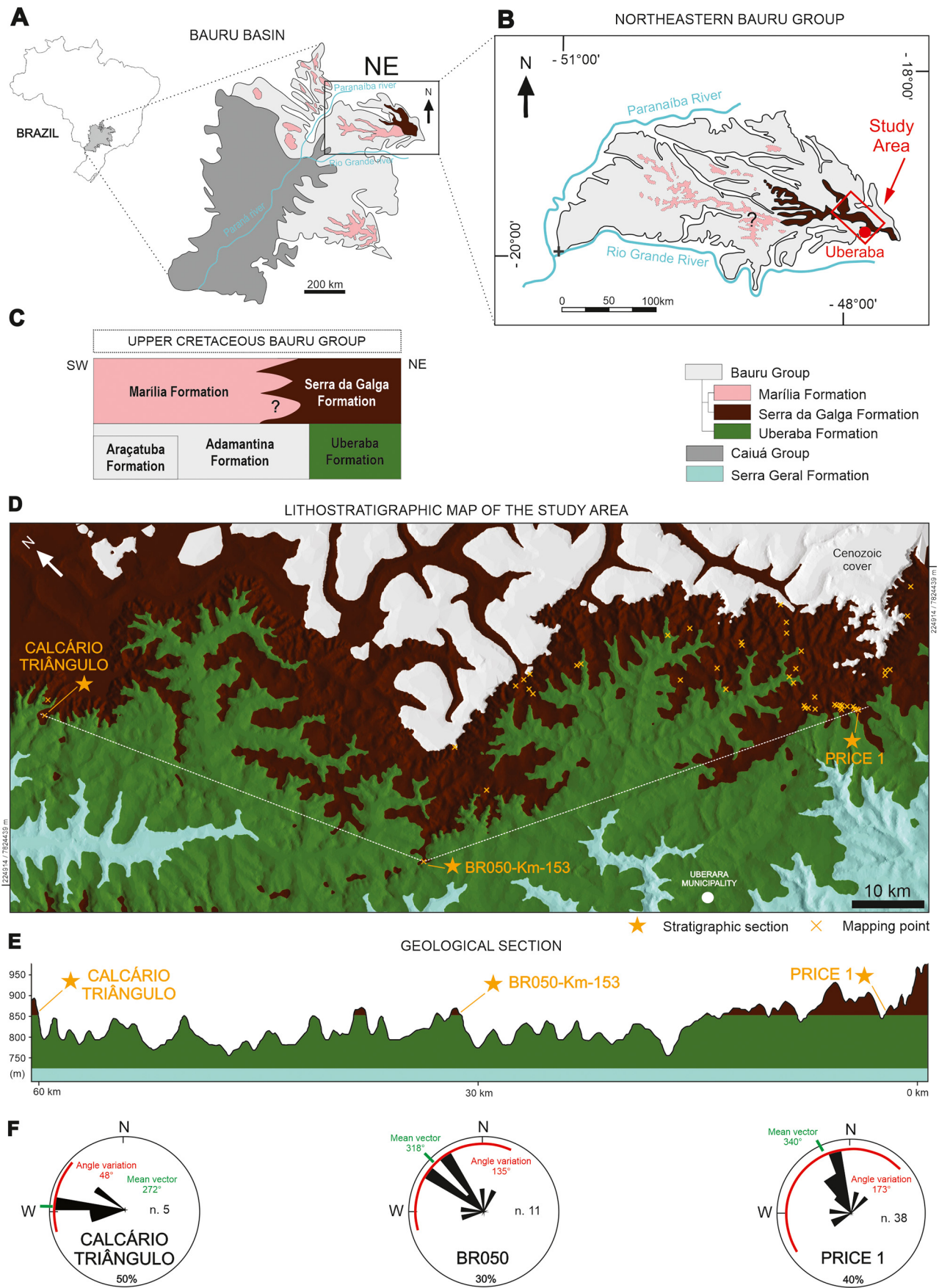
Fig. 1. (A) Location map of the Bauru Basin in Brazil. (B) Distribution of the Serra da Galga Formation within the northeastern margin of the Bauru Basin. (C) Stratigraphy of the Bauru Group. (D) Lithostratigraphic map of the study area with the location of studied outcrops and stratigraphic sections. (E) Geological section of the downdip transect betwween the Price 1, BR050-Km-153 and Calcário Triângulo stratigraphic sections. (F) Rose diagram plots of palaeocurrent data from the stratigraphic sections. This figure was modified from Soares et al. (2018).

The Araçatuba Formation is c. 70 m thick and characterised by interlayered very fine-grained sandstones and siltstones; they display massive character with scarce planar-parallel lamination, desiccation cracks, dolomite pseudomorphs and root traces. The origin of the Araçatuba Formation is related to a palustrine environment (Fernandes and Coimbra, 2000). The Uberaba Formation is a c. 85 m thick unit formed of very fine-grained sandstone showing cross- and planar-laminated strata interbedded with silty mudstone, claystone and conglomerates. This unit is interpreted as the preserved record of a braided fluvial system (Fernandes and Coimbra, 2000). The Adamantina Formation comprises well-sorted, very fine- to fine-grained sandstones showing through cross-strata that occur interlayered with intraformational conglomerates and subordinate shales. The unit represents the interplay between aeolian sand sheets and ephemeral fluvial deposition (Goldberg and Garcia, 2000; Basilici and Dal' Bo, 2010). The Marília Formation (sensu Soares et al., 2020) is formed of very fine-grained sandstones alternated with conglomeratic sandstones and sandy mudstone layers; the sandstones display planar parallel- and cross-laminated strata. This unit is interpreted as the product of a sand-sheet environment punctuated by ephemeral fluvial activity (Basilici and Dal' Bo, 2010). The Marília and Serra da Galga formations are time-equivalent (Fig. 1C). The latter occupies the northeast margin of the Bauru Basin, and is defined by Soares et al. (2020) as the preserved sedimentary product of a distributive fluvial system in which sedimentation was influenced by high-frequency wet-dry depositional cycles (Soares et al., 2018). This study focuses on the Serra da Galga Formation.

2.2. Study area

The study area is located within the Uberaba municipality (Fig. 1B, D) where the Serra Geral, Uberaba and Serra da Galga formations crop out. The Serra da Galga Formation has an average thickness of c. 100 m and is observed as a laterally continuous tabular and horizontal unit; the lower boundary with the underlying Uberaba Formation is planar, horizontal and locally erosive, whereas the upper boundary corresponds to a Cenozoic lateritic soil profile (Fig. 1D, E). The Serra da Galga deposits vary from conglomerate to fine-grained sandstone, and subordinate muddy sandstone and mudstone. The deposits are organised as large-scale and small-scale sheet-like channel bodies and overbank layers. Palaeosol are ubiquitous features of this unit; they have been classified as Inceptisols, Vertisols and Entisols (Soares et al., 2020). Additionally, groundwater calcrete lithosomes are randomly distributed within the deposits. The Serra da Galga Formation in the study area is interpreted as product of a distributive fluvial system, associated with a fan surface having an apex-to-toe distance of c. 70 km. The DFS stratotype sections defined by Soares et al. (2020) for the proximal (Price 1 site), medial (BR050-Km-153 site), and distal (Calcário Triângulo site) zones are applied to this work; they are considered laterally correlative based on: (i) continuous NW palaeocurrent trend (Fig. 1F), (ii) presence of common species in their fossil assemblages (e.g., titanosaur sauropods, abelisaurid theropods, peirosaurid crocodyloforms, podocnemidoid turtles and amiid fishes) (Novas et al., 2008; Martinelli et al., 2013; Martinelli and Teixeira, 2015) and (iii) similar mineralogical composition of channel sandstones formed of monocrystalline quartz (66–64%), polycrystalline quartz (11–18%), volcanic fragments (5%), feldspar (4–7%), mudstone intraclasts (3–4%), muscovite (4%) and others (2–7%). A DFS interpretation is made for this succession, partly based on the down-system change in architecture of the fluvial strata, varying from amalgamated sheet channel bodies in the proximal zone (Price 1) towards medial (BR050-km-153) and distal (Calcário Triângulo) zones that display abundant overbank deposits interbedded with sheet and ribbons channel bodies (Soares et al., 2018, 2020).

3. Methods

The analyses of sediments and palaeosols were conducted over an area of 450 km². Detailed analyses were undertaken at three main locations (Price 1, BR050-Km-153 and Calcário Triângulo sites) (Fig. 1D), which have excellent exposures and are well suited to the three-dimensional study of sedimentary architecture. Three detailed stratigraphic sections were measured and analysed at a centimetre resolution. Thirty-four additional outcrops were evaluated in the area around the Uberaba municipality.

Lithofacies with genetic significance (Harms et al., 1982; Walker, 2006) were identified and further grouped into architectural elements using the classification schemes and hierarchies of Miall (2006). Palaeosols were identified and described macroscopically in the field by the absence of sedimentary structures and the presence of vertical colour trends (applying colour codes of the Munsell Soil Colour Chart), root marks, mottles, nodules, and bioturbation (Retallack, 1988; Catt, 1990). The micromorphological description of palaeosols was conducted on thin sections from the collected samples; they were investigated by their coarse/fine (c/f) related distribution pattern after Stoops and Jongerius (1975), with a size limit between coarse and fine fraction set at 2 μm. Microstructures, groundmass and pedofeatures were described according to Bullock et al. (1985) and Stoops (2003). Chemical weathering ratios (CWR) were determined to evaluate the degree of weathering of palaeosol profiles based on their major oxide percentage of elements in the bulk horizons. The bulk horizon composition was determined on fused beads by X-ray fluorescence spectrometer (Philips-PW2404). The CWR were applied to climofunctions along the studied stratigraphic interval to evaluate the climate influence on palaeopedogenesis (for further details see Supplementary material). Finally, individual palaeosol profiles were grouped into palaeosol types according to their similar macro- and microscopic characteristics (pedotype sensu Retallack, 1994).

4. Sedimentology

Eleven lithofacies were identified in the Serra da Galga Formation (Table 1). These are interpreted as the product of channel and overbank fluvial sedimentation. These lithofacies occur frequently interstratified with palaeosol profiles, the presence of which indicates significant breaks in sedimentation associated with the fluvial dynamics. Sedimentary lithofacies were grouped into five types of architectural elements: (i) perennial-flow main channel fill, (ii) ephemeral-flow main channel fill, (iii) overbank deposit, (iv) floodplain channel fill, and (v) distal channel fill. They are described and interpreted in detail below; details are summarised in Table 2.

4.1. Perennial-flow main channel fill

4.1.1. Description

This channel fill (architectural element CP) forms sheet-like conglomeratic sandstone bodies (2–7 m thick) that extend laterally for more than 110 m (width:thickness ratio > 15) perpendicular to the palaeoflow (Fig. 2A, B). These bodies present a flat and erosive basal boundary with underlying palaeosols and/or other deposits, whereas their upper boundary displays a gradual transition to palaeosol profiles. Internally, the perennial-flow main channel fills are typically formed, from base to top, by: (i) massive conglomerate and (ii) conglomeratic sandstone.

The massive conglomerate (lithofacies Cm) occurs locally and lies over the erosive base of the channel fill and forms tabular layers that are c. 0.5 m thick. The conglomerate is massive and shows predominant clast-supported texture (Fig. 2C). The sandy matrix is formed of very coarse to pebbly litharenite. Gravels are formed of lithoclasts and intraclasts; the lithoclasts (80%) range from granules to pebbles of rounded to well-rounded oligomictic clasts (quartzite, schist, gneiss),

Table 1
Summary of descriptions and interpretations of lithofacies.

Lithofacies	Code	Description	Interpretation
Massive conglomerate	Cm	Tabular layers (c. 0.5 m thick) of massive and clast-supported conglomerate with very coarse to pebbly lithoarenite matrix. Extraformational clasts (80%) are rounded to well-rounded, granules to pebbles; intraformational clasts (20%) are subangular to angular, pebbles to cobbles.	Gravel bars.
Sandy conglomerate	Cs	Tabular layers (c. 0.5 m thick) showing matrix-supported and normally graded pebbles. Extraformational clasts are subrounded to rounded; intraformational clasts are angular to subangular.	Rapid deposition from hyperconcentrated flows marked by transient turbulence.
Intraformational conglomerate	Ci	Lens-shaped layers (up to 1.5 m thick) of matrix-supported and poorly sorted intraformational conglomerate. Intraclasts are angular to subangular pebbles and cobbles (sandstone, mudstone and palaeosol fragments) and locally display poor normal grading.	Rapid deposition from hyperconcentrated flows fed from reworking of overbank material.
Conglomeratic sandstone	Sc	Tabular sandstone (2–3 m thick) organised in thinning and fining sets of planar and trough cross-stratifications showing bimodal grain size distribution.	Small transverse bars and sinuous and linguoid crested three-dimensional dunes with superimposed smaller bedforms.
Large-scale cross-bedded sandstone	Sl	Tabular sandstone organised in: (type A) lenticular sets of low-angle cross-strata (up to 15°) commonly marked by granule- to sand-sized mudstone aggregates; foresets show a slightly concave-up shape and taper towards the toeset; (type B) tabular sets of trough cross-beds showing fining- and thinning-upward with slightly inclined (<5°) set-bounding surfaces.	Large-scale transitional dunes formed by saturated high-velocity flows (type A); upstream-accretion bars (type B) formed by sinuous to linguoid-crested dunes.
Planar cross-bedded conglomeratic sandstone	Sp	Tabular sandstone (up to 1 m thick) organised in tabular sets (0.15–0.4 m thick) of planar cross-beds; sets show fining-upward trend from conglomeratic sandstone at the base towards medium- to fine-grained sandstone at the top.	Two-dimensional dunes formed on the axial scoured base of floodplain channels.
Cross-laminated fine sandstone	Sfc	Tabular layers (>0.3 m thick) arranged in lenticular sets (10–30 mm thick) of low-angle, tabular cross-laminated fine sandstone. The facies is composed of rounded to subrounded very fine sand, with silty matrix.	Ripples formed at low flow stage in floodplain channels
Planar-laminated fine sandstone	Sfp	Tabular layers (up to 0.6 m thick) of very fine-grained sandstone organised in laminae with bimodal grain size distribution in which laminae of fine-grained sand alternate with laminae of very fine-grained sand and silt.	Upper-stage plane beds formed during floodplain channel overflow.
Fine sandstone	Sf	Fine-grained sandstone organised in two geometries: (i) tabular layers (up to 0.5 m thick) displaying cross-laminations outlined by mud drapes; (ii) lenticular patches (up to 10 mm thick) of isolated single sets of cross-laminated sandstone encase by mudstone.	Mutually erosive climbing ripples formed during early stages of overbank flood.
Planar- to wrinkly-laminated claystone	Cl	Encountered between layers of the fine sandstone lithofacies in three forms: (i) horizontal to slightly sinuous laminae (up to 50 mm); (ii) laterally discontinuous wavy-crinkly laminae that internally show highly irregular mm-scale sand patches; (iii) flat-lying, planar to curved, flakes (up to 3 mm in thick and up to 50 mm long).	Periods of stagnant water formed by (i) settling of silt and clay particles on the climbing ripples; (ii) when associated with microbial activity, laminae assume wavy-crinkly geometry; (iii) the reworked microbial laminae are deposited as curved clay flakes.
Mudstone	M	Laterally discontinuous layers (up to 0.5 m thick) of massive mudstone that sharply overlie the large-scale cross-bedded sandstone.	Periods of stagnant water formed by settling of silt and clay particles on the large-scale cross-bedded sandstone, marking the abrupt cessation of the channelised flow.

whereas the intraclasts (20%) range from pebbles to cobbles of subangular fragments of mudstones and pedogenic nodules.

The conglomeratic sandstone (lithofacies Sc) erosively overlies the massive conglomerate and forms laterally continuous tabular layers (2–3 m thick). Internally, the sandstone is mostly organised in lenticular sets of trough cross-stratification with only few sets of planar cross-stratification localised at the base of the channel fill. In either case, the sets are made of either gravel or sandy gravel cross-strata. In addition, these sets are vertically arranged in a thinning- and fining-upward succession where they vary from 0.2 - 0.6 m thick at the base (Fig. 2A, D) to less than 0.2 m thick at the top (Fig. 2A, E). The boundary between each set is marked by a thin surface with aligned granules and pebbles. Overall, foresets show a unidirectional palaeocurrent trend towards WNW (mean vector = 340°; angle variation = 173°; n = 38) (Fig. 1F).

4.1.2. Interpretation

The overall fining- and thinning-upward trends of the channel fill indicate that channelised sedimentation occurred due to a gradual decrease in flow energy and depth that can be separated in two stages.

The first stage of in-channel sedimentation is represented by the massive conglomerate. The clast-supported texture is compatible with deposition from gravel bars at early stages of channel

development, as observed by Blair and McPherson (1994) for gravel beds of the proximal Rakaia River, New Zealand (see their Fig. 23A). In addition, the occluded framework of the conglomerate beds might indicate settling of finer sediments between gravel clasts (Smith, 1974). The second stage in channel hydraulics can be inferred from the overlying conglomeratic sandstone, which is representative of the prevailing hydraulic character of the channel. At the base, the limited presence of tabular sets of planar cross-beds most likely reflects the transition from the previous gravel bars to the emplacement of small transverse bars (Smith, 1972; Martinelli et al., 2019). The predominance of lenticular sets of cross-stratification suggests deposition from sinuous and linguoid crested three-dimensional dunes (Miall, 2006; Collinson and Mountney, 2019) during most of the episode of channel sedimentation. The overall thinning- and fining-upward organisation of the sets marks a progressive decrease in flow depth and energy (Bridge, 2006). In addition, the bimodal grain-size distribution of cross-strata suggests the migration of superimposed bedforms over dunes and/or small transverse bars (Reesink, 2019). In this case, the sandy gravel cross-strata are linked to the migration of superimposed small-scale asymmetrical bedforms. By contrast, gravel cross-strata are associated with superimposed coarser material concentrated into leeside scour pockets that were deposited from avalanching at the edge of dunes and/or bars (Smith, 1972; Lunt and Bridge, 2007).

Table 2
Summary description and interpretation of architectural elements.

Architectural element	Code	Lithofacies	Description	Interpretation
Permanent-flow main channel fill	CP	Massive conglomerate; conglomeratic sandstone	Sheet-like conglomeratic sandstone bodies (2–7 m thick and >110 m wide; w/t > 15) displaying erosive bottom and diffuse transition to palaeosols at the top. The channel fill records a fining-upward succession of massive clast-supported conglomerate at the base, overlain by tabular or trough cross-bedded pebbly sandstone; sets thin upward.	Large-scale channels characterised by flows that experienced a progressive decrease in flow energy and depth over time. Channel sedimentation initiates with the formation of gravel bars followed by the emplacement of small transverse bars and finally sinuous- and linguoid-crested three-dimensional dunes. The formative flows relate to humid climatic episodes.
Ephemeral-flow main channel fill	CE	Sandy conglomerate; large-scale cross-bedded sandstone	Sheet-like sandstone bodies (1.5–8.0 m thick and >110 m wide; w/t > 15) with lower flat erosive boundary and palaeosol at the top. The channel fill records two architectural types: (i) matrix-supported conglomerate at the base, overlain by large-scale, low-angle inclined lenticular cross-bedded sandstone (CE-A); and (ii) sets that thin upward and which contain scattered mudstone pebbles and cobbles (CE-B).	Large-scale channels characterised by flows that may have been initially hyperconcentrated, but which then evolved to either high-velocity, sediment-saturated flows in which transitional dunes formed (Price 1 site), or less energetic flows with high sedimentation rates as recorded by upstream accretion bars (BR050). The high-velocity, sediment-saturated flows are associated with dry climatic episodes.
Overbank deposit	OV	Fine sandstone; planar- to wrinkly-laminated claystone	Tabular layers (0.2–2.5 m thick and 4–110 m wide) with erosive bottom and top. Composed internally of fine sandstone (up to 0.5 m thick) and planar- to wrinkly-laminated claystone (up to 50 mm thick) arranged into alternating layers.	Overbank deposits that record floods from adjacent active channels. Wavy-crinkly laminations indicate probable microbial activity.
Floodplain channel fill	CF	Planar cross-bedded conglomeratic sandstone; cross-laminated fine sandstone; planar-laminated fine sandstone	Sheet-like bodies (1.0–1.4 m thick and >110 m wide; w/t > 15) with concave-up erosive bottom and depositional top boundary. There are 2 types of channel fill: (i) massive mudstone and (ii) fining-up sandstone characterised by an upward transition from cross-bedded conglomeratic sandstone, to cross-laminated and planar-laminated fine sandstone.	Floodplain channels that emanate from channel belts and occur isolated on the alluvial-plain surface; they are supplied with water and sediment from nearby large-scale active channels. Secondary channel fills located adjacent to major channel belts are dominantly sand-prone, whereas those located more distally from major channel belts are dominantly mud-prone.
Distal channel fill	CD	Intraformational conglomerate	Slightly asymmetric ribbon-like bodies (0.3–1.5 thick and <10 m wide; w/t < 7) that show single-storey fill formed of intraformational conglomerate facies with poorly developed normal grading. These bodies are commonly cemented by carbonate showing alpha-type fabrics.	Small-scale and laterally stable fixed channels with low-sinuosity or straight margins; they record deposition from single episodes of hyperconcentrated flows initiated as interchannel overland flows; they occur encased in interchannel elements, indicating that avulsion was a recurrent mechanism of channelisation. Calcretisation is associated with post-depositional near-surface phreatic cementation.

Together, the transition from closed-framework gravel bars to sandy transverse bars and three-dimensional dunes is likely indicative of perennial channel flow experiencing very gradual waning conditions (Colombera and Mountney, 2019).

4.2. Ephemeral-flow main channel fill

4.2.1. Description

This channel fill (architectural element CE) occurs as sheet-like bodies (1.5–8.0 m thick) that extend laterally for more than 110 m (width: thickness ratio > 15) oblique to palaeoflow (Figs. 3, 4). The lower boundary is erosional whereas the upper boundary is marked by a gradual transition to palaeosols. The facies association of this element is typically composed of two facies arranged in a fining-upward trend, from the base to the top: (i) sandy conglomerate, (ii) large-scale cross-bedded sandstone, and (iii) mudstone.

The sandy conglomerate facies (lithofacies Cs) (Fig. 3C) occurs locally at the base of this architectural element. It appears as a tabular layer that extends laterally up to 15 m and vertically up to 0.5 m thick. The lower boundary is irregular to undulating, whereas the upper boundary is defined by the erosive base of the overlying large-scale cross-bedded sandstone sets. Pebbles show a normal grade distribution and are matrix-supported. The matrix is formed of very-coarse to medium sublitharenite. Lithoclast pebbles are formed of subrounded to rounded clasts of quartz, chalcedony and gneiss whereas intraclast pebbles are formed of angular to subangular clasts of mudstone and pedorelicts. The transition from the sandy conglomerate to the uppermost large-scale cross-bedded sandstone is gradual. The large-scale cross-bedded

sandstone (lithofacies Sl) (Figs. 3, 4) composes more than 70% of the ephemeral-flow channel element, appearing as laterally extensive tabular layers (1.4–7.5 m thick) marked by erosive bases.

Two different types of internal architecture are observed in the ephemeral-flow main channel fills. The Type A architecture (observed in the Price 1 site; Fig. 3A, B) is organised in sets showing lenticular geometry. Internally, the sets show low-angle cross-strata (up to 15°) commonly marked by granule- to sand-sized mudstone aggregates. The foresets show a slightly concave-up shape and are marked by extended toeset. Type B architectures (observed at the BR050-Km-153 site; Fig. 4) are organised in tabular sets of trough cross-beds varying in thickness from 1.4 m at the base to 0.1 m at the top. Sets are arranged into cosets and show a thinning- and fining-upward trend. In places, set-bounding surfaces are slightly inclined (<5°) towards southwest, whereas foresets within sets indicate a unidirectional northwest palaeocurrent trend (Fig. 1F). Foresets are traced laterally for up to 5 m, with scattered mudstone intraclasts distributed along the cross-strata. The base of cosets is erosive and displays lags of massive angular mud blocks (up to 1.3 m in length) that are organised internally in subangular blocky peds (Fig. 4). The top of the cosets is bounded by scoop-shaped erosive surfaces with a symmetrical profile; they resemble scoop-shaped scours varying in size from 1 - 2 m deep and 5 to more than 10 m long. This surface is overlain by trough cross-strata dipping radially into the deepest part of the scour. Foresets at the upstream slope are steeper than at the downdip slope (Fig. 4). The sandstone is composed of medium to coarse sand, poorly to moderately sorted, with subangular to subrounded grains. The matrix is composed of fine to very fine sand. Finally, the ephemeral-flow main channel fill is bounded by a laterally discontinuous layer (up to 0.5 m thick) of massive mudstone (lithofacies M).
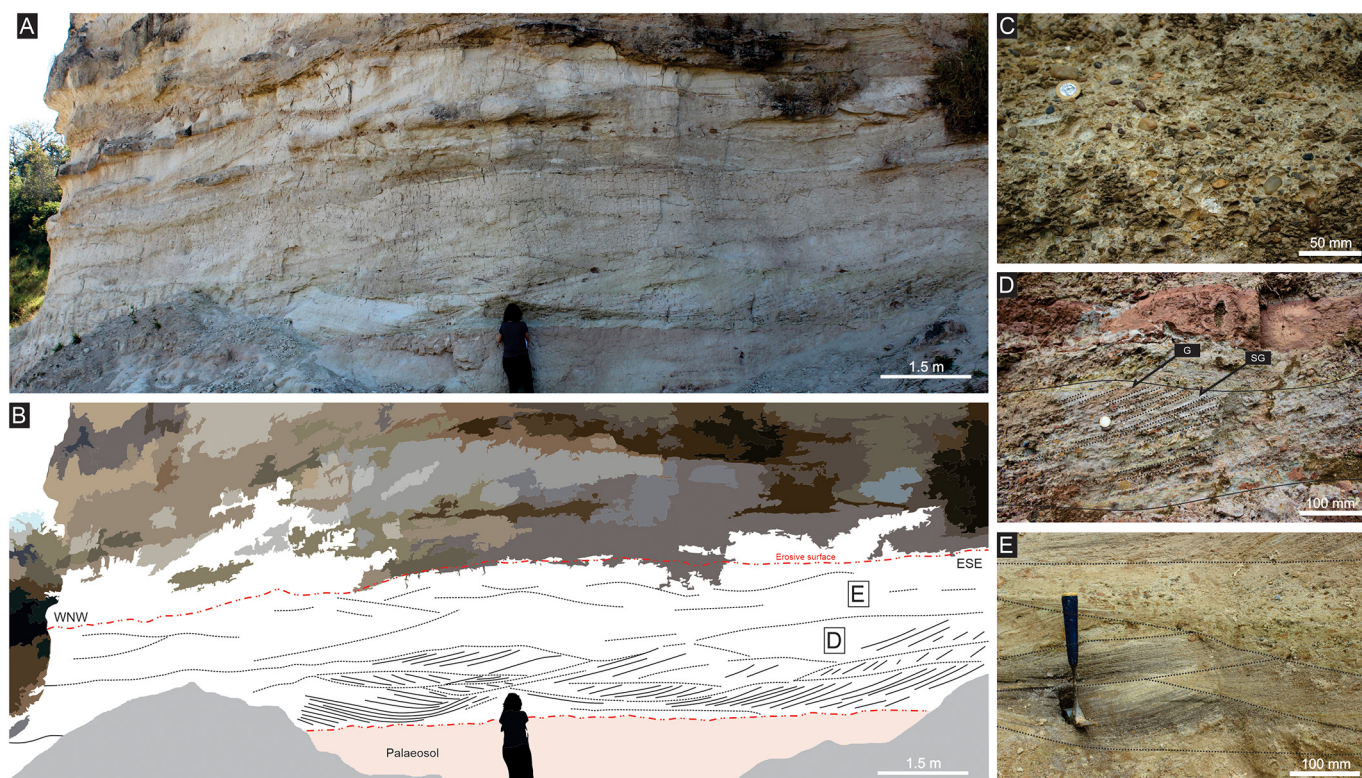
Fig. 2. (A) Outcrop view in the Price 1 site and (B) architectural sketch of the perennial-flow main channel fill. (C) Massive conglomerate showing clast-supported arrangement of clasts. (D) Conglomeratic sandstone at the base of the channel fill arranged in larger sets of cross-stratifications showing cross-beds with bimodal grain-size distribution between gravel [G] and sandy gravel [SG] strata. (E) Thin trough cross-stratified sets of the conglomeratic sandstone occupying the top of the channel fill.
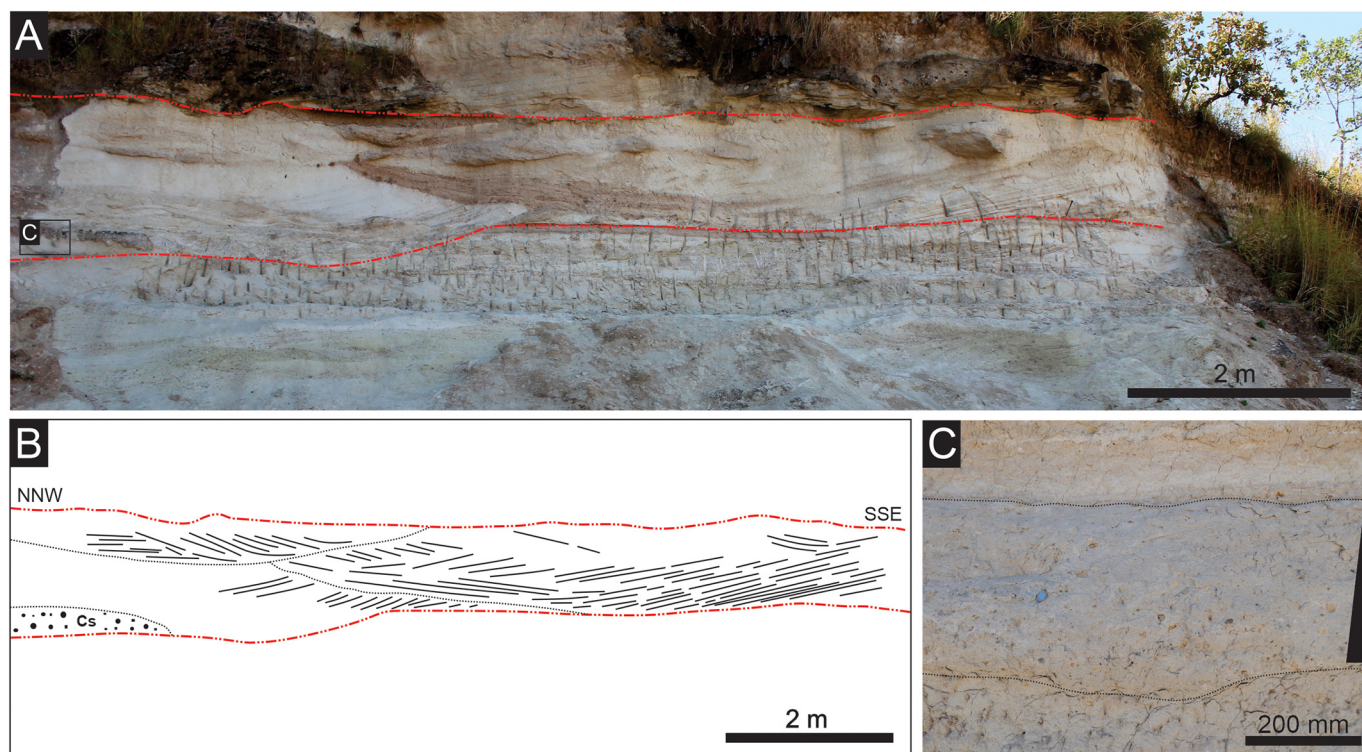

Fig. 3. (A) Outcrop extension and (B) architectural sketch of the ephemeral-flow main channel fill in the Price 1 site (Fig. 1D). The sandstone is arranged in lenticular sets showing cross-strata with foreset angles less than 15° and scattered mudstone intraclasts along concave-up foresets that taper towards the toeset. (C) The sandy conglomerate at the base of the channel fill showing normal grading and matrix-supported arrangement of clasts.
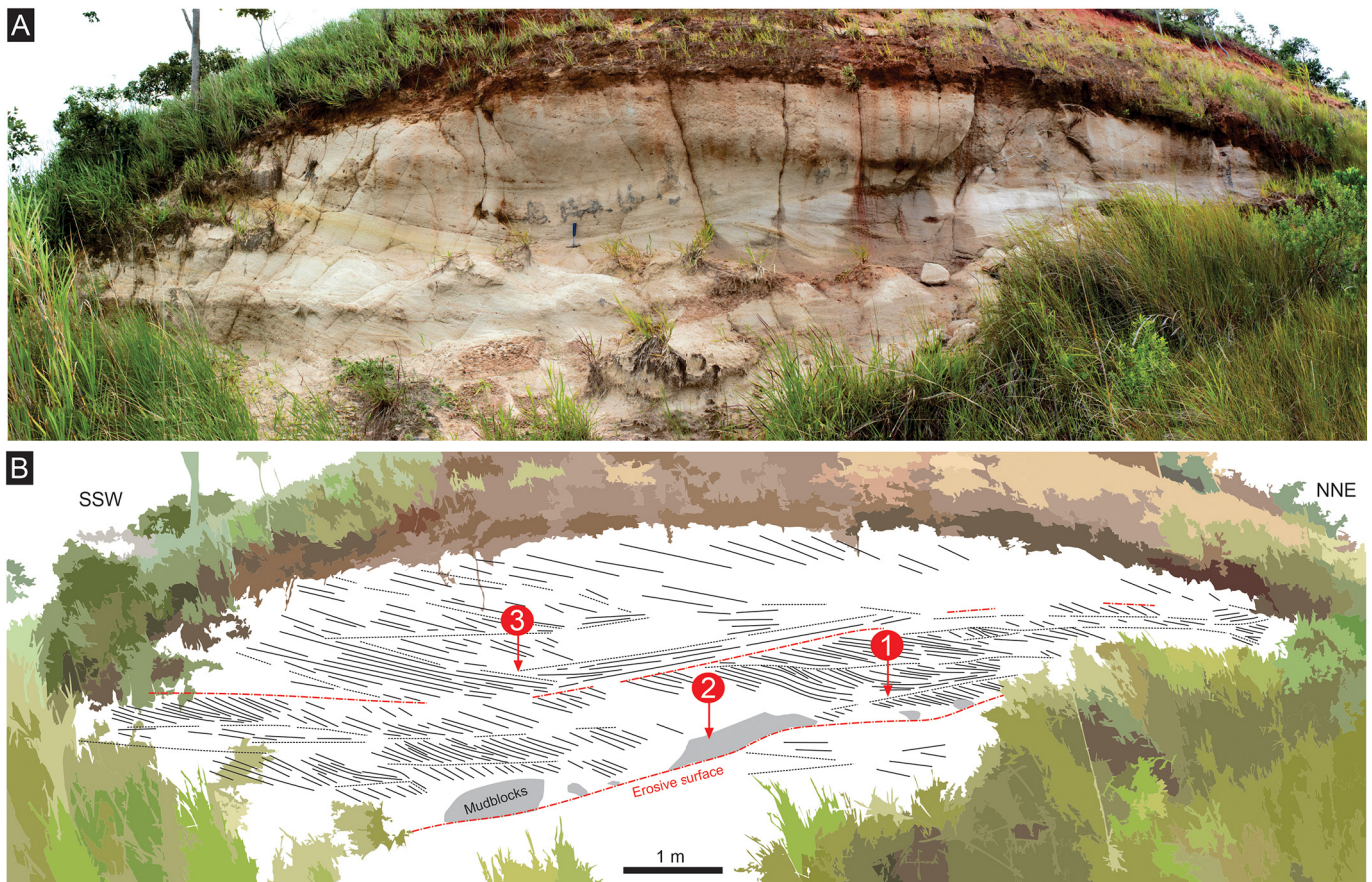
Fig. 4. (A) Outcrop extension of the ephemeral-flow main channel fill and (B) sketch of the internal architecture of the channel fill in BR50-Km-153 site (Fig. 1D). Channel fills show tabular sets of trough cross-beds forming cosets that display thinning- and fining-upward; limits of sets are slightly inclined downstream [1] and mud-blocks are observed at the base of the channel fills [2]. Detail of the trough cross-strata dipping radially into the deepest part of the scour at the top of channel fill [3].

4.2.2. Interpretation

The depositional history of the ephemeral-flow channel corresponds to episodes of high-energy, prevalently transcritical and supersaturated flows. Deposition is first initiated by hyperconcentrated flows. The structureless character of the conglomerate indicates rapid deposition during which organisation of clasts was not achieved. The erosive base and the crude normal grading indicate transient turbulence acting as a secondary mechanism, forcing coarser and denser clasts to settle from suspension (Nemec and Steel, 1984).

At the Price 1 site (Fig. 3), Soares et al. (2018) have interpreted the type A large-scale cross-bedded sandstone as products of large-scale transitional dunes by virtue of (i) their low-angle, (ii) asymptotic, and (ii) concave-up foresets, which suggest flows saturated in material transported under suspension at high velocities over transitional dunes (sensu Chakraborty and Bose, 1992). Type A deposits record strengthening of the current from dune to upper-stage plane bed stability fields. Under these conditions, the dune profile undergoes morphological changes, progressively lowering the leeside angle because deposition from suspension overcomes deposition from avalanching (Jopling, 1965). The ubiquitous sand-sized mudstone intraclasts further demonstrate the erosive character of flows affecting the floodplain areas. The ubiquitous presence of sand-sized mudstone aggregates in fluvial deposits is attributed to the washing out of deeply cracked floodplain soils during dry periods, a process that is recognised in both modern and ancient fluvial systems (Rust and Nanson, 1989; Ekes, 1993; Gierlowski-Kordesch and Gibling, 2002; Wright and Marriott, 2007; Dasgupta et al., 2017; Simon and Gibling, 2017; Li et al., 2020). Mud-aggregate texture similar to that described here has been recognised in clay-rich soils by Fitzpatrick (1983). Experiments

conducted by McIntyre (1976) showed how clay-rich soils quickly slake into sand-sized aggregates when immersed in water. The presence of clay-rich palaeosols in the Serra da Galga Formation (see Section 5.3) further supports the interpretation of a pedogenic origin for the mudstone aggregates.

At the BR050-Km-153 site (Fig. 4), however, the type B ephemeral-flow main channel fill is organised differently and indicates deposition from less energetic currents in upstream-accretion bars. The coset arrangements into thinning- and fining-upward sets of trough cross-beds record the progressive filling of the channel, from large-scale sinuous- to linguoid-crested dunes at the bottom, becoming progressively smaller towards the top of the channel (cf., Miall, 2006). The upstream-dipping erosive surfaces that delimit the cosets and cut the set boundaries with a higher upstream-dipping angle suggest upstream-facing accretion surfaces in fluvial bars. These surfaces further demonstrate the multi-storey character of the history of infill of the channel, a probable consequence of recurrent oscillations in the water level (Miall, 2006). The cross-strata that fill the scoop-shaped erosive surface at the top of the fluvial bars, demonstrating foresets dipping towards the centre, could be associated with the bar-top hollows described by Best et al. (2006), because: (i) they occupy the top surface of the bars; (ii) they show inward filling of the scour; (iii) the upstream slope is higher than the downstream slope; and (iv) the hollow profile is approximately symmetrical. In this case, because hollows occur on the upstream accretion surface, it appears that the formation of bar-top hollows develops from bar-head accretion according to the mechanism proposed by Best et al. (2006; see their Fig. 8C), whereby an accretionary unit bar merges with a bar-head and encloses a trough area in between the two bars. The presence of mud-blocks at the base of the cosets has been previously

interpreted as riverbank collapse assisted by formation of deeply incised desiccation cracks during periods of falling water level (cf., Gibling and Rust, 1984). These blocks can survive disaggregation when quickly buried on channel floors when the sedimentation rate is high (e.g., Klimek, 1974). Similar to the sand-sized mud aggregates, the mud blocks also show pedogenic origin by their internal organisation in subangular blocky peds. The gradual transition from the lowermost conglomerate to the uppermost sandstone reveals that deposition occurred during a single and continuous episode. Finally, the abrupt burial of the sandstones by mudstones further indicates the sudden abandonment of the channel system.

4.3. Overbank deposits

4.3.1. Description

The overbank deposits (architectural element OV) commonly occur as eroded tabular units placed between the perennial- and ephemeral-flow channel fills (Fig. 5). The lower boundaries are flat whereas the top are erosive. The lateral extent of this element is highly variable (4–110 m), as so the thickness (0.2–2.5 m). The overbank deposits are organised in a series of repeated cm-scale alternations between fine sandstone and planar- to wrinkly-laminated claystone.

The fine sandstone facies (lithofacies Sf) (Fig. 5A, B) corresponds to the majority of the overbank deposits. It occurs as either (i) tabular layers that laterally overcomes the outcrop extension (more than 110 m) and are up to 0.5 m in thickness (Fig. 5A-i), or (ii) lenticular bodies that extend from 10 to 100 mm laterally and up to 10 mm vertically (Fig. 5A-ii). The tabular layers have erosive bases, and are organised in lenticular sets that internally show cross-laminations outlined by mud drapes. The lenticular patches of fine sandstone occur encased by claystone, as isolated single sets of cross-laminated sandstone that preserve bedform morphology, showing non-erosive, planar bases and asymmetrical undulatory tops. The dip angles of foresets vary from 6° to 20°. The sandstone is composed of immature, poorly to moderately sorted, subangular to subrounded sand.

Laminated claystone (lithofacies Cl) is encountered between the layers of fine sandstone (Fig. 5A). The clay laminae form beds up to 50 mm thick that are laterally traceable up to 10 m. They conformably drape the tabular and lenticular fine sandstone. Laminations occur as: (i) horizontal to slightly sinuous laminae that are usually thicker (up to 50 mm) and flat and that display internally asymmetrical lenticular patches of fine sandstone (Fig. 5A-iii); (ii) wavy-crinkly laminae that are more discontinuous laterally, and internally show highly irregular, millimetre-scale, structureless sand patches (Fig. 5B-iv); and (iii) flat-lying, planar to curved, flakes that occur isolated in the fine sandstone, up to 3 mm in thickness and up to 50 mm long (Fig. 5A-v). In thin section, both the wavy-crinkly laminae and the clay flakes reveal floating grains of medium to fine, subangular to subrounded sand (Fig. 5C).

4.3.2. Interpretation

The marked textural variations encountered in the overbank deposits are associated with flow oscillations, marked by two distinct phases. The first corresponds to the incursion of flood waters across the floodplain surface. Sediment was most likely sourced from nearby active channels. Sedimentation begins with the accumulation of ripple strata, for which ripple forms do not preserve their stoss side ('mutually erosive climbing ripples' sensu Jopling and Walker, 1968), indicating that suspension fall out was not rapid enough to bury moving grains, preventing preservation of stoss-side laminations. The presence of interlaminated clay in between foresets attests pauses in ripple migration during phases of water stagnation, or associated with the slow return of flood waters back to the active channels during falling water stages (Miall, 2006). The second phase of sedimentation corresponds to periods of stagnant water. At this stage, sedimentation operates predominantly by settling of silt and clay particles, forming a blanket of muddy material on top of the previous sandy substrate (horizontal to slightly sinuous laminae), assuming its original even
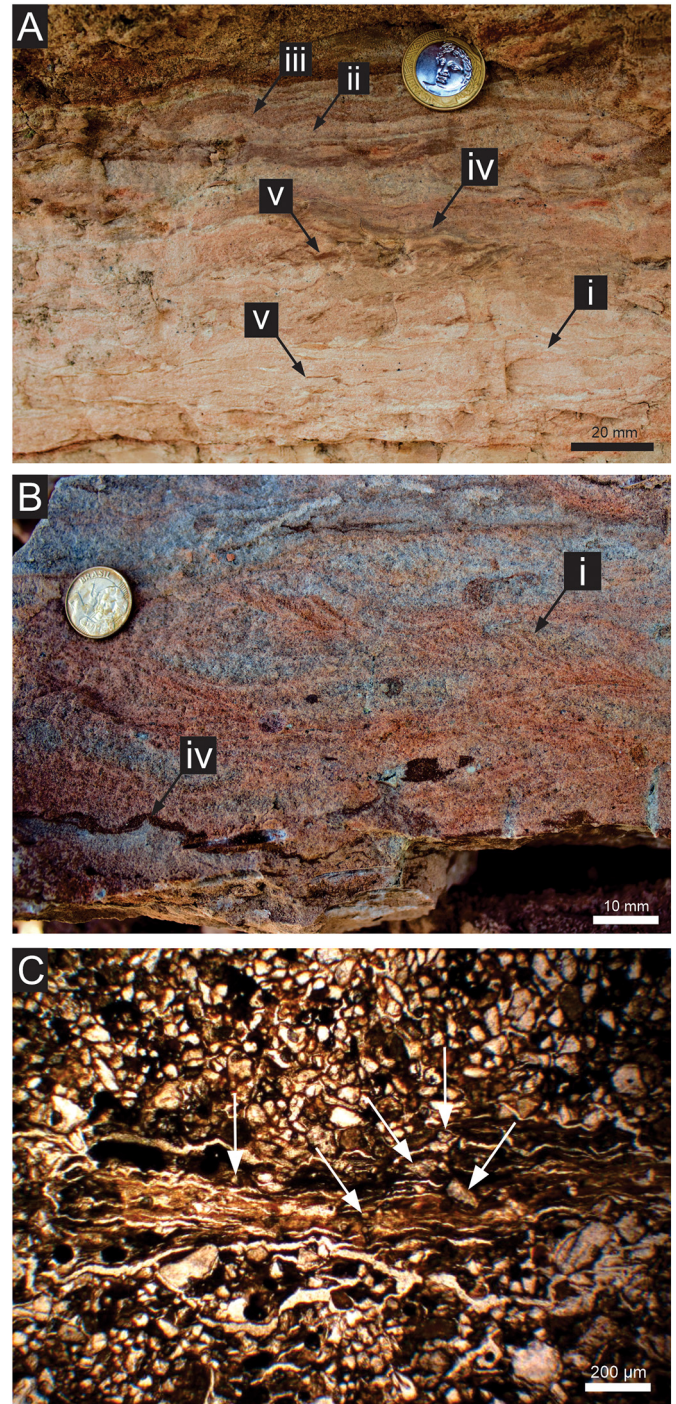

Fig. 5. (A) Overbank deposits architectural element showing repeated alternations between the fine sandstone facies as [i] tabular layers and [ii] lenticular patches and the laminated clay presented as [iii] horizontal to slightly sinuous laminae, [iv] wavy-crinkly laminated clay and [v] flat-lying planar to curved isolated flakes. (B) Detail to the internal organisation of the tabular fine sandstone as lenticular sets of cross-laminations [i] and the presence of [iv] wavy-crinkly laminated clay. (C) XPL photomicrography of wavy-crinkly laminae displaying floating grains of medium to fine, subangular to subrounded sand. [XPL = cross-polarised light].

geometry (Miall, 2006). The wavy-crinkly laminations might be indicative of microbial activity (Schieber, 1998). The biological origin can be further inferred from the cohesive character of the material during erosion, transport and deposition. Laminae at the margin of sandy patches that are steeper than the angle of repose might indicate the binding of sediments by microbial mats (Schieber, 1999; Ulmer-Scholle et al., 2015). When microbial mats are subaerially exposed, they might dry out, crack and curl up.

Subsequently, when flood waters return to the floodplain surface, the curved fragments of sandy-clay laminae are transported and deposited as single entities, their deposits being widespread across rippled surfaces. In this case, the presence of curved clay flakes holding abundant sand grains at angles higher than the angle of repose can attest for the cohesive nature of the microbial mats similarly found in the wavy-crinkly laminae (Gill, 1977; Schieber, 1999). The four-stage cycle of (1) clay settling, (2) microbial-mat colonisation, (3) exposure, and (4) reworking and redeposition, likely occurred repeatedly in the floodplain areas of the Serra da Galga Formation, as demonstrated by the fine-scale alternations in textural character in this architectural element.

4.4. Floodplain channel fill

4.4.1. Description

This channel fill (architectural element CF) occurs as sheet-like depositional bodies (1.0–1.4 m thick) that are laterally continuous for at least 110 m (width:thickness ratio > 15) and occur interlayered with overbank deposits (Fig. 6). The lower boundary is characterised by a slightly concave-up erosive surface, whereas the upper boundary is sharp and planar horizontal. Two types of floodplain channel fills are observed. The first, and rarer type, is filled exclusively by massive mudstone facies (lithofacies M) (Fig. 6A). The second, more abundant, exhibits a fining-upward sequence with a combination of three facies, from base to top: (i) planar cross-bedded conglomeratic sandstone, (ii) cross-laminated fine sandstone, and (iii) planar-laminated fine sandstone (Fig. 6B). The planar cross-bedded conglomeratic sandstone (lithofacies Sp) (Fig. 6C) appears as laterally continuous tabular layers (0.4–1.0 m thick) overlying the erosive bases of the floodplain channels. This facies is organised in tabular sets (0.15–0.4 m thick) of planar cross-beds with foresets dip angles of 20°–25°. Sets are organised in a fining-upward trend, varying from conglomeratic sandstone at the base towards medium- to fine-grained sandstone at the top. The gravel fraction (granules to fine-grained pebbles) is composed predominantly of intraclasts of angular to subangular mudstone and carbonate cemented sandstone, whereas lithoclasts show rather rounded to subrounded textures. The sandstone is composed of immature, very coarse- to medium-grained, subangular to subrounded sand and silt. The cross-laminated fine sandstone facies (lithofacies Sfc) (Fig. 6D) occurs as laterally continuous tabular layers (>0.3 m thick) and is arranged in lenticular sets (10–30 mm thick) of low-angle, tabular cross-laminated fine sandstone. The facies is composed of rounded to subrounded very-fine sand and silt. The planar-laminated fine sandstone facies (lithofacies Sfp) (Fig. 6E) is composed of laterally
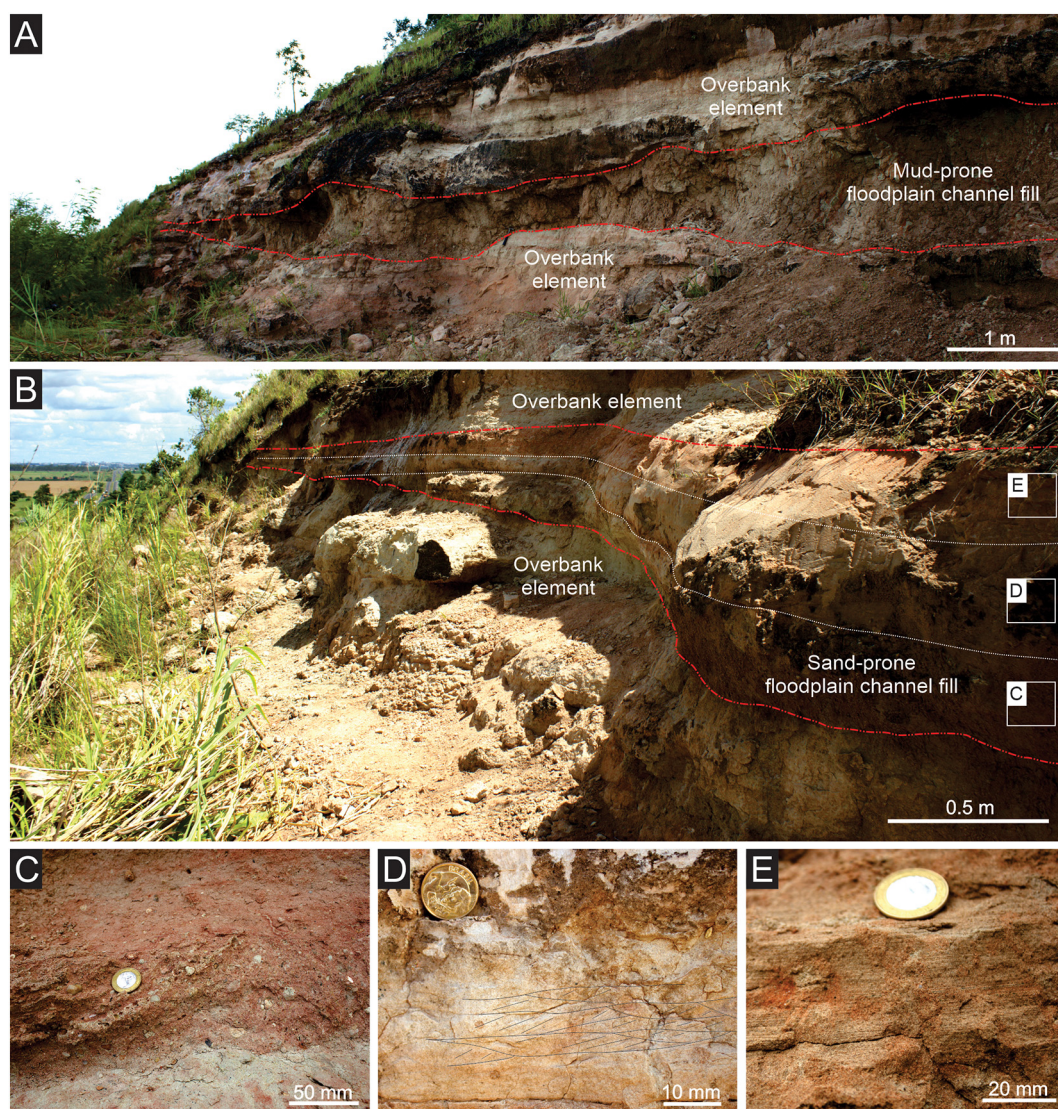

Fig. 6. Floodplain channel fill architectural element. (A) Mud-prone fill showing concave-up erosive base and horizontal irregular top; notice the lateral thinning of the channel fill. (B) Sand-prone fill formed of a superposition of (C) planar cross-bedded conglomeratic sandstone, (D) cross-laminated fine-grained sandstone and (E) planar-laminated fine-grained sandstone.

continuous tabular layers (up to 0.6 m thick) showing erosive bases and sharp horizontal tops. The sediment is composed of rounded to subrounded, very fine-grained sand, with a silty matrix. This facies is organised in subhorizontal and submillimetric laminae (a few grain diameters) that display bimodal grain-size distribution where a lamina of fine-grained sand is overlaid by a lamina of very fine-grained sand and silt; the boundary between the laminae is sharp.

4.4.2. Interpretation

The stratigraphic arrangement of the floodplain channel fills, as small-scale sheet-like bodies embedded in overbank deposits, demonstrates that they correspond to isolated scoured features on the floodplain surface. Sedimentation started on the axial scoured base of the channel with the planar cross-bedded conglomeratic sandstone as a result of deposition from small-scale two-dimensional dunes. Subsequently, ripples were formed (cross-laminated fine sandstone), indicating a decrease in flow energy, depth and capacity (Jopling and Walker, 1968). The planar-laminations that overlie the ripple cross-laminations are interpreted as upper-stage plane beds based on the following criteria: (i) range of fine- to very fine-grained sand, (ii) submillimetric lamina thickness, (iii) sharp lamina boundaries and (iv) subhorizontal lamination (Paola et al., 1989; Fielding, 2006). Therefore, an increase in flow energy took place during the filling of the upper portion of the channel form, probably as a consequence of the decrease in the cross-sectional area of the flow in parallel with a decrease in flow depth and increase in flow velocity. Observations of (i) poorly channelised tabular bodies with (ii) fining-upward trend, followed by an (iii) upward reversion of flow energy, may be indicative of sand-prone channels on the floodplain surface that were occupied by floods from nearby main active channels (perennial- and ephemeral-flow channels) that exceeded their flow capacity (Nichols and Fisher, 2007). Conversely, the mud-prone channel fills are inferred to have occupied a more distal position on the floodplain surface where the supply of water and bedload from the main active channels was limited; in this case, sediment was likely supplied via suspended load, probably leading to their clay-rich infill (Burns et al., 2017, 2019). Because the existence of these floodplain channels depended on hydraulic connection with the main river channels, they probably did not extend for great distances laterally on the floodplain.

4.5. Distal channel fill

4.5.1. Description

This type of channel fill (architectural element CD) occurs as slightly asymmetric ribbon-like bodies (0.3–1.5 thick) that are laterally traceable for up to 10 m along-strike (width:thickness ratio < 7); the orientation of ribbon axes indicates palaeoflow towards WNW (Figs. 1F, 7A). The lower boundary is erosive and concave-up, whereas the top is flat and displays a sharp depositional contact with overlying overbank deposits and/or diffuse transition to palaeosol profiles (Fig. 7A, B). Internally, these ribbon-like bodies are filled solely by intraformational conglomerates (lithofacies Ci); the conglomerate is matrix-supported and poorly sorted (Fig. 7B); up to 90% of gravels are angular to subangular intraclast pebbles and cobbles (sandstone, mudstone and palaeosol fragments; Fig. 7C-1), with only a minor amount of rounded to well-rounded lithoclast granules and pebbles (quartz, chalcedony and gneiss; Fig. 7C-2). These gravels occur dispersed in very-fine to pebbly litharenite matrix and locally demonstrate poorly developed normal grading (Fig. 7B). Additionally, the distal channel fills commonly appear cemented by carbonate; calcite-filled cracks (crystallaria sensu Wright and Tucker, 1991) are observed as subhorizontal and interconnected planes (Fig. 7B); gravels display fractures (up to 2 mm thick) filled by micritic calcite groundmass with floating-grain fabric (Fig. 7D) and are commonly outlined by circum-granular crystallaria features composed of microsparitic to sparitic calcite infill (Fig. 7C-1). In thin section, the litharenite matrix further demonstrates micritic groundmass where

sand grains show microfractures (Fig. 7D-1) and outer rims of micritic to microsparitic calcite (Fig. 7D-2).

4.5.2. Interpretation

The ribbon geometry of these bodies and their single-storey infill make them relatable to the simple distal channel class of Friend et al. (1979). The slightly asymmetric profile of these channel fills is usually considered to represent deposition in laterally stable fixed channels (Gibling, 2006) associated with low sinuosity (cf. Jobe et al., 2010) or straight planforms (Bridge, 2003). The massive conglomeratic deposits encountered in these channel fills indicate rapid deposition from high-energy flows that inhibited any internal organisation of sediments (Costa, 1988; Cain and Mountney, 2009; Banham and Mountney, 2014); their poorly developed normal grading and matrix support suggest origin from hyperconcentrated flows that experienced transient turbulence (Nemec and Steel, 1984). The erosional juxtaposition of distal channels on overbank deposits and palaeosols, combined with their inferred lateral stability, suggests that channelisation initiated from avulsion episodes (Khadkikar et al., 1998). The abundance of intraclasts further corroborates the hypothesis that flows traversed overbank areas where erosion was probably facilitated by the non-cohesive nature of the floodplain surface (Gómez-Gras and Alonso-Zarza, 2003). Finally, the carbonate features commonly observed in distal channel fills correspond exclusively to alpha-type carbonate microstructures (sensu Wright, 1990), which are linked to abiotic genesis. The predominant floating-grain texture indicates a displacive and replacive carbonate growth from the evaporation of moisture infiltrated in the pores of sediments (Wright and Tucker, 1991). The suite of alpha-fabrics identified in these bodies can be related to different stages of calcretisation; the micritic calcite forming rims around sediments demonstrate that cementation formed firstly at grain contacts; afterwards, with intensification of pores saturation, the displacive growth forced grains contacts to form microfractures, ultimately progressing to the stage of forming large cracks (Buczynski and Chafetz, 1987). These abiotic mechanisms of carbonate growth are probably related to post-depositional phreatic cementation from carbonate-saturated groundwater in the capillary fringe of shallow groundwater and could be caused by climatically controlled mechanisms (e.g. evaporation and evapotranspiration) (Mann and Horwitz, 1979; Netterberg, 1969; Pimentel et al., 1996; Wright and Tucker, 1991).

5. Palaeosols

Palaeosol profiles are associated with all the previously described architectural elements. Their total thickness varies from c. 28% among channel fill successions up to c. 92% in overbank successions. The studied palaeosols are organised in five main pedotypes: (I) Inceptisols type 1, (II) Inceptisols type 2, (III) Entisols, (IV) Vertisols type 1 and (V) Vertisols type 2. The description and interpretation of pedotypes are presented below (see Supplementary material 2 for glossary on descriptive terms).

5.1. Inceptisols

The parent material of the Inceptisols consists of sediments associated with the following architectural-element types: (i) perennial-flow main channel fill, (ii) ephemeral-flow main channel fill and (iii) floodplain channel fill. These palaeosols form 1–2 m thick profiles. A total of 14 Inceptisol profiles were distinguished in two pedotypes, based on their distinct sequences of horizons: A-Bw-Bk-C(k) and Ag-Bwg, respectively. They are described and interpreted below.

5.1.1. Inceptisol type 1: A-Bw-Bk-C(k)

5.1.1.1. Description. The first Inceptisol type (Fig. 8A) is characterised by a pinkish colour (7.5YR 7/3). The parent material is formed by the
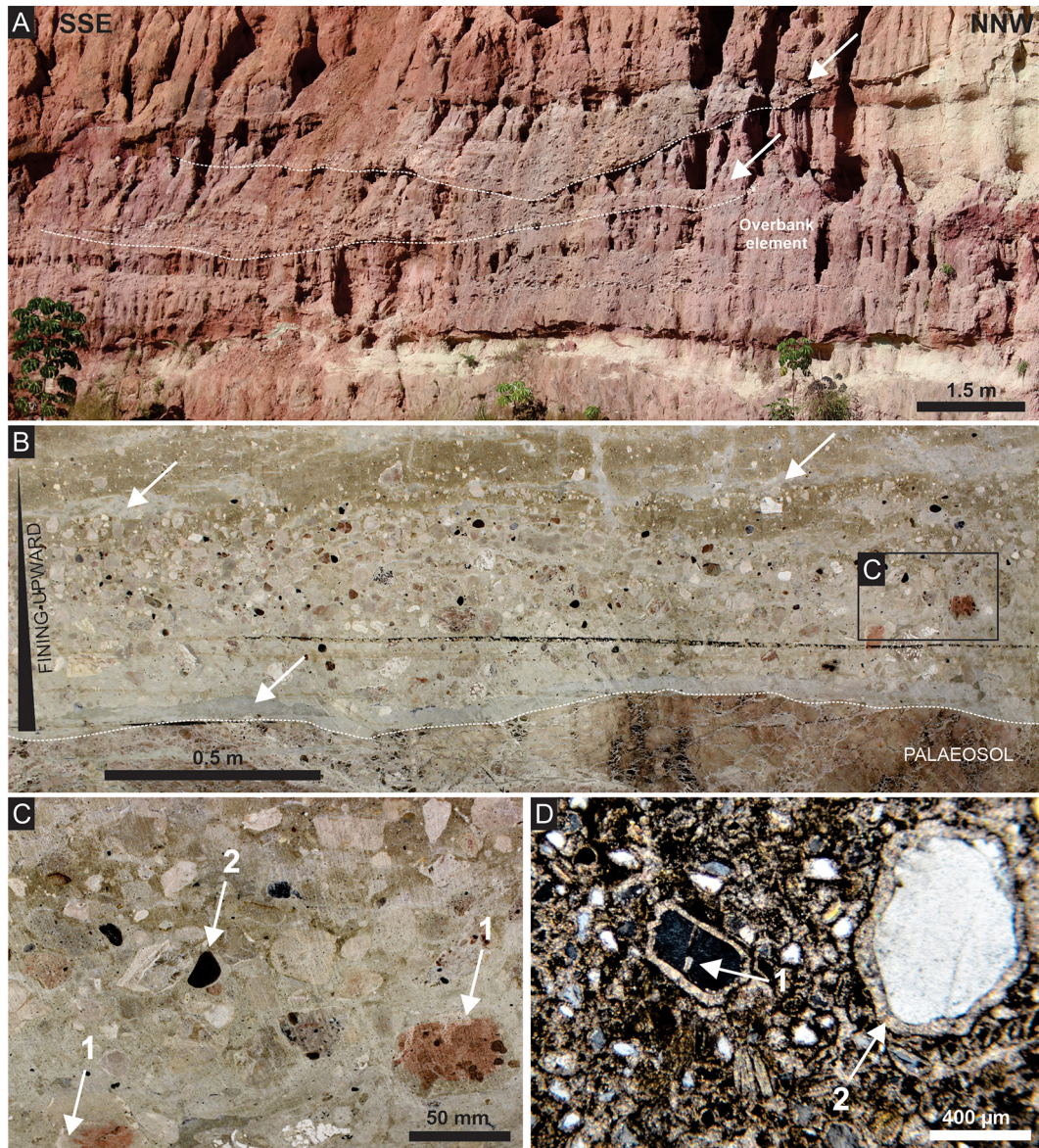
Fig. 7. Distal channel fill architectural element. (A) Ribbon-like channel bodies emplaced among overbank deposits with concave-up erosive bottom (dashed line) and flat and sharp depositional top (arrows). (B) Intraformational conglomerate displaying matrix-supported texture with gravels that exhibit weakly developed normal grading. (C) Angular to subangular intraclasts showing outer rims of invasive carbonate cementation (1) and scarce rounded to subrounded lithoclasts (2). (D) Photomicrography in XPL of the sandy matrix depicting micritic calcite filling microfractures (1) and outlining (2) sand grains.

perennial-, ephemeral-flow and floodplain channel fills. The A horizon is rarely observed; when present, it is associated with profiles developed over the floodplain channel fills, and it is thin (up to 0.4 m thick), whitish pink (7.5YR 7/3) and formed of muddy sand. This horizon further displays drab haloed root traces that branches and tapers vertically and horizontally (Fig. 8B); their drab-haloed fringes are marked by an inward diffuse colour transition from pink (7.5YR 7/3) to white (7.5YR 9.5/1). At places, the central part of root traces exhibit tubules (1–4 mm thick) of massive sparry calcite (Fig. 8C). In thin section, the A horizon demonstrates single-grain microstructure where sand-sized grains show little or no fine material in intergranular spaces (coarse monic c/f related distribution pattern) forming simple packing voids. Finally, the A horizon is marked by a diffuse and smooth transition with the underlying B horizon.

The B horizon is 0.3 to 1.2 m thick and organised into an uppermost cambic (Bw) and a lowermost calcic (Bk) horizons; their colours vary from pink (7.5YR 7/3) to light pink (7.5YR 8/3); the B horizon is formed of sand to muddy sand. The uppermost cambic

(Bw) horizon is marked by very coarse and weakly developed platy structures that are outlined by laminar sparry calcite. These laminae are horizontal to subhorizontal, submillimetric and are laterally interconnected, crossing each other at angles of 60–120°, locally forming flat and lenticular structures (Fig. 8D); they are laterally continuous for no more than 0.2 m and show discrete drab haloes (up to 3 mm thick) that vary inwards from pink (7.5YR 7/3) to white (7.5YR 9.5/1). In plan view, the sparry calcite laminae display a smooth and homogeneous surface, whereas in cross-section they demonstrate sharp and irregular contact with detrital grains. The laminar sparry calcite is also encountered in the underlying Bk horizon. Bioturbation in the Bw horizon shows weak or absent carbonate cementation; bioturbation takes the form of tubular structures (up to 0.1 m long and 5–20 mm in diameter) that are vertical to subvertical (up to 10°), filled with medium to fine sandstone and mudstone, and show drab haloes; when coalesced, this bioturbation is of irregular form, up to 0.25 m wide and 0.15 m thick (Fig. 8E). In thin section, the Bw horizon appears similar to the A horizon;
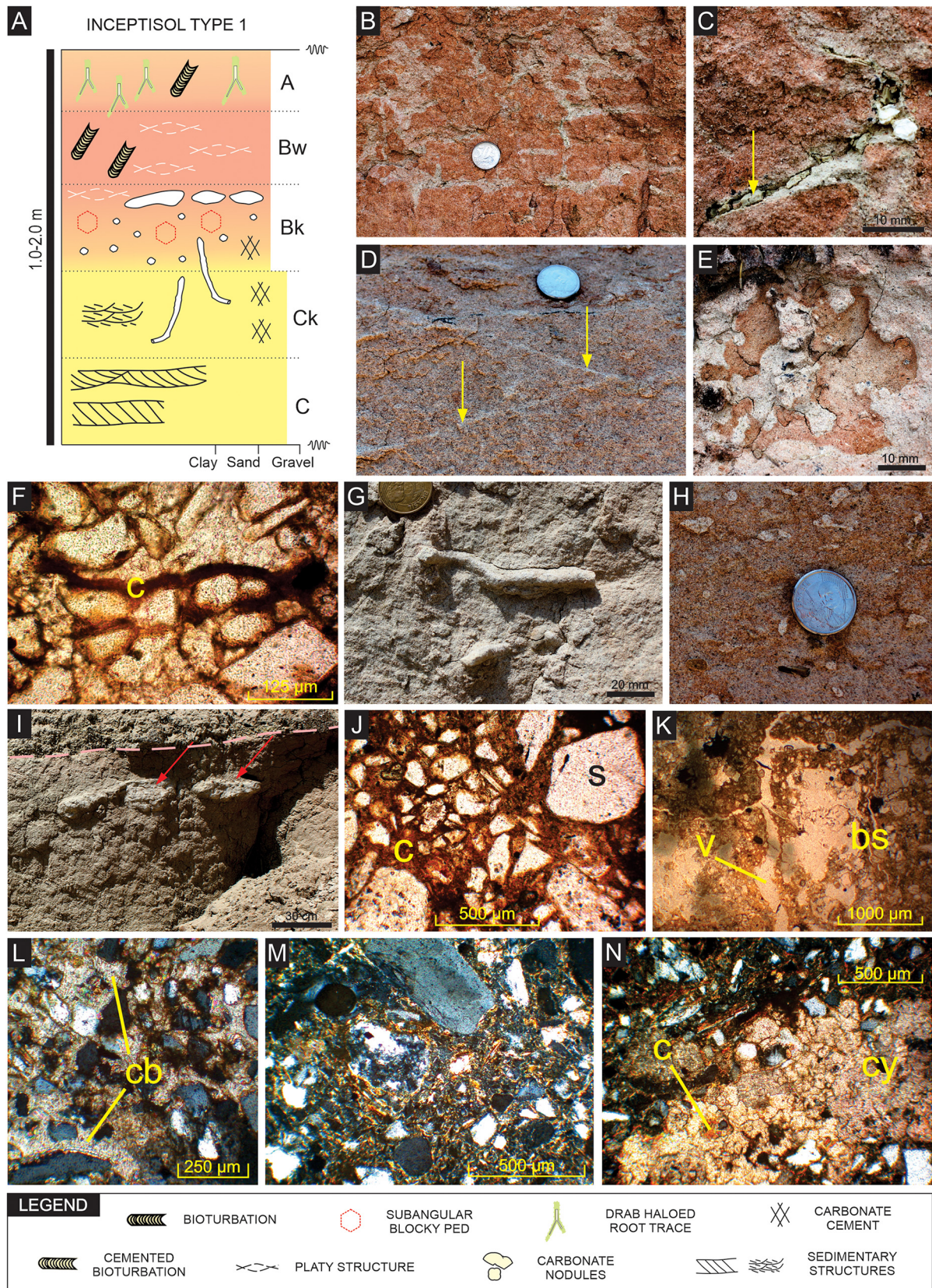
Fig. 8. Summary features of Inceptisols type 1. (A) Synthetic profile of the Inceptisol type 1. (B) Vertical rhizohaloes with laterally horizontal branching. (C) Root trace marked by mm-scale tubules of sparry calcite in its centre. (D) Weakly developed platy structures outlined by subhorizontal laminar calcite. (E) Coalescent bioturbation marks displaying irregular forms. (F) Photomicrography in PPL of Bw horizon showing pellicular grain microstructure where clay [c] outlines sand grains. (G) Rhizotubule cemented by calcium carbonate. (H) Isolated subspheric nodules of calcium carbonate in Bk horizon. (I) Carbonate lenses near the erosive top of the Inceptisol profile. (J) Close porphyric c/f related distribution pattern in Bk horizon displaying sand grains [s] interspersed in clay groundmass [c] (PPL). (K) Subangular blocky microstructure [bs] separated by planar voids [v] (PPL). (L) Crystallitic b-fabric [cb] in Bk horizon (XPL). (M) Cross striated b-fabric in Bk horizon (XPL). (N) Cytomorphic calcite [cy] formed of equigranular and subangular sparry calcite with interspersed clay [c] (PPL). [PPL = plane-polarised light; XPL = cross-polarised light.]

however, the single grain microstructure is locally replaced by a pellicular grain microstructure (Fig. 8F) forming a chitonic c/f related distribution pattern.

By contrast, the carbonate concentration in the lowermost calcic (Bk) horizon is strong. Root marks in this horizon appear as subvertical to subhorizontal rhizoliths filled with sand grains floating in micritic cement (Fig. 8G); at places, the walls of tubules are outlined by sparry calcite. Such rhizoliths usually occur isolated and are observed in the C horizon below; they display morphological and compositional similarity to rhizotubules described by Kraus and Hasiotis (2006). However, in this horizon, the carbonate is predominantly concentrated in nodules, which are spherical to subspherical in shape (no more than 5 mm in diameter), white in colour, and appear frequently isolated and with sharp contact with the enclosing sediments (Fig. 8H). The interior of nodules exhibit micritic cement with floating sand grains. Additionally, carbonate lenses (up to 1.0 m wide and 0.3 m thick) are observed and form distinct calcareous levels at depths of 0.1–0.7 m from the top boundary of the palaeosol profile (Fig. 8I). The interior of these nodules holds few remnants of bioturbations and laminar sparry calcite. In thin section, the Bk horizon differs from the Bw horizon by the increase in fine material filling intergranular spaces (close porphyric c/f related distribution pattern, Fig. 8J) where a subangular blocky microstructure is observed (Fig. 8K); the groundmass around the blocky microstructures displays vugh and channel voids as also small birefringent calcite crystals (crystallitic b-fabric, Fig. 8L) and less commonly streaks of oriented clay (cross striated b-fabric, Fig. 8M). Furthermore, the voids are locally occupied by cytomorphic calcite crystals and surrounded by a decalcification zone; the calcite crystals are equigranular and occur interspersed with clay (Fig. 8N). The transition from the Bk to the C horizon is diffuse and smooth.

The C horizon is 0.4–1.2 m thick, pink to pinkish white (7.5YR 8/1, 8.5/2, 8/3, 7/3, 9/1) and formed of sand. This horizon does not show pedogenic features, but exhibits "ghosts" of planar-laminated and cross-laminated fine sandstones (Fig. 6D, E), trough and planar cross-bedded sandstones (Fig. 2D, E) and conglomerates (Fig. 3C). Carbonate cementation is weak or absent in the C horizon and moderate to strong in the Ck horizon.

5.1.1.2. Interpretation. Inceptisols are soil types that show a weak, but noticeable, degree of development. Because of their poor grade of evolution, they do not meet the criteria of other, more evolved, soil Orders. The diagnostic features that permitted classification of the studied profiles as Inceptisols are: (i) an A horizon that resembles a thin, low-chroma, ochric epipedon; (ii) a cambic (Bw) horizon, and/or (iii) a calcic (Bk) horizon in which both display their upper boundaries within the first metre of the preserved palaeosurface (Soil Survey Staff, 2015). The cambic (Bw) horizon was recognised by the following criteria: (i) thickness higher than 0.15 m, (ii) muddy sand texture, (iii) evidence of weakly developed soil structure (e.g., subangular blocky microstructure), (iv) higher chroma relative to the overlying A horizon; and (v) depletion in carbonates.

The Inceptisols type 1 developed over channel deposits that formed topographically elevated alluvial ridges in the distributive fluvial system (Soares et al., 2018, 2020). The single to pellicular grain microstructure of the A-Bw horizons ensured good drainage conditions to these soils (Kühn et al., 2010). In this condition, during rainfall, suspended clay particles in percolating soil water could disperse downwards through conductive pores of the cambic horizon (Theocharopoulos and Dalrymple, 1987). After slow evaporation of solutions, the gradual drying of water menisci caused the adhesion of clay particles onto the surface of sand grains by adsorption and capillary forces, forming the observed chitonic c/f related distribution patterns in the Bw horizons (Sullivan, 1994).

The crystallitic b-fabric is concentrated mostly in the groundmass and nodules in Bk horizons and developed as a result of the progressive precipitation of fine calcite crystals in the micromass during rapid

drying of the vadose solution in the soil (Durand et al., 2010). Indeed, the relative increase in carbonate accumulation can be related to different degrees of soil development; Bk horizons with small-scale interspersed carbonate nodules indicate a lower stage of soil development (stage II of Gile et al., 1966) whereas Bk with distinct and indurated layers of large-scale carbonate nodules relate to a more advanced pedogenesis (stage III of Gile et al., 1966). Another mechanism of carbonate accumulation in these pedotypes can be associated with roots. The carbonate cementation in rhizotubules most likely developed from the evaporation of soil water percolating along root moldic porosity within the soil after root decay (Kraus and Hasiotis, 2006). Together, the crystallitic b-fabric in Bk, and the vertical distribution of rhizotubules along the entire profile, demonstrates a fairly well-drained soil profile where soil moisture percolated effectively via conductive soil pores and root pathways. Additionally, the localised occurrence of sparry cytomorphic calcite filling and/or outlining root traces and pre-existing platy structures corroborates the inference of root-induced carbonate cementation. The platy structures most likely developed from initial disruption of relict beddings in the parent material (Retallack, 2001). In thin section, the sparry calcite infill in the platy structures resembles cytomorphic calcite crystals possibly linked to petrification of living root cells that occupied these disruption planes (Klappa, 1980). In this case, the laminar sparry calcite observed in Bw-Bk horizons might correspond to the emplacement of wide and horizontal root mats after the disruption of the parent material, which plants enact as a strategy to better hydrate from a profile that poorly retains water (Alonso-Zarza, 1999). Finally, the local increase of fine material in Bk is observed as isolated patches of close porphyric c/f related distribution pattern. The weakly developed subangular blocky microstructures and cross striated b-fabric inside the patches of close-porphyric c/f related distribution patterns are probably related to the argilloturbation (sensu Castellet and FitzPatrick, 1974) of the horizon through shrinking and swelling of clays (Kühn et al., 2010).

5.1.2. Inceptisol type 2: Ag-Bwg

5.1.2.1. Description. This pedotype (Fig. 9A) shows a greenish-grey homogeneous colour (5GY 8/1, 8/2) (Fig. 9B). The parent material is related to overbank and distal channel-fill deposits. The Ag horizon is up to 0.5 m thick and formed of muddy sand. The horizon is marked by abundant drab-haloed root traces and coalescent bioturbations. The drab-haloed root traces appear as vertical to subvertical tubules (up to 0.5 m in length) that taper and branch horizontally and coalesce laterally; the tubules vary from 4 - 50 mm in diameter and are internally coated by thin laminae of manganese oxide (Fig. 9C). Bioturbation is observed near the top of the horizon and occurs as coalesced vertical tubules (50–400 mm in length and 10–50 mm wide) showing irregular walls (Fig. 9D). In thin section, the margins of quartz grains are often outlined by pellicular alteration displaying highly irregular boundaries with the muddy groundmass, resembling single spaced porphyric c/f related distribution pattern (Fig. 9E). Additionally, the sandy mud groundmass reveals packing and vugh voids that are commonly infilled by pure black Fe-Mn oxides limited by rough and irregular surfaces (Fig. 9F). Finally, the top of the Ag horizon is sharp, undulate and erosive, whereas the transition to the lowermost Bwg horizon is diffuse.

The Bwg horizon is 0.1–0.8 m thick, pale green (5GY 8/2) and formed of muddy sand. The macro- and microfeatures observed in the Ag horizon are also encountered in the Bwg horizons; however, a change is observed from a single to double spaced porphyric c/f related distribution pattern. Such a distribution is further linked to the appearance of subangular blocky microstructures (Fig. 9G) delineated by channel voids coated by clay and Fe-Mn oxides (Fig. 9H). Elongated domains of oriented clay outline the altered quartz grains to form granostriated b-fabric (Fig. 9I). Finally, the bottom of the Bwg horizon is marked by an abrupt boundary (Fig. 9D).
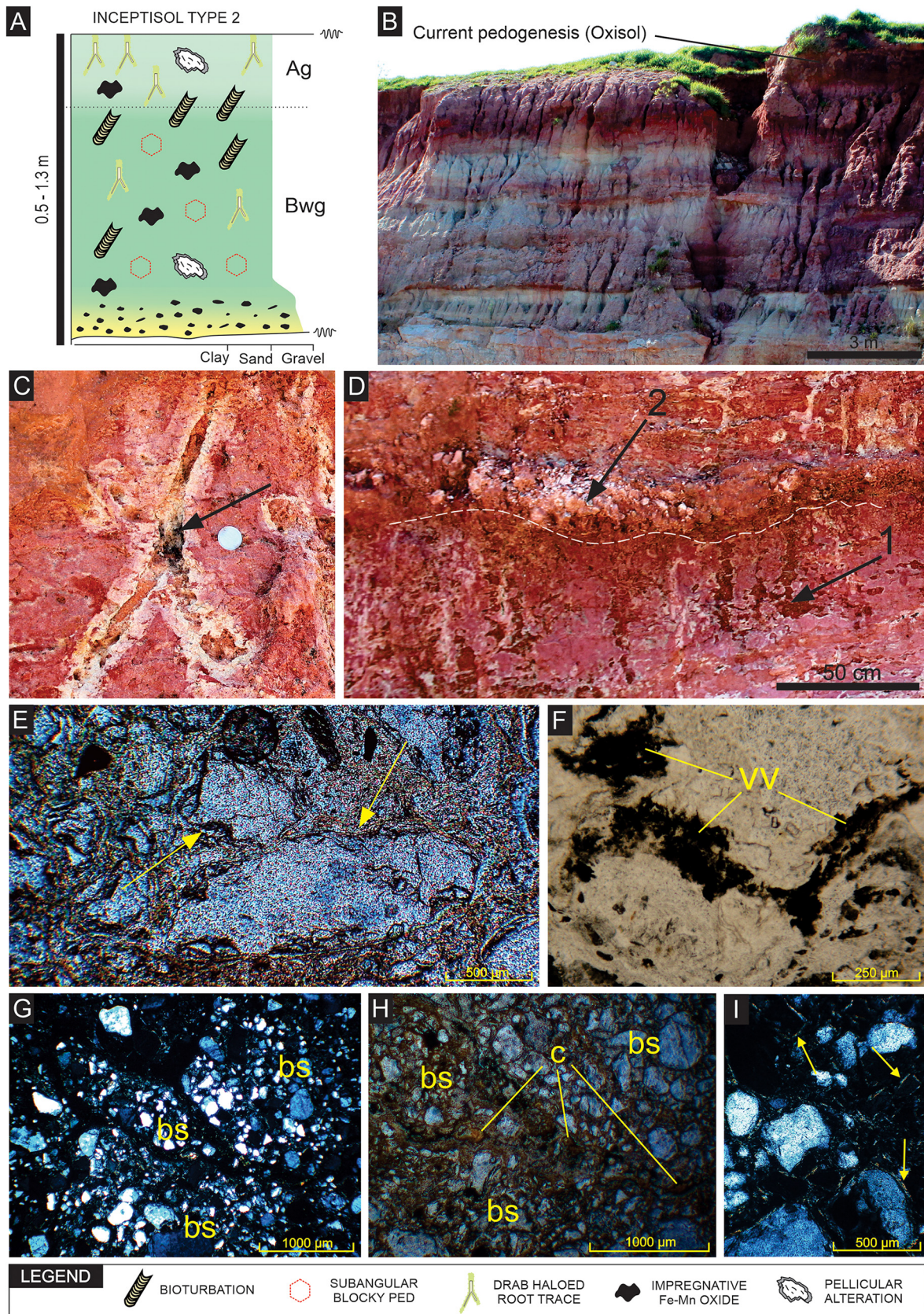
Fig. 9. Summary features of Inceptisols type 2. (A) Synthetic profile of the Inceptisol type 2. (B) Outcrop view of Inceptisol type 2 profiles displaying greenish grey colour. Red colours in the upper profile are due to current pedogenesis from Oxisols. (C) Drab-haloed root trace internally coated by Mn oxide (arrow). (D) Overlaid Bwg horizons showing coalescent bioturbation as vertical tubules, in the top of the horizon [1], and erosive surface marking the base of the horizon [2]. (E) Quartz grains in stage 2 pellicular alteration showing highly irregular borders (XPL). (F) Mn oxide impregnation in vugh voids [vv] (PPL). (G) Subangular blocky peds [bs] separated by planar voids in which appear clay pedofeatures [c] (XPL). (H) Same view as (G) in PPL. (I) Granostriated b-fabric outlining quartz grains (XPL). [PPL = plane-polarised light; XPL = cross-polarised light].

5.1.2.2. Interpretation. The Inceptisol type 2 differs considerably from the first Inceptisol type in parent material, drainage conditions and grade of development. The Inceptisols type 2 was developed over fine-grained overbank and distal channel-fill deposits, which correspond to lowland areas on the alluvial surface of the DFS (Soares et al., 2020). In this palaeoenvironment, the palaeosol profiles developed under poor drainage conditions.

The shallow hydromorphic formative conditions of these Inceptisols can be inferred from their frequent impregnative Fe-Mn oxide features. The presence of these features outlining blocky microstructures, voids and root traces can be related to a reduced soil environment due to stagnant waters. In these conditions, Fe and Mn are mobilised as reduced ions and put into solution (Kyuma, 2004); once they reach locally oxidising environments in the soil profile (e.g., air-filled voids and peds surface), Fe and Mn locally oxidise and precipitate from the soil solution to form the observed impregnative features (Vepraskas, 2000). Additionally, greyer or lighter colours of these pedotypes suggest that their entire groundmass is depleted in Fe and Mn oxides, which, where associated with the ubiquitous presence of impregnative Fe-Mn features, indicates conditions dominated by long periods (weeks to months) of stagnant reducing water (McCarthy and Plint, 1998; Vepraskas, 2004). Murphy and Kemp (1984) have related such protracted water stagnation to near-surface water-table gleying during wet seasons. Under these conditions, soil solutions become anoxic, increasing the solubility of quartz (Sommer et al., 2006). Indeed, evidence of quartz dissolution is frequently encountered in this pedotype as quartz grains with corroded margins, which can be associated with stages 1 and 2 of mineral alteration sensu Stoops et al. (1979). Root traces contoured by rhizohaloes indicate very poorly drained profiles affected by near-surface water gleying as a consequence of a perched water table in a muddy parent material (Kraus and Hasiotis, 2006). Subsequently, the presence of illuvial clay outlining weathered quartz grains depicts a better drained profile probably caused by a drop in the water-table level during drier periods, allowing clay particles to percolate downwards in the profile (Theocharopoulos and Dalrymple, 1987). Finally, the predominance of single to double spaced porphyric c/f related distribution pattern, subangular blocky microstructures and granostriated b-fabric point to a more advanced stage of pedogenesis when compared with the Inceptisol type 1 (Castellet and FitzPatrick, 1974; Kühn et al., 2010).

5.2. Entisols

5.2.1. Description

Entisols are developed exclusively on overbank deposits, and their parent material ranges from fine-grained sandstone to mudstone (Fig. 10A). Profiles vary from 0.2 - 0.5 m in thickness; when vertically stacked, they form sequences up to 2.5 m thick (Fig. 10B). Their complete sequence is formed of A–C horizons.

The A horizon is 0.1–0.3 m thick, pink (7.5YR 7/3) in colour, and shows sandy mudstone materials. This horizon is marked by the presence of root casts, platy structures and bioturbation. Root casts are filled with mudstone and distributed vertically in the palaeosol horizon (Fig. 10C); they are up to 0.2 m in length, 10–20 mm in width, and display branching downward morphologies with walls that are irregular and abrupt. Commonly, roots cross the A–C boundary. The platy structures are coarse, weakly-developed and outlined by sparry calcite (Fig. 10D); the calcite forms subhorizontal laminae (<1 mm thick) that cross laterally at angles of 60–120° to each other, giving rise to lenticular platy structures. In cross-section, the laminae display a central part of white sparry calcite bordered by a drab-haloed fringe of diffuse colour transition that is in sharp and irregular contact with detrital grains. Bioturbations in the A horizon are observed as vertical and submillimetric tubules filled with sandstone. In thin section, the A horizon reveals single to pellicular grain microstructure where quartz grains are partly or wholly surrounded by isotropic clay and Fe-Mn oxides

(chitonic c/f related distribution pattern) (Fig. 10E); locally, coarse units are linked by bridges of fine material (gefuric c/f related distribution pattern) (Fig. 10E). Furthermore, clay pedorelict fragments are observed throughout the A–C profile and occur as rounded to subrounded sand-sized grains (Fig. 10F). The transition between the A and C horizons is diffuse and smooth to undulated, whereas the top of the A horizon is locally bounded by erosive surfaces that display erosive marks with concave-up shape and that are 0.2 m deep and 2 m wide.

The C horizon is 0.2–0.4 m thick, white to light pink (7.5YR 8/0, 8/2), and formed of sandy mudstone. Relicts of the muddy sandstone facies are observed as an alternation of clay-rich laminae and lenticular sets of cross-laminated fine sandstone (Fig. 5A, B). Bioturbations in the C horizon consist of tubules (10–100 mm in length and up to 10 mm in width) that internally show bowlike distribution patterns (Fig. 10G).

5.2.2. Interpretation

The recognition of Entisols is based on the absence of a B horizon (Soil Survey Staff, 2015). The predominance of single to pellicular grain microstructures demonstrates a fairly well-drained profile where fine material could percolate downwards along conductive pores (Theocharopoulos and Dalrymple, 1987; Kühn et al., 2010). The pink colour of the profile, which is microscopically related to the brown coloured clay and oxides outlining quartz grains, might indicate near-surface evaporation of solutions (Sullivan, 1994), corroborating the hypothesis of good drainage conditions. The platy structures likely formed from the initial disruption of relict bedding of the parent material (laminated claystone and fine sandstone) (Retallack, 2001). Additionally, the sparry calcite infill in platy structures (as similarly observed in the Inceptisol type 1) might result from early stages of emplacement of wide and horizontal root mats in the upper horizons of the soil as a mechanism for plants to better hydrate from a profile that does not retain water effectively (Alonso-Zarza, 1999); because levels with calcrete laminae are very thin and sharply in contact with parent material showing low pedogenic weathering, they were likely formed when sedimentation was relatively low and episodic, such that a new vegetation cover would be able to occupy a progressively higher surface in the floodplain environment (Alonso-Zarza, 1999). In this regard, mud-filled root casts also suggest episodic flooding of the previously vegetated surface followed by the filling of remaining root casts (Retallack, 2001). Furthermore, the presence of scattered pedorelicts of impure clay coating corresponds to papules (sensu Brewer, 1964) and might possibly be involved in the erosion of the groundmass of more clay-rich horizons (e.g., Inceptisols type 1) that formed nearby active channels (Kühn et al., 2010). Finally, the absence of B horizons, the sole presence of poorly developed roots and the limited thickness of the profiles indicate very brief pedogenesis frequently interrupted by sporadic flooding of nearby channels. After each episode of sedimentation, the renewed surface was colonised by a vegetation cover. The continuation of this process ultimately formed the observed compound sequence of A–C horizons (sensu Kraus, 1999). The presence and position of these soils in the alluvial surface can be discerned due to their overbank parent material and the presence of papules: both originated from floodwaters coming from topographically elevated nearby active channel belts.

5.3. Vertisols

Vertisols are formed over the clay-rich facies of the overbank deposits. They are up to 1.4 m thick. The described occurrences of Vertisols can be organised in two different sequences of horizons: Assk-Bssk and Assk(m)-Bssk-Bsskg-Bssg.

5.3.1. Vertisol type 1: Assk-Bssk

5.3.1.1. Description. In the Vertisol type 1 (Fig. 11A), the Assk horizon is light pink (7.5YR 8/2), 0.1–0.3 m thick, and formed of sandy mudstone materials. The horizon is recognised by the presence of gilgai
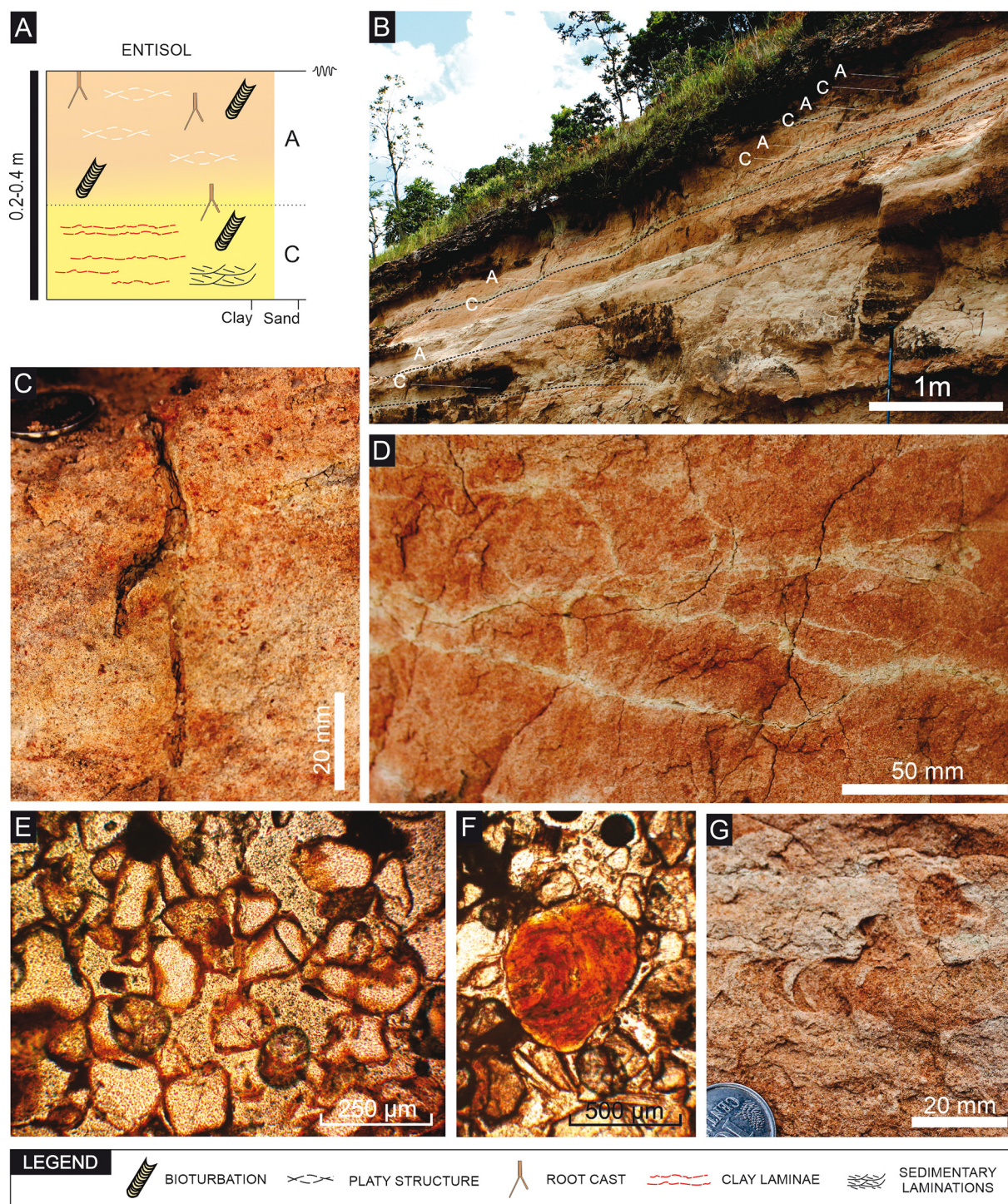
Fig. 10. Summary features of Entisols. (A) Synthetic profile of the Entisol pedotype. (B) Outcrop overview displaying a compound sequence of A–C profiles. (C) Mud-filled root cast. (D) Platy structure outlined by laminae of sparry calcite crossing subhorizontally. (E) Pellicular grain microstructure of A horizon where quartz grains are coated by clay and oxides, locally displaying braces of fine material (PPL). (F) Rounded clay pedorelicts (papule sensu Brewer, 1964) in B horizon (PPL). (G) Bioturbation that internally shows backfills forming a bowlike distribution pattern. [PPL = plane-polarised light; XPL = cross-polarised light.]

microrelief, which is characterised by undulated surfaces (spacing of 0.6 m and amplitude of 0.2 m) overlain by overbank deposits (Fig. 11B). Below the microlows the horizon is formed of lenticular peds, up to 40 mm thick and 0.3 m wide (Fig. 11C), whereas below the microhighs it is more intensely deformed and displays smaller dimensions of both angular blocky peds (2–20 mm in diameter) and lenticular peds (up to 20 mm thick and 0.1 m wide) (Fig. 11D). Carbonates in the Assk and Bssk horizons concentrate in rhizoliths. The rhizoliths appear in circular to subcircular forms, 10–50 mm in diameter (Fig. 11C) and usually coalesce, reaching up to 0.5 m laterally (Fig. 11E). The centre of rhizoliths display a white depleted zone (rhizohalo) cemented by micritic carbonate. An outer rim of red iron oxide outlines the rhizoliths. The oxidised rim shows abrupt transition with the central rhizohalo and diffuses with the surrounding soil matrix (Fig. 11E). The A-B boundary is diffuse and the top boundary of the A horizon is undulated (gilgai microrelief).

The Bssk horizon is light pink in colour (7.5YR 8/0), 0.1–0.4 m thick, and formed of sandy mudstone material. This horizon displays poorly to
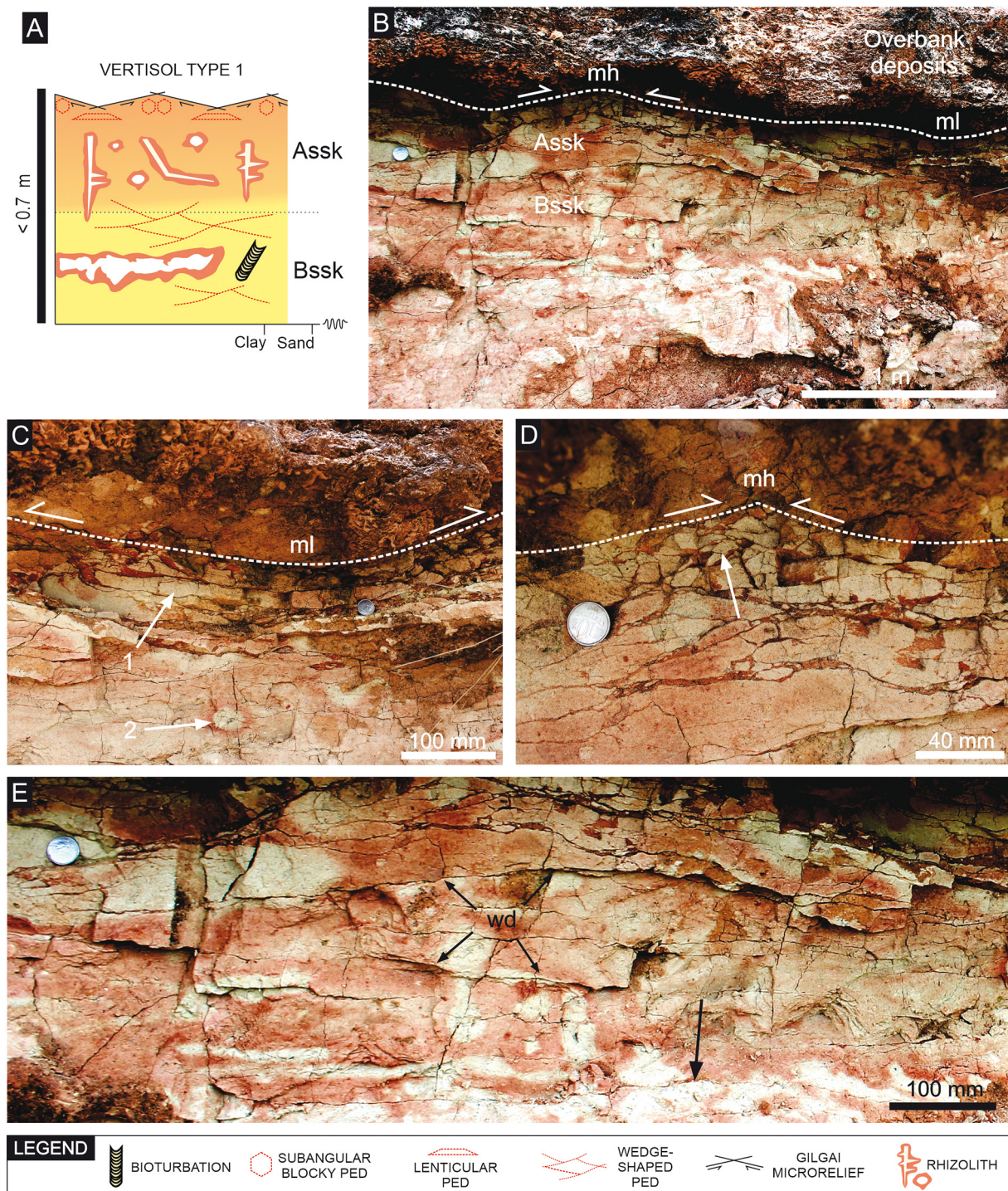
Fig. 11. Summary features of the Vertisol type 1. (A) Synthetic profile of the Vertisol type 1 pedotype. (B) Profile overview showing Assk-Bssk horizons bounded at the top by gilgai microrelief displaying microhighs [mh] and microlows [ml]. (C) Details of lenticular peds [1] and circular cross section of rhizoliths [2] formed below the microlow surface. (D) Details of the subangular blocky peds [arrow] formed under the microhigh topography. (E) Bssk horizon showing poorly developed wedge-shaped peds [wd] and horizontally coalesced rhizoliths [arrow] with well-developed rhizohaloes outlined by red coloured iron oxide rims.

moderately developed, horizontal to slightly inclined wedge-shaped peds (up to 80 mm thick and 0.3 m wide) that are delimited by slickenside planes (Fig. 11E). In the Bssk horizon, rhizoliths are also observed and appear horizontally coalesced (Fig. 11E). Bioturbation occurs as circular to subcircular forms. The burrows show basal sections that are 5–20 mm in diameter and filled with pinkish-red oxidised fine sandstone from the A horizon. The lower boundary of the Bssk horizon is locally marked by abrupt and irregular concave-up surfaces.

5.3.1.2. Interpretation. Vertisols are classified based on the following morphological aspects, seen within the first metre of the soil palaeosurface: (i) wedge-shaped peds limited by fractures crossing at 20°–45° (acute angles) and 135°–160° (obtuse angles); (ii) surface of peds constituted by slickenside planes; (iii) abundant clay fraction in the groundmass; (iv) upper boundary showing preserved gilgai microrelief displaying microhighs and microlows (Mermut et al., 1996; Soil Survey Staff, 2015). Vertisols develop on surfaces that do not exceed 5% in slope

(Mohr et al., 1972). Since the parent material of the study palaeosols is formed of overbank and floodplain channel fill deposits, it is possible to associate them with the lowland areas of the DFS. Vertisols have limited value as palaeoclimate proxies (Retallack, 2001), but indicate marked wet-dry seasonality (Ahmad, 1983; Coulombe et al., 1996). The Vertisol type 1 (Assk-Bssk) is marked by gilgai microrelief, which is a superficial morphology resulting from repeated shrink and swell of the clay material in the soil, which causes the upward buckling of the soil material forming microhighs and microlows (Ahmad, 1983). Such variation is a direct product of a marked wet-dry seasonality. The presence of rhizoliths with depleted rhizohaloes and well-marked red oxidised rims indicates early to moderate gleying, likely induced by stagnating surface waters that become O_2 starved locally around root channels. Additionally, the presence of horizontally dispersed rhizoliths in the Bssk horizon points to a near-surface rise of water table during more humid periods (Wright et al., 1995). Conversely, the carbonate cementation at the centre of rhizoliths indicates the drying of these waters for a sufficiently long period after root decay (Kraus and Hasiotis, 2006), probably from the lowering of the water table.

5.3.2. Vertisol type 2: Asskm-Bssk-Bsskg-Bssg

5.3.2.1. Description. In the Vertisol type 2 (Fig. 12A), the A horizon is calcic (Assk), 0.4 m thick, light brown (7.5YR 6/4) and formed of mudstone (Fig. 12B). The carbonate concentration in the Assk horizon is distributed as cutans of platy structures as moderate carbonate cementation. Rhizoliths occur widespread throughout the profile and vary in shape from small-scale, circular to subcircular (30–40 mm in diameter) to large-scale vertical to subvertical tubular geometries (up to 0.5 m in length, 30 mm in width) (Fig. 12C). The rhizoliths display a central grey depleted zone (rhizohalo) cemented by micritic carbonate that is outlined by a rim of red iron oxide. At the top of the profile, rhizoliths form a laterally coalesced horizon of intense carbonate cementation (Asskm) that is up to 0.3 m thick. The platy structures outlined by carbonate cutans (Fig. 12D) are similar to those described in Inceptisols type 1 and Entisols. However, in the case of Vertisols type 2, the laminar calcrete is commonly encountered adjoined and spreading radially from the rhizoliths. In thin section, the Assk(m) horizon displays a platy structure where aggregates are horizontally elongated and separated by planar voids filled with sparry calcite (Fig. 12E). The clay-rich groundmass displays single- to double-spaced porphyric c/f related distribution pattern where cross streaks of aligned clay are observed in the fine material (cross striated b-fabric) and around the quartz grains (granostriated b-fabric) (Fig. 12F). Additionally, the groundmass reveals interspersed patches of micritic calcite cement occupying the spaces between the sand grains (crystallitic b-fabric, Fig. 12G). The top boundary of the Assk(m) horizon is undulated to irregular, forming a *gilgai* microrelief, whereas the Assk(m)-Bssk transition is diffuse.

The B horizon is 1 m thick, light brown (7.5YR 6/4) and formed of mudstone. This horizon is commonly marked by mukkara structures, sparse rhizoliths and bioturbation. The mukkara structures form wedge-shaped peds (5–300 mm wide and 3–100 mm thick) with subhorizontal long axis and limited by slickenside planes that cross each other at a wide range of angles, as conjugate sets that dip at angles of 20° to 45° (Fig. 12H). Slickenside planes are laterally continuous for up to 0.7 m; they are smoothly polished surfaces that normally display submillimetric striations and grooves. In the upper portion of the horizon (Bssk), the surfaces of mukkara structures are coated by sparry calcite (*calcans*) whereas lower in the profile (Bssg) they are marked by the accumulation of manganese oxide coatings (mangans). Bioturbation takes the form of subvertical tubular structures (up to 10 mm in diameter and 0.2 m in length) surrounded by greenish white depletion zones cemented by micritic calcite; locally, bioturbation walls are coated by a submillimetric film of manganese oxide (Bsskg). In thin section, the Bssk-Bsskg horizons are similar to the Assk(m) horizon,

showing similar calcic features (e.g., interpedal sparry calcite and crystallitic b-fabric), microstructure (platy structure) and groundmass (single to double spaced porphyric c/f related distribution patterns and cross striated to granostriated b-fabric). However, the Bsskg-Bssg horizons can be differentiated by the occurrence of Mn oxide nodules and Fe oxide hypocoatings. The nodules are formed of impregnative Mn oxides showing black and pure intrapedal void infilling and limited by rough and irregular surfaces (Fig. 12I), whereas the hypocoatings constitute brown Fe oxide fringes outlining irregular to subcircular voids (Fig. 12J). Finally, the transitions between the Bssk-Bsskg-Bssg horizons are diffuse and homogeneous in colour; the lowermost Bssg horizon is bounded at the bottom by abrupt and irregular concave-up surfaces (Fig. 12B).

5.3.2.2. Interpretation. The Vertisol type 2 shares the same Assk-Bssk horizons observed in the Vertisol type 1; however, in this case, peds are outlined by carbonates. This particular difference, as well as the crystallitic b-fabric, might be associated with the progressive drying of stagnant solutions trapped among soil aggregates (Durand et al., 2010). Rodrigues et al. (2019) performed an in-depth study of the calcretes in these Vertisols. They showed a clear genetic association between root activity and the horizontally coalescent rhizoliths and peripheral laminar calcretes. As a consequence, this bioinduced calcretisation resulted in an impermeable horizon (Asskm) near the palaeosurface, which served as indicator of the advanced stage of calcretisation (Wright et al., 1995).

Relative to the Vertisol type 1, profiles of Vertisol type 2 can be differentiated by their abundance of redoximorphic features. Rhizoliths are normally accompanied by well-developed grey colour rhizohaloes, which indicate depletion of Fe and Mn from the microenvironment created by the roots responsible for the remobilisation of these elements (Schoeneberger et al., 2001; Vepraskas, 2004; Kraus and Hasiotis, 2006). The dissolved Mn ions migrated in the soil solution to locally oxidised sites forming the intrapedal impregnative nodules, the interpedal mangans outlining wedge-shaped peds and the Mn oxide coatings outlining bioturbations and rhizoliths of the Bsskg-Bssg horizons (Vepraskas, 2000). The combined presence of impregnative Mn oxide and the Fe oxide hypocoatings indicates several days of stagnant water conditions (Veneman et al., 1976). The combination of the described redoximorphic features permits association of the pedogenesis of Vertisols type 2 with short to medium periods of stagnant surface water gleying. Such a condition can be further related to a combination of rapid rise of the water table (Murphy and Kemp, 1984) and poor drainage associated with high water retention and low permeability of the clay-rich groundmass, as attested from the porphyric c/f related distribution pattern of these profiles (Lindbo et al., 2010).

The coexistence of calcium carbonate and redoximorphic features reveals the oscillatory character of the Eh conditions in these palaeosols, where carbonate was precipitated during dry periods and redoximorphic features developed during wetter periods. Finally, the recurrent shifts between wet-dry periods in the clay-rich groundmass was likely responsible for the development of the cross and granostriated b-fabrics in these Vertisols (Castellet and FitzPatrick, 1974; Kühn et al., 2010).

6. Spatial distribution of sediments and palaeosols

The distribution of sediments and palaeosols was examined along a downdip transect (c. 70 km long) from southeast to northwest of the basin margin (Fig. 1D). Along this sector, the Serra da Galga Formation displays a systematic variation in sedimentary architectures and associated palaeosols, such that proximal, medial and distal zones of the distributive fluvial system can be differentiated. From fan apex to toe, the distribution of sediments and palaeosols demonstrates a progressive variation from (i) a proximal zone dominated by channel belts and associated well-drained Inceptisols (type 1), towards (ii) a medial zone
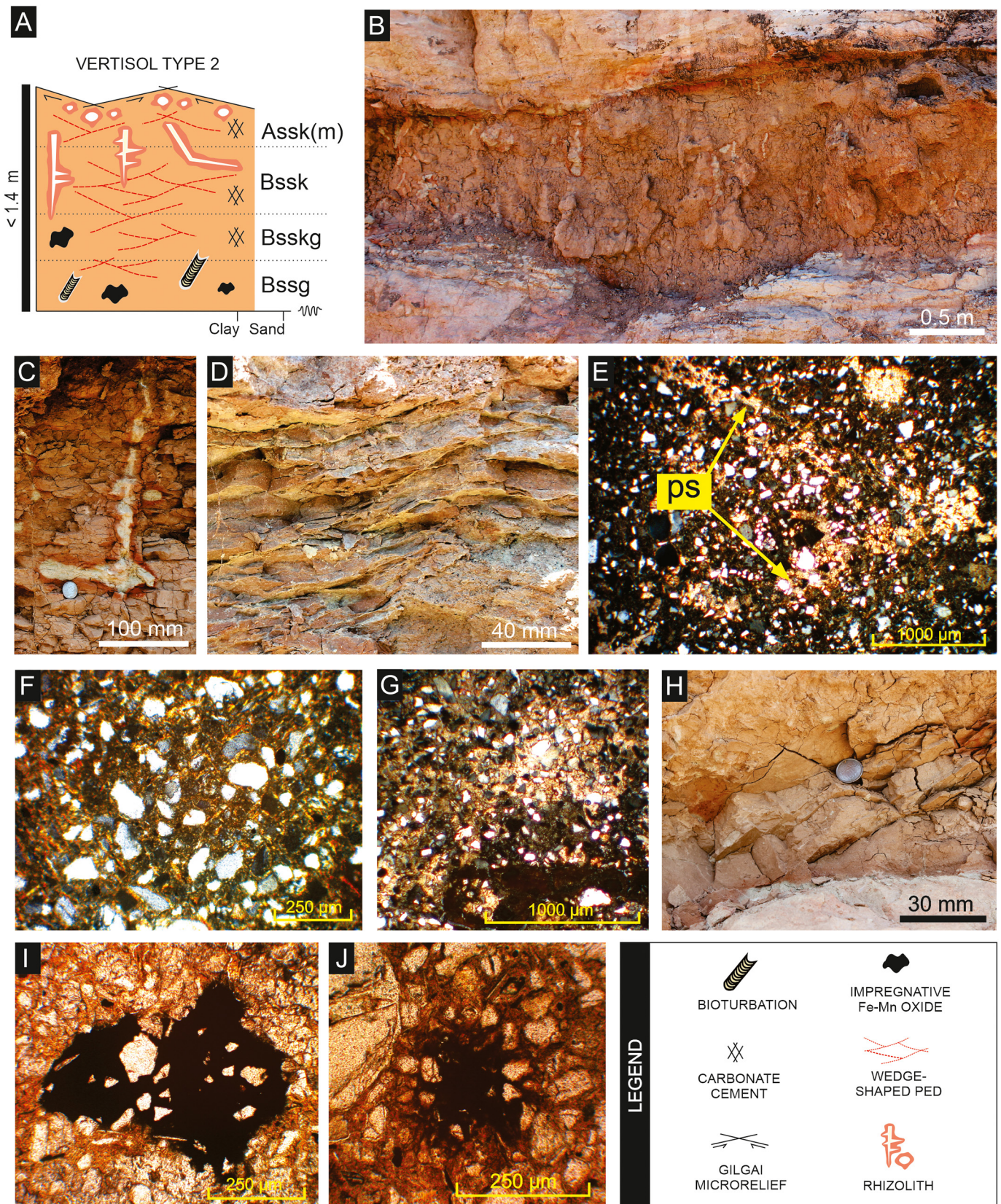
Fig. 12. Summary features of the Vertisol type 2. (A) Synthetic profile and (B) outcrop overview of the Vertisol type 2 pedotype. (C) Large-scale subvertical rhizolith showing central depleted rhizohalo outlined by well-developed red coloured iron oxide rim. (D) Platy structures coated by laminar calcrete. (E) Photomicrography of platy structure [ps] showing aggregates bounded by planar voids with sparry calcite (XPL). (F) Groundmass displaying single to double spaced porphyric c/f related distribution pattern with granostriated and cross striated b-fabric (XPL). (G) Crystallitic b-fabric (XPL). (H) Wedge-shaped mukkara structures. (I) Intrapedal vugh void filled with irregular, strongly impregnative, black nodule of Mn oxides (PPL). (J) Ferruginous hypocoating related to circular void (PPL). [PPL = plane-polarised light; XPL = cross-polarised light.]

where the channel belt deposits and floodplain channel fills occur interstratified with overbank deposits and are associated with Entisols and Vertisols (types 1 and 2), to finally reach (iii) a distal zone characterised mostly by overbank deposits with interspersed distal channel fills, both associated with poorly drained Inceptisols (type 2).

6.1. Proximal zone (Price 1 site)

The proximal zone is observed in the Price 1 type section (Fig. 1D). At this location, the stratigraphic interval is organised in amalgamated channel belts (c. 8 m thick) overprinted with Inceptisols type 1 and rare occurrences of overbank deposits (Fig. 13); the proximal zone shows channel to overbank thickness ratio (c/o) of 7.9 and unaltered sediment to palaeosol thickness ratio (s/p) of 1.7. Overall, in-channel cross-strata show a unidirectional palaeocurrent trend towards WNW (mean vector = 340°; angle variation = 173°; n = 38) (Fig. 1F).

The channel-belt successions are organised into high-frequency c. 10-m thick stratigraphic cycles that alternate between the type A ephemeral-flow main channel fill (c. 30% of the total succession) and perennial-flow main channel fill (c. 70% of the total succession). Locally, floodplain channel fills occur interspersed as laterally restricted lenticular bodies displaying incised concave-up bases and flat erosive top boundaries (Fig. 13). Overall, the top and bottom of the amalgamated channel-fill succession is formed of well-drained Inceptisols of type 1, whereas, internally, each channel-fill unit is separated by an erosive surface with little to no sign of pedogenesis.

The observed stratigraphic arrangement depicts a twofold depositional style of the fluvial system. First, the alternation between ephemeral- and perennial-flow main channel fills reveals the depositional history of channels that experienced high oscillations in water and sediment discharge; the discharge regime varied between (i) high discharge and sharply peaked flood events that produced supersaturated flows with transcritical to supercritical hydraulic conditions established during periods of episodic and sudden overland runoff (ephemeral-flow main channel fill); (ii) low discharge flows of longer duration and lower sediment saturation that were likely maintained from water and sediment derived from the catchment area (perennial-flow main channel fill). Because the erosive boundaries between each channel fill do not show evidence of pedogenesis, it is reasonable to assume that the variations in discharge regime occurred in less than a few hundred years, which is the time necessary to develop initial stages of soil horizonation (for further details, see Soares et al., 2018). Second, the amalgamated succession of channel fills is bounded by Inceptisols of type 1, which indicate long pauses in sedimentation until the reoccupation of a depositional site by the channel belt and sedimentation of a new channel-fill succession. Overall, a depositional history characterised by high discharge variability, inferred from the internal architecture of the channel bodies, corroborates a fluvial-fan hypothesis, since fluvial systems with large fluctuations in water discharge are thought to be more prone to develop fans due to channel instability and avulsion where fans can emanate from outlets in front of mountain ranges (Leier et al., 2005). Fan-forming channel networks with high discharge variability are often associated with highly seasonal climates (Hansford and Plink-Björklund, 2020), and this is in agreement with the seasonal palaeoclimate inferred for the Upper Cretaceous of the Bauru Basin, marked by wet-dry cyclicity (e.g. Basilici et al., 2009, 2016; Soares et al., 2018).

The inferred depositional behaviour indicates that the proximal zone was a site where channels systematically reoccupied the same depositional area. The progressive aggradation of the channel belt gave rise to an elevated alluvial ridge (Törnqvist and Bridge, 2002), which, in association with the erodible sandy substrate, acted as a precondition to avulsion of the channel belt to a lower position laterally on the fan surface (Jones and Schumm, 1999; Makaske, 2001; Slingerland and Smith, 2004; Aslan et al., 2005). As a consequence, avulsion (sensu Allen, 1965) is inferred to be the key mechanism that controlled the stratigraphic arrangement of the distributive fluvial system. After complete

abandonment of the elevated alluvial ridge, the channel deposits were subject to pedogenesis for a duration sufficient to develop Inceptisols type 1. These pedotypes recorded well-drained conditions due to their porous sandy parent material and to the vertical separation between the topographic surface and the water table. As a result, the pedotypes show a profile with single-grain microstructures with connective packing voids that allowed effective downward percolation of solutions, forming link cappings and chitonic c/f related distribution pattern in the uppermost A-Bw horizons. When associated with longer periods of stability, these palaeosols recorded argilloturbation in their lowermost Bk horizon (forming subangular blocky microstructures), suggesting more advanced stages of soil development. The carbonate accumulations in Bk horizons of the proximal zone show stages I and II of Gile et al. (1966), suggesting a palaeopedogenetic evolution in the order of 2.6 ky (see Table 1 in Gile et al., 1966) to 10 ky (see Table 2 in Machette, 1985). Because these pedotypes constitute boundaries between the amalgamated channel belts, their time of formation corresponds to intervals between successive avulsion episodes; as such, their estimated time of pedogenesis serves as a proxy with which to estimate the minimum interavulsion frequency of channel belts in the proximal zone. Finally, the absence of preserved overbank deposits corroborates the highly mobile and cannibalistic behaviour of the channels (Steel and Thompson, 1983), which might be explained by high bedload and relative lack of cohesive bank sediments (Hassan, 2005).

6.2. Medial zone (BR050-Km-153 site)

The medial zone of the DFS is recorded at the BR050-Km-153 type-section (Fig. 1D). At this locality, the amalgamated channel belts occur interstratified with overbank deposits and floodplain channel fills (Fig. 14); the medial zone shows c/o thickness ratio of 2.5 and s/p thickness ratio of 0.6. Overall, in-channel cross-strata show a unidirectional palaeocurrent trend towards NW (mean vector = 318°; angle variation = 135°; n = 11) (Fig. 1F).

The amalgamated channel fills that occur in the medial zone form successions (up to 8 m thick) that are laterally extensive throughout the outcrop. In this zone, the internal architecture of channel fills is differentiated from that of the proximal zone. In this case, the perennial-flow main channel fill (c. 16% of the total succession) alternates with type B ephemeral-flow main channel fill (c. 36% of the total succession). The latter type relates to less energetic flows with deposition of unit bars that amalgamate through bar-head accretion (Best et al., 2006). The preservation of bar heads and their accretion is possibly explained by the selective deposition of coarse particles at their upstream end (e.g., mud blocks; Fig. 4) that collectively acted as an armoured layer, deflecting the flow laterally and decreasing shear stress on the bar head; the decrease in bottom stress would cause particles carried onto the bar head to be deposited, and deflection of the flow around the bar would promote erosion of channel margins (Lisle et al., 1991). Even though the type B ephemeral flow channels of the medial zone preserve evidence for lower flow velocities (as opposed to near-critical flows of the proximal zone), the cannibalistic behaviour of these intraclast-rich channels persisted during dry periods, indicating their origin via overland flow. In this regard, the relative decrease in flow discharge from the proximal to the medial zone most likely permitted the preservation of fluvial bars in the internal architecture of the amalgamated channel belts. Finally, similar to the proximal zone, the amalgamated channel-fill succession of the medial zone is bounded by Inceptisols type 1; however, the carbonate accumulation in the Bk horizons is associated with the stage III of Gile et al. (1966), suggesting longer periods of pedogenesis, in the order of 10 ky (see Table 2 in Machette, 1985).

The overbank deposits (up to 3 m thick) occur interbedded with the amalgamated channel belts and are laterally extensive throughout the outcrop. The sand-prone intervals of the overbank deposits
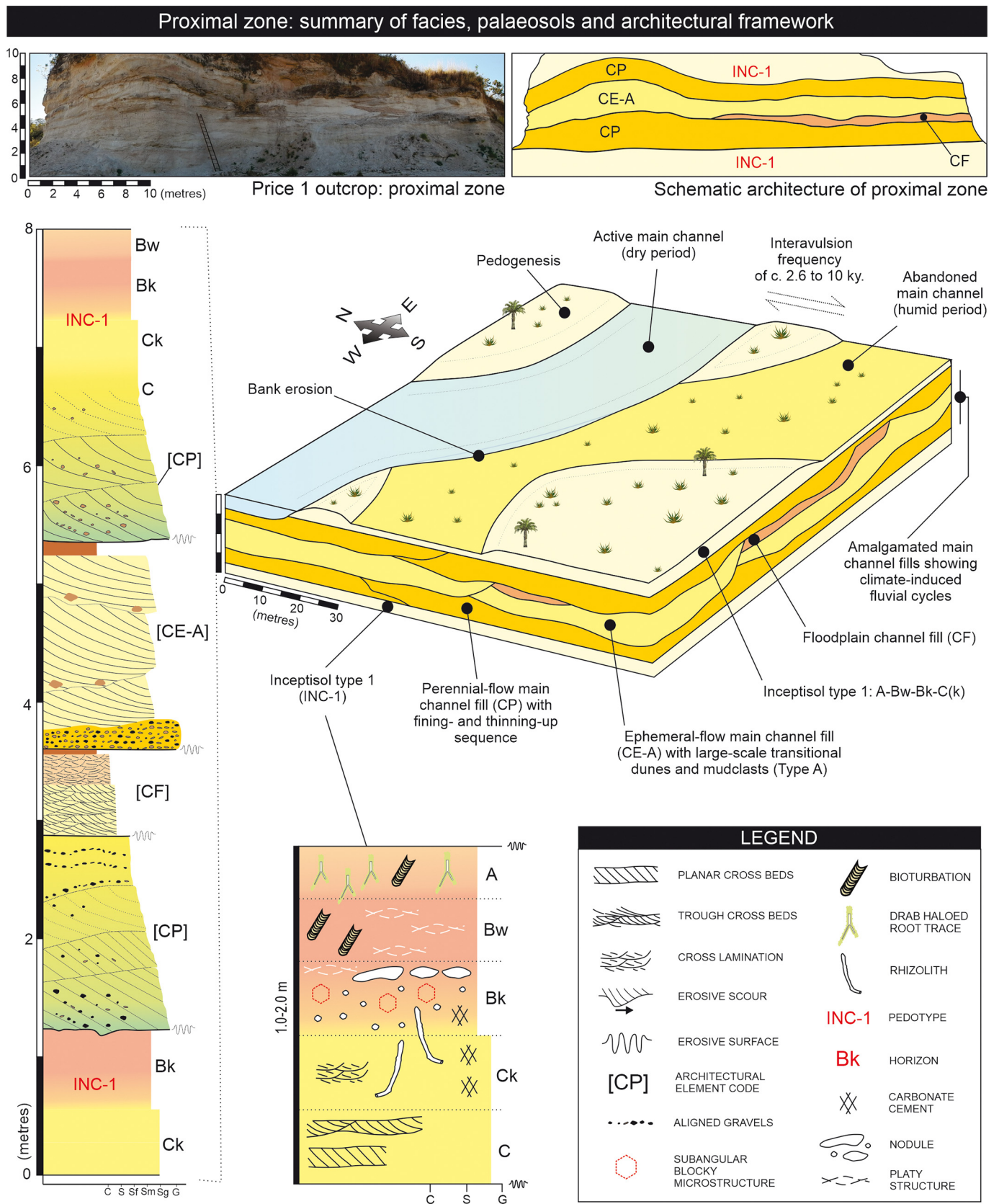
Fig. 13. Summary model depicting the typical vertical and lateral sedimentary architecture and distribution of palaeosols in the proximal zone of the distributive fluvial system (Price 1 site, Fig. 1D). Architectural elements shown are (CP) perennial-flow main channel fill, (CE-A) ephemeral-flow main channel fill with type A architecture and (CF) floodplain channel fill.
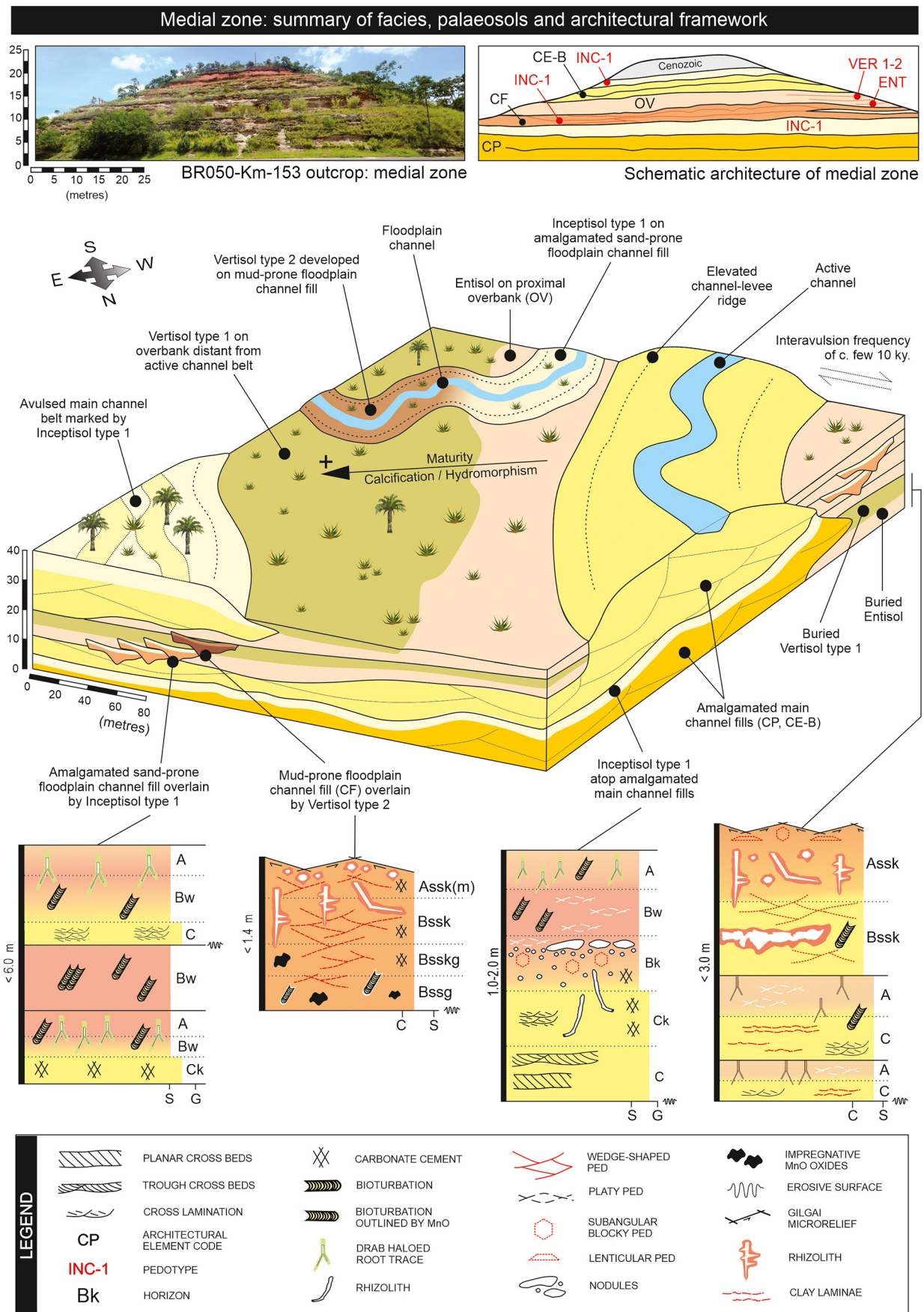
Fig. 14. Summary model depicting the typical vertical and lateral sedimentary architecture and distribution of palaeosols in the medial zone of the distributive fluvial system (BR050-Km-153 site, Fig. 1D). Architectural elements shown are (CP) perennial-flow main channel fill, (CE-B) ephemeral-flow main channel fill with type B architecture, (CF) floodplain channel fill and (OV) overbank deposit.

are associated with proximal lowland areas of the floodplain environment where Entisols developed. In these areas, floods coming from nearby active channels were frequent, as attested by the presence of pedorelict fragments (Fig. 10F) (Kühn et al., 2010); as a result of the short interflooding period, only poorly developed roots (laminar calcrete in platy structures; Fig. 10D) were achieved (Alonso-Zarza, 1999). Following each episode of flood sedimentation, a new surface was established, resulting in a compound sequence of Entisols. The time required for development of these palaeosols probably did not exceed few hundred years (Allen and Wright, 1989), i.e., the period between each flood episode. The top of the compound interval is bounded by the Assk-Bssk horizons (Vertisol type 1) developed in more mud-prone deposits. In this case, these Vertisols mark the deviation of feeder channels from the depositional site; indeed, their superficial and coalescent root system further indicates a water table near to the surface (Wright et al., 1995), probably associated with a floodplain environment at greater distance from the active channel belt.

The floodplain channel fills occur amalgamated vertically and laterally, and form a fining- and thinning-upward succession (up to 6 m thick) between the amalgamated channel fill and the overbank deposits (Fig. 14). At the base, sand-prone floodplain channel fills are associated with Inceptisols of type 1 developed close to channel ridges; the incipient or absent carbonate accumulation of these Inceptisols indicates their poor grade of development, which probably did not exceed 2.6 ky (Gile et al., 1966). Conversely, at greater distance from the channel ridge, mud-prone floodplain channel fills are encountered. In this case, the greater distance from the active channels and the low-permeability parent material permitted the development of poorly drained Vertisols of type 2. The various redoximorphic features (e.g., mangans, impregnative Fe-Mn oxide nodules and hypocoatings; Fig. 12I-J) present in these pedotypes recorded several episodes of rapid rise of the water table (Murphy and Kemp, 1984) and stagnant water conditions that persisted for several days (Veneman et al., 1976). Furthermore, Rodrigues et al. (2019) associated the coexistence of well-developed rhizoliths, Fe-Mn oxides and vertic features in Vertisol type 2 of the medial zone with the stages III to IV in the Vertisol chronosequence of Robinson (2002), suggesting a palaeopedogenetic evolution in the order of 4 ky. Finally, the fining- and thinning-upward organisation of the floodplain channel fills, and their stratigraphic position between the amalgamated channel fills and the overbank deposits, suggests the progressive deviation of the active channel belt away from the depositional site (Burns et al., 2017, 2019).

6.3. Distal zone (Calcário Triângulo site)

The analysis of the distal zone of the DFS was carried out at the Calcário Triângulo type-section (Fig. 1D). The stratigraphic framework of the distal zone is composed of overbank deposits interspersed with distal channel fills, both associated with Inceptisols of type 2 (Fig. 15); the distal zone shows a c/o thickness ratio of 0.23 and an s/p thickness ratio of 0.11. Overall, channels axes are oriented towards WNW (mean vector = 272°; angle variation = 48°; n = 5) (Fig. 1F).

The distal zone is marked by a significant decrease in (i) the incision depth of channels, (ii) their discharge, and (iii) overall drainage conditions. Gleyed Inceptisols (type 2) correspond to up to 87% of the entire succession and mark an environment associated with long periods when the water table was near the surface. However, the stratigraphic arrangement of interbedded distal channel fills, and the micromorphological features encountered in the Inceptisol type 2, reveal a history of repeated wet-dry cycles, most likely connected to oscillations of a shallow water table.

During wetter periods, river floods invaded the distal surface of the DFS; as a result, the deposited sediments constantly accumulated in a setting with high water table, where reducing conditions controlled their pedogenetic alteration. Under such conditions, Fe and Mn are promptly removed from the iron oxides and clay sediments, free to migrate in solution (Kyuma, 2004) and later precipitate in locally oxidising voids in the soil profile, forming the impregnative Fe-Mn features (Vepraskas, 2000). As a result of the wet stage of pedogenesis, palaeosol profiles in the distal zone are marked by intense gleying colours (Murphy and Kemp, 1984; McCarthy and Plint, 1998; Vepraskas, 2004). Protracted conditions of high water-table level were responsible for the establishment of anoxic conditions in the soil profile, which increased the solubility of silica, and resulted in the pellicular dissolution of quartz grains in the parent material (Sommer et al., 2006).

Afterwards, during drier periods, the water table was lowered, leading to full subaerial exposure of the palaeosol profile. At this stage, distal channels were fed by hyperconcentrated overland flows that entrained intraclasts from the nearby overbank (i.e., their intraformational conglomerate fill; Fig. 7C). Pedogenesis during the drier periods took place over the renewed surface. At this stage, root traces and bioturbations were formed, attesting to colonisation of the surface by vegetation. Additionally, under conditions of a lowered water table, the substrate experienced an increase in drainage and clay pedofeatures (possibly clay coatings) were formed around subangular blocky peds (Fig. 9H). Moreover, the single to double spaced porphyric c/f related distribution pattern (Fig. 8I), the abundance of subangular blocky peds (Fig. 8M) and the composite arrangement of the palaeosol profiles indicate a more advanced stage of pedogenesis, attesting to the higher stability of the surface in the distal zone of the distributive fluvial system (Castellet and FitzPatrick, 1974; Kühn et al., 2010).

7. Geochemical trends in palaeosols

From the proximal to the distal zones, the spatial distribution of palaeosols incorporated in the stratigraphic record of the studied succession reveals a number of factors that acted to control their pedogenesis (notably time, topography, parent material, biological communities and sedimentation rate). The intensity with which the different factors operated varied across the different pedotypes, in part as a function of the position that each soil type occupied on the fan surface. However, in the stratigraphic record, palaeosol profiles emerge as fragmented pieces and rarely preserve a clear lateral continuum between pedotypes; as such, direct observation of palaeopedogenetic evolutionary trends is generally not possible. In this regard, as an attempt to trace a common line on the evolution of the various analysed pedotypes, a suite of geochemical proxies (palaeosol weathering index, hydrolysis, calcification and oxidation) has been assessed to evaluate the common processes of alteration acting on palaeosols of the Serra da Galga Formation.

The degree of alteration of the palaeosols was measured by the palaeosol weathering index (PWI, after Gallagher and Sheldon, 2013), which considers the higher susceptibility of Na and K to leaching in comparison to Ca and Mg during soil development (Fig. 16A). The PWI effectively captures how the palaeosol composition differs from that of its parent material, whereby higher values indicate a similar composition to the parent material (i.e., low degree of development), and lower values indicate a higher geochemical differentiation (i.e., higher degree of development) (Gallagher and Sheldon, 2013). The PWI is applied in combination with other soil-forming processes (e.g., clay formation, calcification, hydrolysis, salinization and oxidation) to evaluate the trends in palaeopedogenetic degree of maturity within the palaeopedogenetic record of the Serra da Galga Formation (Fig. 16). The combination of the weathering indices permits the recognition of two trends in the degree of palaeopedogenetic evolution of pedotypes according to their apex-to-toe and channel-to-floodplain position.

7.1. Downdip geochemical trends in palaeosols

From apex-to-toe, the Inceptisols of the channel belt demonstrated a decrease in PWI values, indicating an increase in soil maturity towards
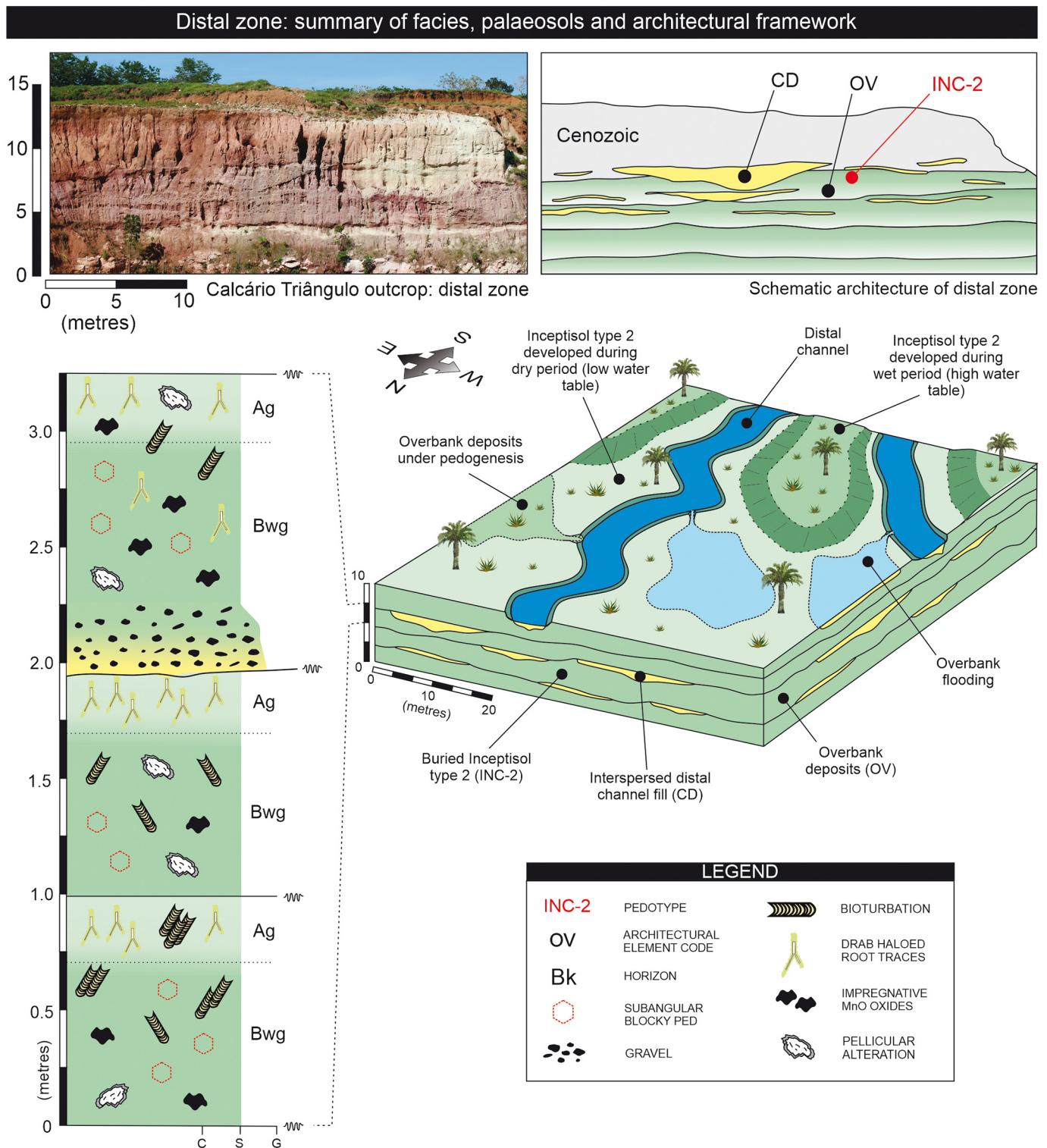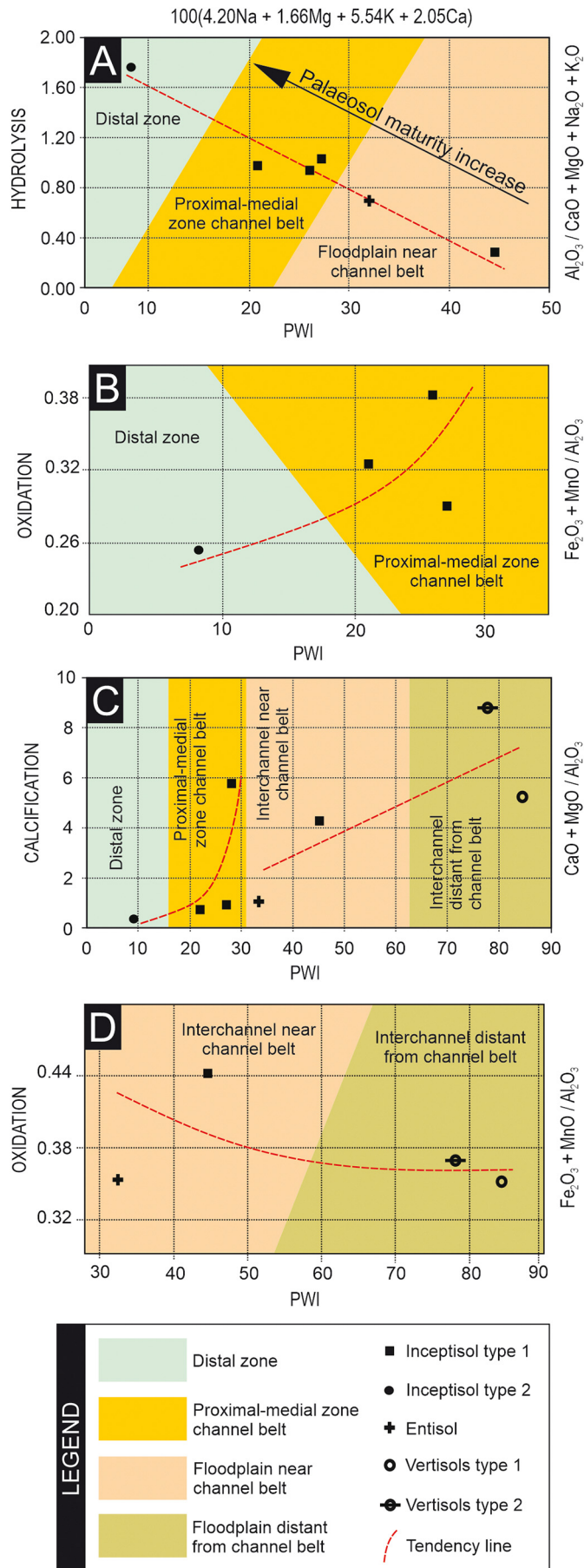
Fig. 15. Summary model depicting the typical vertical and lateral sedimentary architecture and distribution of palaeosols in the distal zone of the distributive fluvial system (Calcário Triângulo site, Fig. 1D). Architectural elements shown are (CD) distal channel fill and (OV) overbank deposit.

the distal zone. This downdip increase in maturity of channel belt palaeosols is also observed as a linear increase between PWI and hydrolysis from c. 1.76 to 1.03 (Fig. 16A). Hydrolysis is a common process associated with the formation of pedogenic clay, and its downdip increase in the Inceptisols probably reflects (i) the progression from chitonic to double-spaced porphyric c/f related distribution patterns, and (ii) the increase in abundance of subangular blocky peds towards the distal zone (Castellet and FitzPatrick, 1974; Kühn et al., 2010). Another

important controlling factor on the pedogenesis of the studied palaeosols is oxidation, which is controlled by topographic changes along the downdip DFS profile. The comparison between PWI and oxidation (Fig. 16B) demonstrates an exponential decrease from proximal, to medial, to distal palaeosols. This decrease in oxidation most likely reflects the downdip increase in reduction state of the Inceptisols, as attested by the intense gleying colours, impregnative MnO and quartz dissolution features encountered on the Inceptisols type 2 of the distal

LEGEND

Distal zone	■ Inceptisol type 1
Proximal-medial zone channel belt	● Inceptisol type 2
Floodplain near channel belt	✚ Entisol
Floodplain distant from channel belt	◯ Vertisols type 1
	⊖ Vertisols type 2
	╌ ╌ Tendency line

zone as a result of a shallow water table (Murphy and Kemp, 1984; McCarthy and Plint, 1998; Vepraskas, 2000, 2004; Kyuma, 2004; Sommer et al., 2006). Finally, the combination of PWI and calcification (Fig. 16C) demonstrates an exponential downdip decrease in carbonate accumulation in these palaeosols, thereby demonstrating a reduction in the effectiveness of drainage conditions towards the distal zone (Wright et al., 1995; Retallack, 2001), further corroborating the downdip shallowing of the water-table profile.

7.2. Along-strike geochemical trends in palaeosols

A second palaeopedogenetic trend (depicted in the medial zone) is observed in palaeosols profiles from channel belts towards floodplain environments. The combination of PWI and hydrolysis (Fig. 16A) shows a linear increase from the floodplain to the abandoned channel belt palaeosols, revealing an increase in palaeosol maturity towards the abandoned channel ridges. The higher maturity of Inceptisols occupying the abandoned channel ridges is a likely indicator of longer periods of stability of these areas due to their topographically elevated position on the alluvial surface (Törnqvist and Bridge, 2002). The relationship between PWI and calcification (Fig. 16C) shows a higher average degree of calcification of floodplain palaeosols compared to palaeosols of the channel belt. This along-strike increase is most likely caused by the increased root activity near the topographically lower floodplain areas closer to the water table; indeed, palaeosols of these areas (Vertisols type 1 and 2) reveal a greater abundance of rhizoliths and cytomorphic calcite. Additionally, the relative calcification increase in floodplain palaeosols away from the active channel belt (Fig. 16C) further indicates that such bioinduced calcification acted for longer periods over more distant floodplain reaches, where sedimentation episodes from channel floods were less frequent. The presence of Entisols near active channels indicate periods of stability in the order of hundreds of years (Allen and Wright, 1989), whereas Vertisols type 2 suggest a pause in local sedimentation for estimated periods of around 4 ky (Rodrigues et al., 2019). Finally, the PWI in combination with the oxidation index (Fig. 16D) reveals a slight decrease in oxidation towards the more distant reaches of the floodplain area, possibly indicating a closer proximity to the water-table level, as also observed from the horizontal rhizoliths and Asskm horizons of the Vertisols (Wright et al., 1995).

7.3. Vertical geochemical trends in palaeosols

Overall, the downdip and along-strike geochemical trends in palaeopedogenesis corroborate the notion that a series of autogenic factors (e.g., topography, sedimentation rate and biological communities) interplay to control the evolution of palaeosol profiles, whereas there is limited to no evidence of influence exerted by allogenic factors. However, the internal architecture of channel fills of the proximal zone demonstrates a stratigraphic organisation governed by high-frequency climate-induced cycles. Therefore, to test a possible palaeoclimatic influence on palaeosol evolution, this work further applied palaeoclimatic proxies (palaeoprecipitation and palaeotemperature) to evaluate the role played by climate on the formation and evolution of pedotypes. The MAP (mean annual precipitation), MAT (mean annual temperature) and MARP (mean annual range of precipitation) climofunctions were combined and plotted against stratigraphic level for the entire studied interval (Fig. 17) from the proximal to the medial zones of the distributive fluvial system (see Supplementary material 1 for further

Fig. 16. Downdip and along-strike geochemical trends in pedotypes. (A) Proximal-to-distal and floodplain-to-channel palaeosol maturity increase captured by the comparison between palaeosol weathering index (PWI) and hydrolysis. (B) Proximal-to-distal exponential decrease in the PWI-oxidation trend. (C) PWI-calcification trends showing exponential decrease from proximal to distal zones and linear increase from channel to floodplain palaeosols. (D) PWI-oxidation trend showing gentle decline in floodplain palaeosols away from the channel belt.
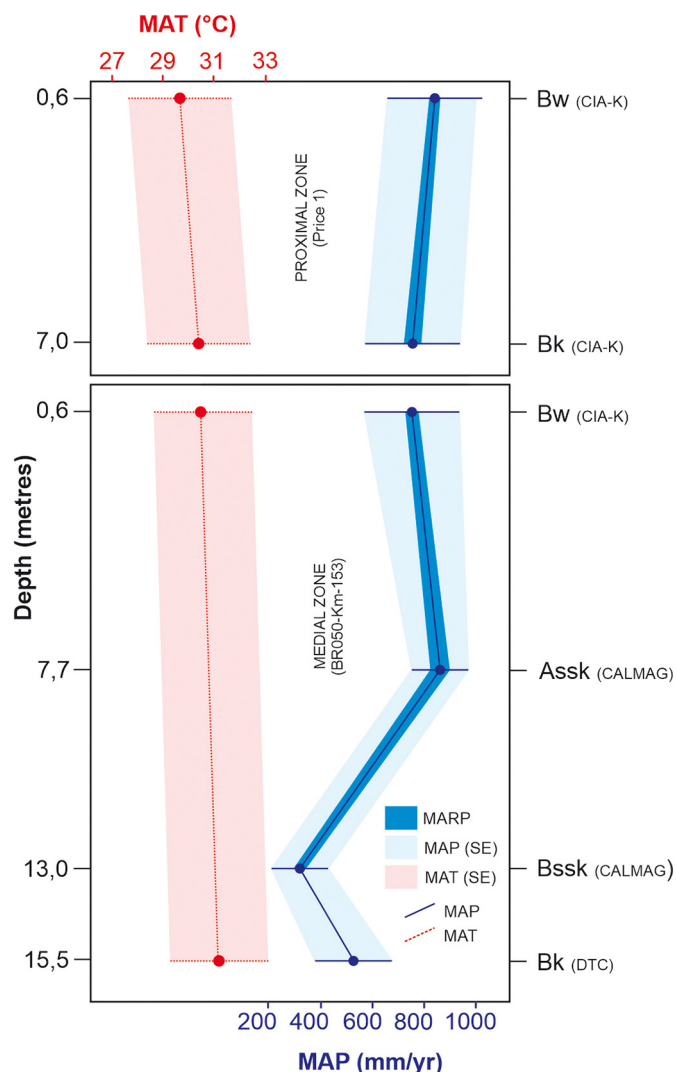
Fig. 17. Mean annual precipitation (MAP), mean annual range of precipitation (MARP) and mean annual temperature (MAT) estimates from pedotypes using CIA-K, CALMAG and DTC geochemical indices (see Supplementary material 1 for further definition). The standard errors are represented in light blue for palaeoprecipitation (MAP-SE) and light pink for palaeotemperature (MAT-SE).

explanation). The vertical analysis of the climofunction values revealed high-frequency variations in MAP, from 319 mm/yr to 866 mm/yr, following a low-frequency increase in precipitation and steady warm temperatures over the time interval. When compared to simulations of ocean-atmosphere global circulation models for the Late Cretaceous, the observed values are in agreement with the range of temperatures (20–35 °C) and palaeoprecipitation (365–1095 mm/yr) simulated for the study area (see Fig. 4 in Zhou et al., 2012); moreover, the climofunction values are in accord with palaeoclimatic reconstructions for the basin (Chumakov et al., 1995; Basilici and Dal' Bo, 2010; Arai and Dias-Brito, 2018). The observed high-frequency oscillations in precipitation might offer a plausible explanation for the variations in facies architecture of fluvial channel deposits (although the exact temporal scale between these two remains unconstrained), but these oscillations did not act as the main controlling mechanism in the vertical distribution of pedotypes. Also, pedotypes in the Serra da Galga Formation show a strong correlation to parent material, which further suggests that climate was not the main controlling factor (cf., Hartley et al., 2013). In this regard, the secondary role of climate on palaeopedogenesis is likely linked to the overall low maturity of the profiles, since this suggests that not enough time was

available for pedogenesis to adapt to the prevailing climatic conditions (Retallack, 2001). Nonetheless, a poorly defined climate-related geochemical signature can be inferred from the vertical organisation of the palaeosols, which demonstrates that climate played some role on the pedogenesis of this DFS succession.

8. Discussion

Along a downdip transect of more than 70 km within the Bauru Basin, the regional palaeodepositional and palaeoenvironmental reconstruction of the Serra da Galga Formation displays some of the typical characteristics of a distributive fluvial system succession, which can be summarised in a downdip change from dominantly sheet-like to dominantly ribbon-like channel bodies, accompanied by a downdip decrease in: (i) the proportion of channel fills, (ii) their degree of amalgamation, (iii) the inferred water discharge of their formative rivers, (iv) and their channel depth and width. These trends are parallelled by a downdip increase in: (v) proportion of overbank deposits and palaeosols, (vi) in palaeosols maturity, and (vii) in the record of hydromorphic conditions (Hartley et al., 2013; Weissmann et al., 2013). The presented data portrays two trends in the distribution of palaeosols and sediments of the studied distributive fluvial system: (i) a regional downdip trend, from proximal to distal zones, and (ii) a local along-strike trend, from channel belts to parts of the floodplain located furthest from contemporaneous channel belts.

8.1. Downdip palaeopedogenetic model

Analyses of downdip trends of the DSF succession highlight that palaeosols display an important variation in proportion, corresponding to c. 37% of the stratigraphic interval in the proximal zone, passing to c. 62% in the medial zone to reach c. 90% of the succession of the distal zone. This variation in cumulative thickness is further followed by a change in pedotypes, which reflects a progressive downdip increase in maturity towards more poorly drained palaeosols (Fig. 18).

The studied proximal zone of the DFS succession preserves exclusively the depositional record of channel fills bounded by Inceptisols type 1. The porous sandy material of these palaeosols, exhibiting single-grain microstructure and connective packing voids, combined with their higher topographic distance to the water table near the DFS apex, resulted in the development of well-drained profiles; stages I to II in carbonate accumulation (sensu Gile et al., 1966) in their Bk horizons suggest that pedogenesis over these abandoned channel belts spanned approximately 2.6–10 ky (Gile et al., 1966; Machette, 1985). This short interavulsion frequency demonstrates the cannibalistic behaviour of channel belts of the proximal zone (Steel and Thompson, 1983), which is most probably the cause for the absence or scarcity of overbank deposits and associated palaeosols (Fig. 13).

Towards the medial zone, the preserved record of overbank deposits and their associated palaeosols (Inceptisols type 1, Entisols and Vertisols type 1 and 2) indicate an increase in the period over which a formerly channelised portion of the fan surface remains abandoned. Accordingly, the Inceptisols type 1 of channel belts of the medial zone demonstrate a more advanced stage of carbonate accumulation (stage III sensu Gile et al., 1966), which indicates pedogenesis in the order of few 10 ky (Gile et al., 1966; Machette, 1985). The increase in abandonment time of the depositional surface most likely results from the radiation of channels from the fan apex (Weissmann et al., 2013). Additionally, the medial zone records a downdip increase in water-saturated profiles, as attested by the appearance of horizontally coalescent rhizoliths in Bssk (Vertisol type 1) and Asskm (Vertisol type 2) horizons as also the redoximorphic hypocoatings, interpedal mangans and impregnative Mn oxides in Bsskg-Bssg horizons (Vertisol type 2) (Fig. 14); this increase in redoximorphic features towards the medial zone suggests that
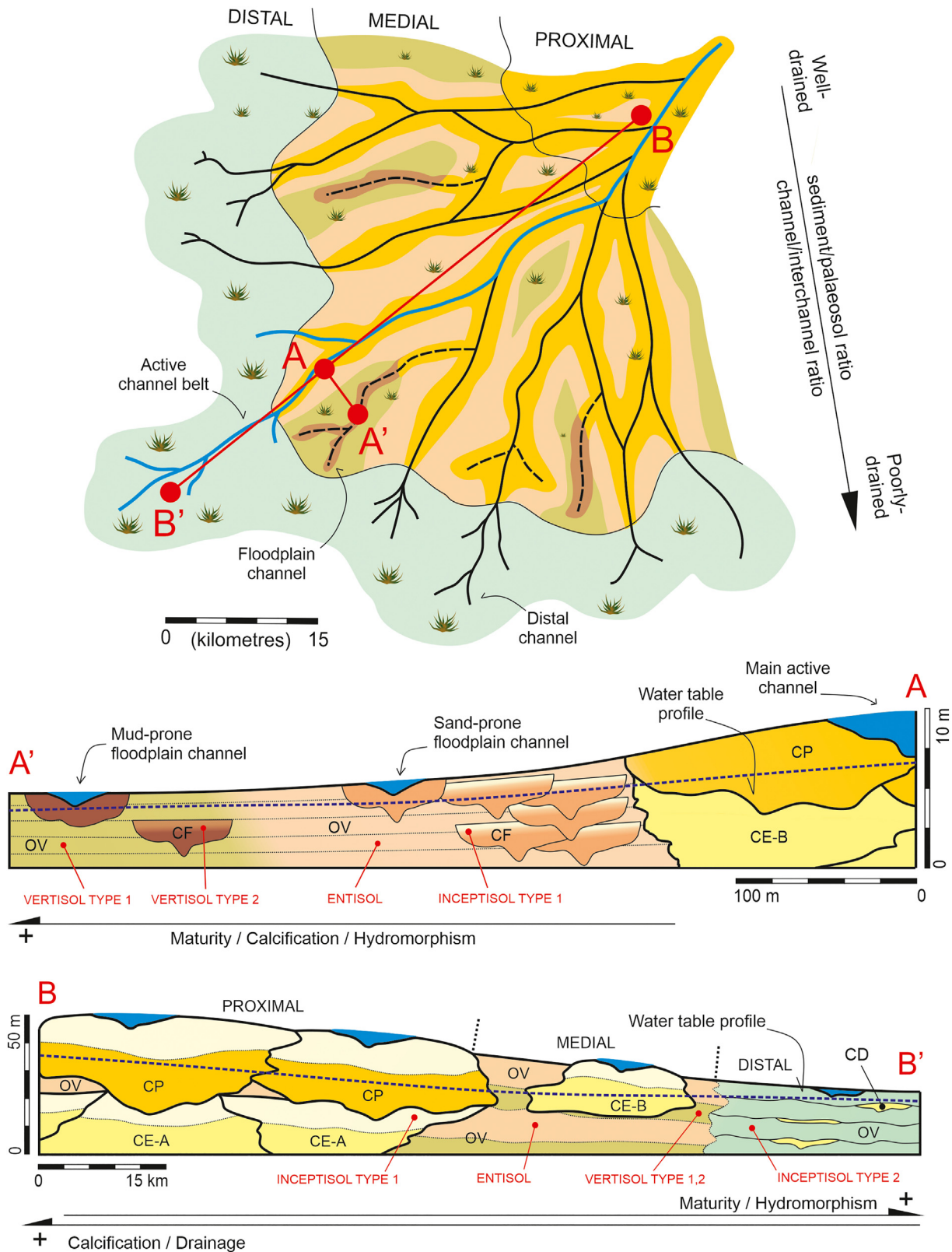
Fig. 18. Palaeopedogenetic model of the Serra da Galga DFS showing schematic plan view, along-strike (A–A′) and downdip (B–B′) organisation of sediments and palaeosols, with further indications of water table profile and geochemical trends. Scales used are for indicative purposes.

topographic lowering of the floodplain areas closer to the water table (Wright et al., 1995).

The lowest topographic elevation of the DFS profile towards the distal zone is recorded by the sole presence of water-saturated palaeosol profiles (Figs. 16B, 18). The distal zone is characterised

by composite profiles formed solely of poorly drained Inceptisols type 2, which reveal redoximorphic grey colours and contain abundant Mn oxide impregnations and quartz grains with corroded margins. In this case, these features indicate a palaeoenvironment marked by excessively long periods of stagnant and anoxic water

(McCarthy and Plint, 1998; Vepraskas, 2004; Sommer et al., 2006) likely associated with a near-surface water table (Murphy and Kemp, 1984), which is further supported by the exponential downdip decrease in palaeosol oxidation towards the distal zone (Figs. 16B, 18). The observed downdip hydrological control has been previously noticed in modern distributive fluvial systems (Hartley et al., 2013), as well as in the geological record (Atkinson, 1986; Besley and Fielding, 1989; Platt and Keller, 1992; McCarthy et al., 1997; Weissmann et al., 2013; Owen et al., 2015). Finally, the increase in palaeosols maturity towards the distal zone is evidenced by the increase in argilloturbation (single to double spaced porphyric c/f related distribution pattern and subangular blocky peds) in the Inceptisols of type 2 and by the linear increase in the PWI-hydrolysis relationship towards the distal zone of the DFS (Fig. 18).

Overall, the analysis of pedotypes in the Serra da Galga Formation DFS revealed poorly developed profiles, most probably due to relatively high sedimentation rates (Kraus, 1999) and to the relatively small radius of the network of distributive channels promoting short abandonment time of fan surfaces (Hartley et al., 2013). In fact, avulsion is a ubiquitous process in DFS construction, so their preserved palaeosols (as well as their modern soils) are naturally poorly developed (e.g., Pilcomayo, Bermejo, Tista and Okavango DFS; Hartley et al., 2013). However, despite the low maturity of the studied palaeosols, the combined application of macro-, micromorphological and geochemical approaches taken in this work offered a more robust diagnostic toolbox for the recognition of downdip changes in palaeosols maturity, compared to the classic macromorphological approach.

8.2. Along-strike palaeopedogenetic model

The palaeosol record of the medial zone (BR050-Km-153 site; Fig. 1D) exemplifies the lateral organisation of pedotypes that increase in maturity, bioinduced calcification and hydromorphism with increasing distance from an active channel belt. This palaeopedogenetic trend is observed on palaeosols developed on both overbank deposits and floodplain channel fills.

In the floodplain environment, hiatuses between each flood allowed pedogenesis to occur. Because pedogenesis was penecontemporaneous with sedimentation, the maturity of the floodplain palaeosols reflects the decrease in rate of sedimentation away from the active channel belt (Bown and Kraus, 1993). Floodplain areas marked by compound Entisols with abundant pedorelicts demonstrate their probable proximity to active channels (Kühn et al., 2010). Moreover, the early stages of root development and poor horizonation of the Entisols show that time intervals between floods probably did not exceed a few hundred years (Allen and Wright, 1989; Alonso-Zarza, 1999). Likewise, the interbedding of sand-prone floodplain channel fills further corroborates the proximity to active channels, and their association with Inceptisols of type 1, which display poor to absent carbonate accumulation, suggests breaks in sedimentation of up to c. 2.6 ky (Gile et al., 1966). Moreover, the single to pellicular grain microstructure and pink colours of the uppermost A horizons (Entisols) and A-Bw horizons (Inceptisols type 1) of these pedotypes indicate well-drained profiles (Theocharopoulos and Dalrymple, 1987; Kühn et al., 2010). However, with increasing distance from the active channels, the floodplain area was subject to the development of Vertisols, formed over mud-prone overbank deposits (Vertisols type 1) and mud-prone floodplain channel fills (Vertisols type 2). The ubiquitous presence of horizontal rhizoliths in the upper horizons of both pedotypes further suggests closer proximity to the water table (Wright et al., 1995). Likewise, the high content in hydromorphic features of Vertisols (e.g., impregnative Mn oxides, reduced hypocoatings, interpedal mangans), and their decrease in oxidation index away from channel deposits (Fig. 16D), indicate more poorly drained conditions due to the higher clay groundmass of their parent material (Lindbo et al., 2010). The combination of well-developed rhizoliths and hydromorphic features indicates a palaeopedogenetic evolution in the order of 4 ky (Rodrigues et al., 2019) for floodplain

areas located furthest from the active channel belts. The increase in palaeopedogenetic maturity is further evidenced by the marked rise in bioinduced calcification (Fig. 16C) and by the increase in the thickness and horizonation of pedotypes away from the active channel belt.

The thick accumulation of poorly developed pedotypes in the floodplain record indicates a relatively low topographic position on the DFS surface, which results from differences in sedimentation rates between the floodplain and the channel belt (Pizzuto, 1987). Channel aggradation led to the rapid growth of the topographic surface of channel belts (Makaske, 2001; Aslan et al., 2005), inhibiting pedogenesis during this process. Consequently, the depositional surface around active channels reached a stage where the gradient away from the channel belt was higher than the down-fan gradient, driving the avulsion of the belt and abandonment of a topographically elevated ridge (Jones and Schumm, 1999; Törnqvist and Bridge, 2002). After avulsion, the elevated ridge remained at some distance laterally away from the new active channel belt; the combination of both the elevated topography and higher lateral distance from the active channel belt probably reduced the susceptibility to channel-belt reoccupation, leading to longer intervals of palaeopedogenetic evolution (in the order of 10 ky at the medial zone). Because of the geomorphologic stability of alluvial ridges, their sandy parent material and their higher separation from the water table, relatively more mature, thicker and well-drained Inceptisols type 1 could develop (Kühn et al., 2010).

9. Conclusions

This study has defined the landscape and depositional controls on palaeosols of a distributive fluvial system, based on the study of the Serra da Galga Formation (Bauru Basin, SE Brazil). The work describes the stratigraphic organisation and the relationships between sediments and palaeosols for a succession embodying the proximal, medial and distal zones of an Upper Cretaceous distributive fluvial system. The genetic association between sediments and palaeosols has permitted the identification of five pedotypes. Macro-, micromorphological and geochemical analyses of pedotypes have been applied to unravel the factors controlling the spatial variability and genesis of the pedotypes. Two major palaeopedogenetic trends describe the distribution of pedotypes in the studied succession:

1. The first palaeopedogenetic trend is depicted in a regional downdip direction (c. 70 km long) from the proximal to the distal zone of the formative fan. Palaeosols demonstrate a clear downdip increase in proportion (from c. 37% to 90% of total succession) and a change in pedotypes that reflects a progressive increase in maturity towards more poorly drained palaeosols. From the proximal to the medial zone, well-drained Inceptisols (type 1) recorded an increase in maturity (from c. 2.6 to more than 10 ky) as result of progressively longer periods of surface abandonment associated with the radial avulsion of channels, which further led to the preservation of floodplain pedotypes recording hydromorphic features formed by intermittent near-surface water table. In the most distal zone, more mature and hydromorphic Inceptisols (type 2) developed during longer periods of stagnant near-surface water table. Finally, from apex to toe, the marked increase in hydromorphism is controlled by the progressive lowering of the topographic surface towards the regional water table, whereas the increase in maturity is associated with a down-system increase in fan-surface stability.

2. The second palaeopedogenetic trend is observed in the medial zone and records the transition of pedotypes from channel-belt to floodplain settings. In the floodplain setting, because pedogenesis was penecontemporaneous with sedimentation, the maturity of the pedotypes was controlled by a decreasing rate of sedimentation away from the active channel belt, varying from Entisols and poorly developed Inceptisols (type 1) close to active channels, to Vertisols (types 1 and 2) in more distant parts of the floodplain environment.

These pedotypes display an increase in maturity indicative of the time required for their development from few hundred years near active channels, to c. 4 ky in more distant parts of the floodplain area. Overall, the thick accumulation of poorly developed pedotypes in the floodplain record reflects the topographically depressed character of this setting in comparison to the superelevated alluvial ridges. Channel-belt avulsion results in a topographically elevated ridge located at some distance away from the new active channel belt, and elevated considerably above the water table, leading to the formation of more mature and better drained Inceptisols (type 1), compared to floodplain pedotypes.

These downdip and along-strike pedosedimentary models reflect the overriding influence of topography, sedimentation rates and parent material on the stratigraphic organisation of palaeosols. Finally, the overall poor grade of development of the studied pedotypes shows that sedimentation rate and accommodation were high enough in this system so as to prevent a significant control by climate on palaeosol development.

Supplementary data to this article can be found online at https://doi.org/10.1016/j.sedgeo.2020.105774.

Declaration of competing interest

The authors declare that they have no known competing financial interests or personal relationships that could have appeared to influence the work reported in this paper.

Acknowledgements

References

Abdullatif, O.M., 1989. Channel-fill and sheet-flood facies sequences in the ephemeral River Gash, Kassala, Sudan. Sedimentary Geology 63, 171–184.

Ahmad, N., 1983. Vertisols. In: Wilding, L.P., Smeck, N.E., Hall, G.F. (Eds.), Pedogenesis and Soil Taxonomy II. The Soil Orders. Developments in Soil Science vol. 11. Elsevier, Amsterdam, pp. 91–123.

Allen, J.R.L., 1965. A review of the origin and characteristics of recent alluvial sediments. Sedimentology 5, 89–191.

Allen, J.R.L., Wright, V.P., 1989. Paleosols in Siliciclastic Sequences. PRIS University of Reading (97 pp.).

Alonso-Zarza, A.M., 1999. Initial stages of laminar calcrete formation by roots: examples from the Neogene of central Spain. Sedimentary Geology 126, 177–191.

Arai, M., Dias-Brito, D., 2018. The Ibaté paleolake in SE Brazil: record of an exceptional late Santonian palynoflora with multiple significance (chronostratigraphy, paleoecology and paleophytogeography). Cretaceous Research 84, 264–285.

Aslan, A., Autin, W.J., Blum, M.D., 2005. Causes of river avulsion: insights from the Late Holocene avulsion history of the Mississippi River, U.S.A. Journal of Sedimentary Research 75, 648–662.

Atkinson, C.D., 1986. Tectonic control on alluvial sedimentation as revealed by an ancient catena in the Capella Formation (Eocene) of northern Spain. In: Wright, V.P. (Ed.), Paleosols: Their Recognition and Interpretation. Princeton University Press, Princeton, New Jersey, pp. 139–179.

Banham, S.G., Mountney, N.P., 2014. Climatic versus halokinetic control on sedimentation in a dryland fluvial succession: Triassic Moenkopi Formation, Utah, USA. Sedimentology 61, 570–608.

Basilici, G., Dal' Bo, P.F., 2010. Anatomy and controlling factors of a Late Cretaceous Aeolian sand sheet: the Marília and the Adamantina formations, NW Bauru Basin, Brazil. Sedimentary Geology 226, 71–93.

Basilici, G., Dal' Bó, P.F.F., Ladeira, F.S., 2009. Climate-induced sediment-palaeosol cycles in a Late Cretaceous dry aeolian sand sheet: Marília Formation (North-West Bauru Basin, Brazil). Sedimentology 56, 1876–1904.

Basilici, G., Dal' Bó, P.F.F., Oliveira, E.F., 2016. Distribution of palaeosols and deposits in the temporal evolution of a semiarid fluvial distributary system (Bauru Group, Upper Cretaceous, SE Brazil). Sedimentary Geology 341, 245–264.

Basilici, G., Fiorelli, L.E., Dal' Bo, P.F., Fiorelli, L.E., 2019. Comment on "Evolution and palaeoenvironment of the Bauru Basin (Upper Cretaceous, Brazil)" by Luiz Alberto Fernandes and Claudia Maria Magalhaes Ribeiro. Journal of South American Earth Sciences 91, 389–393.

Besley, B.M., Fielding, C.R., 1989. Paleosols in Westphalian coal-bearing and red-bed sequences, central and northern England. Paleogeography, Paleoclimatology, Paleoecology 70, 303–330.

Best, J., Woodward, J., Ashworth, P., Smith, G.S., Simpson, C., 2006. Bar-top hollows: a new element in the architecture of sandy braided rivers. Sedimentary Geology 190, 241–255.

Blair, T.C., McPherson, J.G., 1994. Alluvial fans and their natural distinction from rivers based on morphology, hydraulic processes, sedimentary processes and facies assemblages. Journal of Sedimentary Research 64, 450–489.

Bown, T.M., Kraus, M.J., 1993. Time-stratigraphic reconstruction and integration of paleopedologic, sedimentologic, and Biotic events (Willwood Formation, Lower Eocene, Northwest Wyoming, U.S.A.). Palaios 8, 68–80.

Brewer, R., 1964. Fabric and Mineral Analysis of Soils. Wiley and Sons, New York (470 pp.).

Bridge, J.S., 2003. Rivers and Floodplains: Forms, Processes and Sedimentary Record. Blackwell Publishing, Oxford, Oxford, U.K. (504 pp.).

Bridge, J.S., 2006. Fluvial facies models: recent developments. In: Posamentier, H.W., Walker, R.G. (Eds.), Facies Models Revisited. Facies Models Revisited, SEPM Special Publication 84, pp. 85–170.

Buczynski, C., Chafetz, H.S., 1987. Siliciclastic grain breakage and displacement due to carbonate crystal growth: an example from the Lenders Formation, Permian of North Central Texas, USA. Sedimentology 34, 837–843.

Bullock, P., Fedoroff, N., Jongerius, A., Stoops, G., Tursina, T., 1985. Handbook for Soil Thin Section Description. Waine Research Publications, Wolverhampton.

Burns, C.E., Mountney, N.P., Hodgson, D.M., Colombera, L., 2017. Anatomy and dimensions of fluvial crevasse-splay deposits: examples from the Cretaceous Castlegate sandstone and Neslen formation, Utah, USA. Sedimentary Geology 351, 21–35.

Burns, C.E., Mountney, N.P., Hodgson, D.M., Colombera, L., 2019. Stratigraphic architecture and hierarchy of fluvial overbank crevasse-splay deposits. Journal of the Geological Society of London 176, 629–649.

Cain, S.A., Mountney, N.P., 2009. Spatial and temporal evolution of a terminal fluvial fan system: the Permian Organ Rock Formation, South-east Utah, USA. Sedimentology 56, 1774–1800.

Castellet, J.T., FitzPatrick, E.A., 1974. Clay cutans and matrix disruption in some soils form central Spain. In: Rutherford, G.K. (Ed.), Soil Microscopy. The Limestone Press, Kingston, Ontario, pp. 632–641.

Catt, J.A., 1990. Field recognition, description and spatial relationships of paleosols: paleopedology manual. Quaternary International 6, 2–95.

Chakraborty, C., Bose, P.K., 1992. Ripple/dune to upper stage plane bed transition: some observations from the ancient record. Geological Journal 27, 349–359.

Chumakov, N.M., Zharkov, M.A., Herman, A.B., Doludenko, M.P., Kalandadze, N.N., Lebedev, E.L., Ponomarenko, A.G., Rautian, A.S., 1995. Climatic zones in the middle of the Cretaceous Period. Stratigraphy and Geological Correlation 3, 3–14.

Collinson, J.D., Mountney, N.P., 2019. Sedimentary Structures. Fourth edition. Dunedin Academic Press, Edinburgh, Scotland (340 pp.).

Colombera, L., Mountney, N.P., 2019. The lithofacies organization of fluvial channel deposits: a meta-analysis of modern rivers. Sedimentary Geology 383, 16–40.

Costa, J.E., 1988. Rheologic, geomorphic and sedimentologic differentiation of water floods, hyperconcentrated flows and debris flows. In: Baker, V.R., Kochel, R.C., Patton, P.C. (Eds.), Flood Geomorphology. John Wiley and Sons, Inc., Chichester, pp. 113–122.

Coulombe, C.E., Dixon, J.B., Wilding, L.P., 1996. Mineralogy and chemistry of Vertisols. In: Ahmad, N., Mermut, A. (Eds.), Vertisols and Technologies for Their Management. Developments in Soil Science vol. 24. Elsevier, Amsterdam, pp. 115–200.

Coutinho, J.M.V., Coimbra, A.M., Brandt Neto, M., Rocha, G.A., 1982. Lavas alcalinas analcimíticas associadas ao Grupo Bauru (Kb) no Estado de São Paulo, Brasil. Congresso Latinoamericano de Geologia 5, 185–196.

Dal' Bó, P.F.F., Basilici, G., Angélica, R.S., 2010. Factors of paleosol formation in a Late Cretaceous eolian sand sheet paleoenvironment, Marilia Formation, Southeastern Brazil. Palaeogeography, Palaeoclimatology, Palaeoecology 292, 349–365.

Dal' Bó, P.F., Soares, M.V.T., Basilici, G., Rodrigues, A.G., Menezes, M.N., 2019. Spatial variations in distributive fluvial system architecture of the Upper Cretaceous Marília Formation, SE Brazil. In: Corbett, P.W.M., Owen, A., Hartley, A.J., Pla-Pueyo, S., Barreto, D., Hackney, C., Kape, S.J. (Eds.), River to Reservoir: Geoscience to Engineering. Geological Society of London Special Publications vol. 488, pp. 97–118.

Dasgupta, S., Ghosh, P., Gierlowski-Kordesch, E.H., 2017. A discontinuous ephemeral stream transporting mud aggregates in a continental rift basin: the Late Triassic Maleri Formation, India. Journal of Sedimentary Research 87, 838–865.

DeCelles, P.G., Cavazza, W., 1999. A comparison of fluvial megafans in the Cordilleran (Upper Cretaceous) and modern Himalayan foreland basin systems. Geological Society of America Bulletin 111, 1315–1334.

Dias-Brito, D., Musacchio, E.A., Castro, J.C., Maranhão, M.S.A.S., Suárez, J.M., Rodrigues, R., 2001. Grupo Bauru: uma unidade continental do Cretáceo do Brasil – Concepções baseadas em dados micropaleontológicos, isotópicos e estratigráficos. Revue Paléobiologie 2, 195–304.

Durand, N., Monger, H.C., Canti, M.G., Verrecchia, E., 2010. Calcium carbonate features. In: Stoops, G., Marcelino, V., Mees, F. (Eds.), Interpretation of Micromorphological Features of Soils and Regoliths, 2nd edition Elsevier, Amsterdam, pp. 205–258.

Ekes, C., 1993. Bedload-transported pedogenic mud aggregates in the Lower Old Red Sandstone in southwest Wales. Journal of the Geological Society of London 150, 469–472.

Fernandes, L.A., Basilici, G., 2009. Transition of ephemeral palustrine to aeolian deposits in a continental arid – semi-arid environment (Upper Cretaceous Bauru Basin, Brazil). Cretaceous Research 30, 605–614.

Fernandes, L.A., Coimbra, A.M., 1994. O Grupo Caiuá (Ks): revisão estratigráfica e contexto deposicional. Revista Brasileira de Geociencias 24, 164–176.

Fernandes, L.A., Coimbra, A.M., 2000. Revisão estratigráfica da parte oriental da Bacia Bauru (Neocretáceo). Revista Brasileira de Geociencias 30, 717–728.

Fielding, C.R., 2006. Upper flow regime sheets, lenses and scour fills: extending the range of architectural elements for fluvial sediment bodies. Sedimentary Geology 190, 227–240.

Fitzpatrick, E.A., 1983. Soils-Their Formation, Classification and Distribution. Longman, London (353 pp.).

Friend, P.F., 1978. Distinctive features of some ancient river systems. In: Miall, A.D. (Ed.), Fluvial Sedimentology. Canadian Society of Petroleum Geologists Memoir vol. 5, pp. 531–542.

Friend, P.F., Slater, M.J., Williams, R.C., 1979. Vertical and lateral building of river sandstone bodies, Ebro Basin, Spain. Journal of the Geological Society of London 136, 39–46.

Gallagher, T.M., Sheldon, N.D., 2013. A new paleothermometer for forest paleosols and its implications for Cenozoic climate. Geology 41, 647–650.

Gibling, M.R., 2006. Width and thickness of fluvial channel Bodies and valley fills in the geological record: a literature compilation and classification. Journal of Sedimentary Research 76, 731–770.

Gibling, M., Rust, B.R., 1984. Channel margins in a Pennsylvanian braided, fluvial deposit: the Morien Group near Sydney, Nova Scotia, Canada. Journal of Sedimentary Petrology 54, 773–782.

Gierlowski-Kordesch, E.H., Gibling, M.R., 2002. Pedogenic mud aggregates in rift sedimentation. In: Renaut, R.W., Ashley, G.M. (Eds.), Sedimentation in Continental Rifts. SEPM Special Publication vol. 73, pp. 195–206.

Gile, L.H., Peterson, F.F., Grossman, R.B., 1966. Morphological and genetic sequences of carbonate accumulation in desert soils. Soil Science 101, 347–360.

Gill, D., 1977. Salina A-1 sabkha cycles and the Late Silurian paleo-geography of the Michigan Basin. Journal of Sedimentary Petrology 47, 979–1017.

Goldberg, K., Garcia, A.J.V., 2000. Palaeobiogeography of the Bauru Group, a dinosaur-bearing Cretaceous unit, northeastern Paraná Basin, Brazil. Cretaceous Research 21, 241–254.

Gómez-Gras, D., Alonso-Zarza, A.M., 2003. Reworked calcretes: their significance in the reconstruction of alluvial sequences (Permian and Triassic, Minorca, Balearic Islands, Spain). Sedimentary Geology 158, 299–319.

Hansford, M.R., Plink-Björklund, P., 2020. River discharge variability as the link between climate and fluvial fan formation. Geology. https://doi.org/10.1130/G47471.1.

Harms, J.C., Southard, J.B., Walker, R.G., 1982. Structures and sequences in clastic rocks. Society of Economic Paleontologists and Mineralogists Short Course, No. 9.

Hartley, A.J., Weissmann, G.S., Battacharayya, P., Nichols, G.J., Scuderi, L.A., Davidson, S.K., Ghosh, P., 2013. Soil development on modern distributive fluvial systems: preliminary observations with implications for interpretation of paleosols in the rock record. In: Dreise, S.G., Nordt, L.C., McCarthy, P.L. (Eds.), New Frontiers in Paleopedology and Terrestrial Paleoclimatology. SEPM, Special Publication vol. 104, pp. 149–158.

Hassan, M.A., 2005. Characteristics of gravel bars in ephemeral streams. Journal of Sedimentary Research 75, 29–42.

Jobe, Z.R., Bernhardt, A., Lowe, D.R., 2010. Facies and architectural asymmetry in a conglomerate-rich submarine channel fill, Cerro Toro Formation, Sierra del Toro, Magallanes Basin, Chile. Journal of Sedimentary Research 80, 1085–1108.

Jones, L.S., Schumm, S.A., 1999. Causes of avulsion: an overview. In: Smith, N.D., Rogers, J. (Eds.), Fluvial Sedimentology VI Special Publication. International Association of Sedimentologists Special Publication vol. 28, pp. 171–178.

Jopling, A.V., 1965. Hydraulic factors and shape of laminae. Journal of Sedimentary Petrology 35, 777–791.

Jopling, A.V., Walker, R.G., 1968. Morphology and origin of ripples-drift cross-lamination, with examples from the Pleistocene of Massachusetts. Journal of Sedimentary Petrology 38, 971–984.

Kelly, S.B., Olsen, H., 1993. Terminal fans - a review with reference to Devonian examples. Sedimentary Geology 85, 339–374.

Khadkikar, A.S., Merh, S.S., Malik, J.N., Chamyal, L.S., 1998. Calcretes in semi-arid alluvial systems: formative pathways and sinks. Sedimentary Geology 116, 251–260.

Klappa, C.F., 1980. Rhizoliths in terrestrial carbonates: classification, recognition, genesis and significance. Sedimentology 27, 613–629.

Klimek, K., 1974. The retreat of alluvial river banks in the Wisloka Valley (South Poland). Geographia Polonica 28, 59–75.

Kraus, M.J., 1999. Paleosols in clastic sedimentary rocks: their geologic applications. Earth-Science Reviews 47, 41–70.

Kraus, M.J., Hasiotis, S.T., 2006. Significance of different modes of rhizolith preservation to interpreting paleoenvironmental and paleohydrologic settings: examples from Paleogene paleosols, Bighorn Basin, Wyoming, U.S.A. Journal of Sedimentary Research 76, 633–646.

Kühn, P., Aguilar, J., Miedema, R., Bronnikova, M., 2010. Textural pedofeatures and related horizons. In: Stoops, G., Marcelino, V., Mees, F. (Eds.), Interpretation of Micromorphological Features of Soils and Regoliths, 2nd edition Elsevier, Amsterdam, pp. 377–423.

Kyuma, K., 2004. Paddy Soil Science. Kyoto University Press and Trans Pacific Press, Melbourne, Australia (280 pp.).

Leier, A.L., DeCelles, P.G., Pelletier, J.D., 2005. Mountains, monsoons, and megafans. Geology 33, 289–292.

Li, J., Vandenberghe, J., Mountney, N.P., Luthi, S.M., 2020. Grain-size variability of point-bar deposits from a fine-grained dryland river terminus, Southern Altiplano, Bolivia. Sedimentary Geology, 105663 https://doi.org/10.1016/j.sedgeo.2020.105663.

Lindbo, D.L., Stolt, M.H., Vepraskas, M.J., 2010. Redoximorphic features. In: Stoops, G., Marcelino, V., Mees, F. (Eds.), Interpretation of Micromorphological Features of Soils and Regoliths, 2nd edition Elsevier, Amsterdam, pp. 129–147.

Lisle, T.E., Ikeda, H., Iseya, F., 1991. Formation of stationary alternate bars in a steep channel with mixed-size sediment: a flume experiment. Earth Surface Processes and Landforms 16, 463–469.

Lunt, I.A., Bridge, S., 2007. Formation and preservation of open-framework gravel strata in unidirectional flows. Sedimentology 54, 71–87.

Machette, M.N., 1985. Calcific soils of the southwestern United States. In: Weide, D.L. (Ed.), Soils and Quaternary Geology of the Southwestern United States. Geological Society of America, Special Paper vol. 203, pp. 1–21.

Makaske, B., 2001. Anastomosing rivers: a review of their classification, origin and sedimentary products. Earth-Science Reviews 53, 149–196.

Mann, A.W., Horwitz, R.C., 1979. Groundwater calcrete deposits in Australia: some observations from Western Australia. Journal of the Geological Society of Australia 26, 293–303.

Martinelli, A.G., Teixeira, V.P.A., 2015. The Late Cretaceous vertebrate record from the Bauru Group at the Triângulo Mineiro, southeastern Brazil. Boletín Geologico y Minero de España 126, 129–158.

Martinelli, A.G., Bogan, S., Agnolin, F.L., Ribeiro, L.C.B., Cavellani, C.L., Ferraz, M.L.F., Teixeira, V.P.A., 2013. First fossil record of amiid fishes (Halecomorphi, Amiiformes, Amiidae) from the Late Cretaceous of Uberaba, Minas Gerais State, Brazil. Alcheringa: An Australasian Journal of Palaeontology 37, 105–113.

Martinelli, A.G., Basilici, G., Fiorelli, L.E., Klock, C., Karfunkele, J., Diniz, A.C., Soares, M.V.T., Marconato, A., Silva, J.I., Ribeiro, L.C.B., Marinho, T.S., 2019. Palaeoecological implications of an Upper Cretaceous tetrapod burrow (Bauru Basin; Peirópolis, Minas Gerais, Brazil). Palaeogeography, Palaeoclimatology, Palaeoecology 528, 147–159.

McCarthy, P.J., Plint, A.G., 1998. Recognition of interfluve sequence boundaries: integrating paleopedology and sequence stratigraphy. Geology 26, 387–390.

McCarthy, P.J., Martini, I.P., Leckie, D.A., 1997. Anatomy and evolution of a Lower Cretaceous alluvial plain: sedimentology and paleosols of the Upper Blairmore Group, southwestern Alberta, Canada. Sedimentology 44, 197–220.

McIntyre, D.S., 1976. Subplasticity in Australian soils. I Description, occurrence and some propertires. Australian Journal of Soil Research 14 (3), 227–236.

Mermut, A.R., Dasog, G.S., Dowuona, G.N., 1996. Soil morphology. In: Ahmad, N., Mermut, A. (Eds.), Vertisols and Technologies for Their Management. Developments in Soil Science vol. 24. Elsevier, Amsterdam, pp. 89–114.

Miall, A.D., 2006. The Geology of Fluvial Deposits: Sedimentary Facies, Basin Analysis and Petroleum Geology. Springer, Berlin.

Mohr, E.C.J., Van Baren, F.A., Van Schuylenborgh, J., 1972. Tropical Soils. Mouton, The Hague (481 pp.).

Mukerji, A.B., 1976. Terminal fans of inland streams in Sutlej-Yamuna Plain, India. Zeitschrift für Geomorphologie 20, 190–204.

Murphy, C.P., Kemp, R.A., 1984. The over-estimation of clay and the under-estimation of pores in soil thin sections. Journal of Soil Science 35, 481–495.

Nemec, W., Steel, R.J., 1984. Alluvial and coastal conglomerates: their significant features and some comments on gravelly mass-flow deposits. In: Koster, E.H., Steel, R.J. (Eds.), Sedimentology of Gravels and Conglomerates. Canadian Society of Petroleum Geologists Memoir vol. 10, pp. 1–31.

Netterberg, F., 1969. The interpretation of some basin calcrete types. South Africa Archaeology Bulletin 24, 117–122.

Nichols, G.J., Fisher, J.A., 2007. Processes, facies and architecture of fluvial distributary system deposits. Sedimentary Geology 195, 75–90.

North, C.P., Warwick, G.L., 2007. Distributive fluvial systems: myths, misconceptions, and the end of the terminal-fan model. Journal of Sedimentary Research 77, 693–701.

Novas, F.E., Carvalho, I.S., Ribeiro, L.C.B., Méndez, A.H., 2008. First abelisaurid bone remains from the Maastrichtian Marília Formation, Bauru Group, Brazil. Cretaceous Research 29, 625–635.

Oest, C., 2015. Paleopedology and Fluvial Sedimentology of the Upper Devonian Catskill Formation, Central Pennsylvania: A Test of the Distributive Fluvial System Model. Temple University, Pennsylvania, USA (Master Thesis, 115 pp.).

Olsen, H., 1987. Ancient ephemeral stream deposits: a local terminal fan model from the Bunter Sandstone Formation (L. Triassic) in the Tønder-3, -4 and -5 wells, Denmark. In: Frostick, L.E., Reid, I. (Eds.), Desert Sediments: Ancient and Modern. Geological Society of London Special Publication vol. 35. Blackwell Scientific Publications, Oxford, pp. 69–86.

Owen, A., Nichols, G., Hartley, A., Weissmann, G.S., Scuderi, L.A., 2015. Quantification of a distributive fluvial system: the Salt Wash DFS of the Morrison Formation, SW U.S.A. Journal of Sedimentary Research 85, 544–561.

Paola, C., Wiele, S.M., Reinhart, M.A., 1989. Upper-regime parallel lamination as the result of turbulent sediment transport and low amplitude bed forms. Sedimentology 36, 47–59.

Parkash, B., Awasthi, A.K., Gohain, K., 1983. Lithofacies of the Markanda terminal fan, Kurukshetra district, Haryana, India. In: Collinson, J.D., Lewin, J. (Eds.), Modern and Ancient Fluvial Systems. Special Publication of the International Association of Sedimentologists No. 6. Blackwell Scientific Publications, Oxford, pp. 337–344.

Pimentel, N.L., Wright, V.P., Azevedo, T.M., 1996. Distinguishing early groundwater alteration effects from pedogenesis in ancient alluvial basins: examples from the Palaeogene of Portugal. Sedimentary Geology 105, 1–10.

Pizzuto, J.E., 1987. Sediment diffusion during overbank flows. Sedimentology 34, 301–317.

Platt, N.H., Keller, B., 1992. Distal alluvial deposits in a foreland basin setting - the Lower Freshwater Molasse (Lower Miocene), Switzerland: sedimentology, architecture and paleosols. Sedimentology 39, 545–565.

Reesink, A.J.H., 2019. Interpretation of cross strata formed by unit bars. In: Ghinassi, M., Colombera, L., Mountney, N.P., Reesink, A.J.H. (Eds.), Fluvial Meanders and Their Sedimentary Products in the Rock Record. International Association of Sedimentologists Special Publication vol. 48, pp. 173–200.

Retallack, G.J., 1988. Field recognition of paleosols. In: Reinhardt, J., Sigleo, W.R. (Eds.), Paleosol and Weathering Through Geologic Time: Techniques and ApplicationsGeological Society of America Special Paper vol. 216, pp. 1–20.

Retallack, G.J., 1994. A pedotype approach to latest Cretaceous and earliest Tertiary paleosols in easter Montana. Geological Society of America Bulletin 106, 1377–1397.

Retallack, G.J., 2001. Soils of the Past: An Introduction to Paleopedology. 2nd edition. Blackwell Science, Oxford (404 pp.).

Riccomini, C., 1997. Arcabouço Estrutural e Aspectos do Tectonismo Gerador e Deformador da Bacia Bauru no Estado de São Paulo. Revista Brasileira de Geociencias 27, 153–162.

Robinson, A.C., 2002. A Chronosequence Study of Modern Vertisols and Application to Interpreting the Time Significance of Paleozoic Paleovertisols. University of Tennessee, Knoxville (MSc Thesis, 177 pp.).

Rodrigues, A.G., Dal' Bó, P.F., Basilici, G., Soares, M.V.T., Menezes, M.N., 2019. Biotic influence in the genesis of laminar calcretes in vertisols of the Marília Formation (Upper Cretaceous, Brazil). Journal of Sedimentary Research 89, 440–458.

Rosario, J.J., 2017. Stratigraphic Record of a Distributary Fluvial System, Paleosols, Soils, and Their Paleoclimatic Implications During the Miocene to Early Pliocene, Northwestern Argentina. Faculty of the Graduate School, Cornell University, USA (PhD Thesis, 275 pp.).

Rust, B., Nanson, G.C., 1989. Bedload transport of mud as pedogenic aggregates in modern and ancient rivers. Sedimentology 36, 291–306.

Sáez, A., Anadón, P., Herrero, M.J., Moscariello, A., 2007. Variable style of transition between Palaeogene distributive fluvial system and lacustrine systems, southern Pyrenean foreland, NE Spain. Sedimentology 54, 367–390.

Santucci, R.M., Bertini, R.J., 2001. Distribução Paleogeográfica e Biocronológica dos Titanossauros (Saurishia, Sauropoda) do Grupo Bauru, Cretáceo Superior do Sudeste Brasileiro. Brazilian Journal of Geology 31, 307–315.

Schieber, J., 1998. Possible indicators of microbial mat deposits in shales and sandstones: examples from the Mid-Proterozoic Belt Supergroup, Montana, USA. Sedimentary Geology 120, 105–124.

Schieber, J., 1999. Microbial mats in terrigenous clastics: the challenge of identification in the rock record. Palaios 14, 3–12.

Schoeneberger, P.J., Wysocki, D.A., Benham, E.C., Broderson, W.D., 2001. Field Book for Describing and Sampling Soils. USDA-NRCS, National Soil Survey Center, Lincoln, NE (228 pp.).

Simon, S.S.T., Gibling, M.R., 2017. Pedogenic mud aggregates preserved in a fine grained meandering channel in the Lower Permian Clear Fork Formation, north-central Texas, USA. Journal of Sedimentary Research 87, 230–252.

Slingerland, R., Smith, N.D., 2004. River avulsions and their deposits. Annual Review of Earth and Planetary Sciences 32, 257–285.

Smith, N.D., 1972. Some sedimentological aspects of planar cross-stratification in a Sandy braided river. Journal of Sedimentary Petrology 42, 624–634.

Smith, N.D., 1974. Sedimentology and bar formation in the Upper Kicking Horse River, a braided outwash stream. Journal of Geology 82, 205–223.

Soares, M.V.T., Basilici, G., Dal' Bó, P.F., Marinho, T.S., Mountney, N.P., Colombera, De Oliveira, E.F., Silva, K.E.B., 2018. Climatic and geomorphologic cycles in a semiarid distributive fluvial system, Upper Cretaceous, Bauru Group, SE Brazil. Sedimentary Geology 372, 75–95.

Soares, M.V.T., Basilici, G., Marinho, T.S., Martinelli, A.G., Marconato, A., Mountney, N.P., Colombera, L., Mesquita, A.F., Vasques, J.T., Junior, F.R.A., Ribeiro, L.C.B., 2020. Sedimentology of a distributive fluvial system (Upper Cretaceous, Bauru Basin, Brazil): the Serra da Galga Formation, a new lithostratigraphic unit. Geological Journal, 1–25 https://doi.org/10.1002/gj.3987.

Soil Survey Staff, 2015. Illustrated Guide to Soil Taxonomy, Version 2. U.S. Department of Agriculture, Natural Resources Conservation Service, National Soil Survey Center, Lincoln, Nebraska.

Sommer, M., Kaczorek, D., Kuzyakov, Y., Breuer, J., 2006. Silicon pools and fluxes in soils and landscapes – a review. Journal of Plant Nutrition and Soil Science 169, 310–329.

Steel, R.J., Thompson, D.B., 1983. Structures and textures in Triassic braided stream conglomerates ('Bunter' Pebble Beds) in the Sherwood Sandstone Group, North Staffordshire, England. Sedimentology 30, 341–368.

Stoops, G., 2003. Guidelines for Analysis and Description of Soil and Regolith Thin Sections. Soil Science Society of America Inc., Madison, Wisconsin, USA (181 pp.).

Stoops, G., Jongerius, A., 1975. Proposal for micromorphological classification in soil materials. A classification of the related distributions of coarse and fine particles. Geoderma 13, 189–200.

Stoops, G., Altemuller, H.J., Bisdom, E.B.A., Delvigne, J., Dobrosvolsky, V.V., FitzPatrick, E.A., Paneque, G., Sleeman, J., 1979. Guidelines for the description of mineral alterations in soil micromorphology. Pedologie 29, 121–135.

Sullivan, L.A., 1994. Clay coating formation on impermeable materials: deposition by suspension retention. In: Ringrose-Voase, A.J., Humphreys, G.S. (Eds.), Soil Micromorphology: Studies in Management and Genesis. Developments in Soil Science vol. 22. Elsevier, Amsterdam, pp. 373–380.

Theocharopoulos, S.P., Dalrymple, J.B., 1987. Experimental construction of illuviation cutans (channel argillans) with differing morphological and optical properties. In: Fedoroff, N., Bresson, L.M., Courty, M.A. (Eds.), Micromorphologie des Sols, Soil Micromorphology. AFES, Paris, pp. 245–250.

Törnqvist, T.E., Bridge, J.S., 2002. Spatial variation of overbank aggradation rate and its influence on avulsion frequency. Sedimentology 49, 891–905.

Tunbridge, I.P., 1984. Facies model for a sandy ephemeral stream and clay playa complex; the Middle Devonian Trentishoe Formation and North Devon, UK. Sedimentology 31, 697–715.

Ulmer-Scholle, D.S., Scholle, P.A., Schieber, J., Raine, R.J., 2015. A color guide to the petrography of sandstones, siltstones, shales and associated rocks. American Association of Petroleum Geologists Memoir 109 (526 pp).

Veneman, P.L.M., Vepraskas, M.J., Bouma, J., 1976. The physical significance of soil mottling in a Wisconsin toposequence. Geoderma 15, 103–118.

Vepraskas, M.J., 2000. Morphological features of seasonally reduced soils. In: Richardson, J.L., Vepraskas, M.J. (Eds.), Wetland Soils: Genesis, Hydrology, Landscapes and Classification. Lewis Publisher, Boca Raton, Florida, USA, pp. 163–182.

Vepraskas, M.J., 2004. Redoximorphic features for identifying aquic conditions. Technical Bulletin 301. North Carolina Agricultural Research Service, Raleigh, NC, USA (33 p.).

Walker, R.G., 2006. Facies models revisited: introduction. In: Posamantier, H.W., Walker, H.G. (Eds.), Facies Models Revisited. SEPM Special Publication vol. 84, pp. 5–22.

Weissmann, G.S., Hartley, A.J., Nichols, G.J., Scuderi, L.A., Olson, M., Buehler, H., Banteah, R., 2010. Fluvial form in modern continental sedimentary basins: distributive fluvial systems. Geology 38, 39–42.

Weissmann, G.S., Hartley, A.J., Scuderi, L.A., Nichols, G.J., Davidson, S.K., Owen, A., Atchley, S.C., Bhattacharyya, P., Chakraborty, T., Ghosh, P., Nordt, L.C., Michel, L., Tabor, N.J., 2013. Prograding distributive fluvial systems: geomorphic models and ancient examples. In: Dreise, S.G., Nordt, L.C., McCarthy, P.L. (Eds.), New Frontiers in Paleopedology and Terrestrial Paleoclimatology. SEPM Special Publication vol. 104, pp. 131–147.

Wright, V.P., 1990. A micromorphological classification of fossil and recent calcic and petrocalcic microstructures. In: Douglas, L.A. (Ed.), Soil Micromorphology: A Basic and Applied Science. Developments in Soil Science vol. 19. Elsevier, Amsterdam, pp. 401–407.

Wright, V.P., Marriott, S.B., 2007. The dangers of taking mud for granted: lessons from Lower Old Red Sandstone dryland river systems of South Wales. Sedimentary Geology 195, 91–100.

Wright, V.P., Tucker, M.E., 1991. Calcretes: an introduction. In: Wright, V.P., Tucker, M. (Eds.), Calcretes. International Association of Sedimentologists Reprint Series 2, Oxford. Blackwell, Oxford, pp. 1–22.

Wright, V.P., Platt, N.H., Marriott, S.B., Beck, V.H., 1995. A classification of rhizogenic (root-formed) calcretes, with examples from the Upper Jurassic–Lower Cretaceous of Spain and Upper Cretaceous of southern France. Sedimentary Geology 100, 143–158.

Zhou, J., Poulsen, C.J., Rosenbloom, N., Shields, C., Briegleb, B., 2012. Vegetation-climate interactions in the warm mid-Cretaceous. Climate of the Past 8, 565–576.